SURFACE ENHANCED RAMAN SPECTROSCOPY STUDIES OF LUMAZINE, PIPERIDINE AND 2-MERCAPTOPYRIDINE ON A SILVER ELECTRODE

by

XINGXING CHEN

A dissertation submitted to the Graduate Faculty in Chemistry in partial fulfillment of the requirements for the degree of Doctor of Philosophy, The City University of New York

2001

This manuscript has been read and accepted for the Graduate Faculty in Chemistry in satisfaction of the dissertation requirement for the degree of Doctor of Philosophy.

7/25/01
Date

Ronald J Bukowski
Chair of Examining Committee

8/2/2001
Date

Gerald Koppel
Executive Officer

Professor John R. Lombardi

Professor Max Diem

Supervisory Committee

THE CITY UNIVERSITY OF NEW YORK

ABSTRACT

Surface Enhanced Raman Spectroscopy Studies of Lumazine, Piperidine and 2-Mercaptopyridine on a Silver Electrode

by

Xingxing Chen

Advisers: Professors Ronald L. Birke and John R. Lombardi

Surface-enhanced Raman spectroscopy (SERS) at a silver electrode was used to obtain the Raman spectrum of lumazine free of interference from fluorescence. The study was carried out varying the experimental conditions of voltage and pH. Ab initio calculations at the Hartree-Fock/6-31G(d) level were made of the vibrational spectra of lumazine [2,4(3*H*,8*H*)-pterdinedione, LUM] and dimethyllumazine [6,7-dimethyl-,2,4(3*H*,8*H*)-pterdinedione, DML], and these were compared with the experimental results. Band assignments were made for LUM and DML. In addition, to determining the structure of the molecules on the metal surface as well as to examining the effects of the surface on the observed spectrum, we compared the results with the FTIR spectrum of a known metal complex of LUM. We also analyzed band shifts and the intensity ratio of in-plane and out-of-plane modes as a function of potential. This analysis indicates that the LUM molecules are tilted at an angle of ca. 45 degree (0.0 to -0.3 V) to the surface interacting as dimers with silver (Ag) sites through the lone pairs on the

1N or 5N atoms of the LUM ring. The tilt angle moves to ca. 50 degree as the potential is made more negative (-0.6 to -0.7 V).

The enhancement factor of the surfaced enhanced Raman scattering spectra of a molecule on metal electrode is well known to be potential and incident wavelength dependent. A quantitative potential-dependence study of SERS of piperidine and 2-mercaptopyridine on the Ag electrode is presented. The result shows that the surface concentration of piperidine adsorbed on the Ag electrode is a constant over the potential range from 0.0V to –0.9V vs. SCE. Two structural isomers exist on the surface. The concentration of each species is a function of applied potential. 2-mercaptopyridine is adsorbed on Ag surface via Ag-S bond. The orientation of the molecule changes with the applied potential. Experimentally, the SERS of 2-mercaptopyridine is much stronger than the SERS of 2-piperidine, which implies that the strength of chemical bond between adsorbate and metal is related to the chemical enhancement factor.

ACKNOWLEDGMENTS

I am deeply grateful to Professor Birke, my dissertation advisor, for guiding this dissertation and for his help and patience.

I also wish to thank my committee members Professor Lombardi, Professor Grossman, and Professor Diem for their valuable assistance and comments and on this dissertation.

Many thanks are due to my coworkers and friends in Birke and Lombardi's group: Dr. Wei Zhang, Dr. Mingfa Wang, Dr. Donghong Zheng, Paula A. Faria, Richard, and Lei Yan.

Finally I want to thank Huaiming Wang and Yuchen Wang for their unfailing encouragement and support along the way.

TABLE OF CONTENTS

LIST OF TABLES

LIST OF FIGURES

CHAPTER 1 THEORY AND OVERVIEW

1.1 Introduction

The fundamental study of the chemical and physical processes occurring at different types of interfaces has been one of the most active research fields for decades. Such an endeavor not only extends our understanding and knowledge of surfaces at the atomic and molecular level but also leads to the development of many important technological areas such as heterogeneous catalysis [1-2], fabrication of thin film microelectronic devices [3], solar energy conversion and storage [4], and corrosion control [5-6].

There are varieties of surface spectroscopy techniques that have been used to characterize interfacial properties. The following is a list of examples [7-15]: Auger Electron Spectroscopy (AES), X-ray Photoelectron Spectroscopy (XPS) and Ultraviolet Photoelectron Spectroscopy (UPS) which provides electronic structure information, Secondary Ion Mass Spectroscopy (SIMS) which provides composition information, Low Energy Electron Diffraction (LEED), Transmission and Scanning Electron Microscopies (TEM and SEM), Scanning Tunneling and Atomic Force Microscopies (STM, AFM), Ion Scattering Spectroscopy (ISS) which provides geometric information, High Resolution Electron Energy Loss Spectroscopy (HREELS), Infrared Spectroscopy (IR) and Raman Spectroscopy which provide adsorbate structural and interaction information. Combined use of

these techniques can provide complementary information on different physical-chemical properties of an interfacial system.

For the study of the charge transfer processes at an electrode/solution interface, until recently the conventional electrochemical techniques dominated. Electrochemical methods, such as polarography, cyclic voltammetry and coulometry can only measure the sum of all the processes at the interfaces, and cannot characterize the molecular species present. So the structural information can only be inferred indirectly. In recently years, research in electrochemistry has turned to the combination of data obtained by traditional electrochemical techniques with those *ex-situ* and *in-situ* surface analytical spectroscopic methods mentioned above. However, while some of those techniques were extended to metal-liquid interfaces, which are particular important to electrochemists, many obstacles have been encountered. For example, some of the spectroscopy techniques that require ultrahigh vacuum condition would be normally excluded at the solid-liquid interface. IR and normal Raman techniques suffered from low detection sensitivity and difficulty in distinguishing the interface signal from the bulk solution signal. In this circumstance, the surface enhanced Raman spectroscopy (SERS) technique provides many advantages over the other spectroscopic techniques. First of all, SERS phenomenon exist at almost all types of interfaces: solid/vacuum, solid/gas, solid/liquid and solid/solid, and does not require high vacuum conditions. Secondly, SERS offers *in-situ* and non-destructive measurement, which gives great convenience to the electrochemist in the study of the electrode/electrolyte interface. Third, it is probably the most

sensitive vibrational spectroscopy technique available as a surface analytical probe. The giant Raman signal enhancement, which is up to six orders of magnitude higher when compared to molecules in the solution, completely solved the low sensitivity problem. In addition, SERS strongly discriminates against signals of molecules in the diffuse layer since the enhancement factor falls off rapidly as the surface-adsorbate separation increases. It can also be used to follow in real time electrochemical or photochemical process occurring at the electrode surface. Another strength of SERS is its complementary nature with respect to surface infrared spectroscopy. IR and Raman are governed by different selection rules, and the vibrational spectra of a molecule obtained by the two techniques exhibit different relative intensity patterns.

For the study of the vibrational spectra of molecules in aqueous environment, SERS has unique advantages comparing to FT-IR technique. Water has a very weak Raman signal, and, therefore, it is an ideal solvent for Raman measurement, which makes SERS an excellent technique to investigate the behavior of the interaction of biological molecules with the metals in aqueous environment. Also the optics and cell materials are made from glass or quartz in Raman instead of the salts used in IR. Photon detectors such as the photon multiplier tube (PMT) and other array detectors used in the UV-Vis range can offer much better sensitivity and signal to noise ratio compared to thermal detectors used in IR. A single Raman spectrometer can cover the entire range of vibrational frequency (100 cm^{-1} to 4000 cm^{-1}), whereas even with FT-IR systems, changes in detectors or beam splitters must be made to cover the whole range.

In this chapter, a brief introduction will be given on theories and fundamentals of normal Raman spectroscopy, resonance Raman spectroscopy and SERS mechanisms. Recent developments and SERS applications will also be reviewed, and then the goals and an overview of this thesis will be discussed in the last section.

1.2 Raman Spectroscopy

Predicted by Smekal in 1923 [16] and experimentally confirmed by Raman in 1928 [17], the Raman effect originates from the interaction between a molecule and the oscillating electric field associated with light. In the classical mechanical model [18], the electromagnetic radiation (excitation source for Raman scattering) can be written as:

$$E = E_m \cos \omega_0 t \qquad (1\text{-}1)$$

Where E_m is the amplitude and ω_0 is the frequency of the excitation light source. When this electromagnetic radiation interacts with the polarizable electron clouds of the sample molecules, it induces a dipole moment μ given by:

$$\mu = \alpha E = \alpha E_m \cos \omega_0 t \qquad (1\text{-}2)$$

If the polarizability α is a time independent constant, the induced dipole moment μ causes oscillating and radiating light in all directions at the same frequency ω_0 as the incident light. This process is well known as Rayleigh scattering.

In addition, if the sample molecule itself has a natural oscillation frequency ω_{if} corresponding to various normal modes of a molecule, the polarizability α is not a constant (time dependent). The polarizability varies with the internuclear separation around its equilibrium value α_0 according to

$$\alpha = \alpha_0 + (r - r_0)(\frac{\partial \alpha}{\partial r})_{r=r_0} \qquad (1\text{-}3)$$

Where α_0 is the polarizability of molecule at the equilibration distance r_0, r is the internuclear separation. The subscript $_0$ indicates evaluation at the equilibrium position. The change in internuclear distance varies with the frequency of the vibration ω_{if} according to

$$r - r_0 = r_m \cos \omega_{if} t \qquad (1\text{-}4)$$

where r_m is the maximum internulcear separation relative to the equilibrium position. Substituting Eq. (1-4) into Eq. (1-3), we obtain

$$\alpha = \alpha_0 + (\frac{\partial \alpha}{\partial r})\Big|_{r=ro} r_m \cos \omega_{if} t \qquad (1\text{-}5)$$

Substituting Eq. (1-5) into Eq. (1-2), we have an expression for the induced dipole moment μ

$$\mu = [\alpha_0 + (\frac{\partial \alpha}{\partial r})\Big|_{r=r_0} r_m \cos\omega_{if} t] E_m \cos\omega_0 t$$
$$= \alpha_0 E_m \cos\omega_0 t + E_m r_m (\frac{\partial \alpha}{\partial r})\Big|_{r=r_0} \cos\omega_{if} t \cos\omega t$$
$$= \alpha_0 E_m \cos\omega_0 t + E_m r_m (\frac{\partial \alpha}{\partial r})\Big|_{r=r_0} \cos(\omega_0 + \omega_{if}) + E_m r_m (\frac{\partial \alpha}{\partial r})\Big|_{r=r_0} \cos(\omega_0 - \omega_{if}) t$$

(1-6)

From Eq. (1-6), we find that the characteristic vibrational frequency can mix with the exciting light to form sum and difference frequencies in the scattering radiation. The first term corresponds to Rayleigh scattering, while the second and the third terms correspond to Anti-Stokes and Stokes frequencies. The actual molecule vibrational frequencies can be detected as shifts from the Rayleigh frequency, and are called normal Raman spectra. The measurement of these shifts reflects the characteristic vibrations of the molecules, and may be utilized as a complement to infrared spectroscopy.

Although this classical treatment predicted Raman scattered radiation at higher or lower frequencies than the excitation radiation, it failed to account for the spectral intensity difference between stokes and anti-stokes lines. A quantum mechanic treatment solved this problem by accounting for the relative populations of the energy levels.

In the quantum mechanical model [19], light scattering is depicted as a two-photon process. In Rayleigh scattering, the molecule is excited to a higher virtual state by combination with a photon, and relaxes "immediately" to the original vibrational state by re-emitting a photon at the same frequency as the incident light. The molecule "adsorbs" no energy from the incident radiation in this case. In Raman scattering, the excited molecule relaxes "immediately" to a different vibrational state, rather than to the original state. Only a very small fraction of molecules undergo Raman scattering (inelastic scattering). The energy carried by an inelastically scattered photon is different from that of the incident light. In anti-Stokes process, the second photon has frequency $\omega_0+\omega_{if}$, and in the Stockes process, the second photon has frequency $\omega_0 - \omega_{if}$.

We have seen that in the Raman spectrum, the energy difference between the incident and scattering light appears as a frequency shift ω_{if} between the excitation light and the scattering light, which corresponds to the energy difference between two vibrational states.

$$\Delta E_{vibration} = h\omega_{if} \qquad (1\text{-}7)$$

where h is Plank constant.

1.3 Resonance Raman Spectroscopy

When the excitation frequency is not within the electronic absorption band of the molecule, the spectrum detected is called the normal Raman spectra (NRS). Normal Raman is a very weak effect, typically one incident photon out of 10^{10}. The total Raman scattered radiation is therefore very small, and this was the major disadvantage that prevented many potential applications.

When the frequency of the exciting radiation coincides with or is in the region of an electronic absorption band, a significant enhancement of some of the vibrational bands are observed, which are called resonance Raman spectra (RRS). Resonance Raman lines can be 10^2 to 10^6 times more intense than in the normal Raman spectra. The enhancement is restricted to vibrational modes that couple with the electronic transition. That is, those vibrations that exhibit a large change in equilibrium geometry upon electronic excitation are enhanced. This usually means that enhancements are observed for totally symmetric vibrations and vibrations that vibronically couple the two electronic states. As the result of such an enhancement, RRS provide low detection limits (10^{-6} to 10^{-8}M for some species), and is suitable for trace analysis. Resonance Raman spectra are often quite simple, since only the bands related to chromophoric groups in the molecule are enhanced. Thus, the resonance Raman effect is closely related to fluorescence emission. The incident photon is absorbed, promoting an electron into an excited vibronic state. Immediate relaxation to a vibrational level of the ground state results in resonance Raman emission. As might be expected, with fluorescent molecules, fluorescence emission can be a major interference in the resonance Raman spectroscopy measurement.

The quantum mechanical treatment [19] gives a better understanding of the intensity enhancement in resonance Raman scattering and will be helpful in understanding the SERS enhancement mechanisms that we will discuss in next section.

Eq. (1-8) gives the total intensity of the scattered light I_s in terms of the intensity of the exciting light I_L:

$$I_s = K_E 8\pi[\frac{(\omega \pm \omega_{IF})^4}{9c^4}]I_L \sum_{\sigma,\rho}|\alpha_{\sigma\rho}|^2 \qquad (1\text{-}8)$$

where K_E is a parameter, which gathers all instrumental factors, and $\alpha_{\sigma\rho}$ is the $\rho\sigma$ component of the transition polarizability tensor (ρ and σ refer to x, y or z). For transitions between states I and F, we may use second-order perturbation theory to obtain the expression of $\alpha_{\rho\sigma}$, in terms of the quantum mechanical wave functions associated with the molecular states as

$$\alpha_{\sigma\rho} = \sum_{K \neq I,F} \left\{ \frac{\langle I|\mu_\sigma|K\rangle\langle K|\mu_\rho|F\rangle}{E_K - E_I - \hbar\omega} + \frac{\langle I|\mu_\rho|K\rangle\langle K|\mu_\sigma|F\rangle}{E_K - E_F + \hbar\omega} \right\} \qquad (1\text{-}9)$$

where μ_σ and μ_ρ are the dipole moment operators for the polarization directions σ and ρ, E_I and E_F are the energies of the initial and final states, while E_K are the energies of all the states other than I and F.

With the fact that nuclei motion is much slower than electronic motion, we may use the zero-order Born-Oppenheimer approximation to separate the

nuclear coordinates from the electronic coordinates by writing the vibronic function as a product of an electronic function and a vibrational one: $|I\rangle = |I_e\rangle|i\rangle$ and $|F\rangle = |I_e\rangle|f\rangle$, and also we integrate over the electronic coordinates:

$$M_{KI}(Q) = \langle I_e|\mu|K_e\rangle \tag{1-10}$$

where Q is a normal coordinate, and represents motion along one of the normal modes. If Q has a slight displacement from equilibrium position Q_0, we have:

$$M_{KI}(Q) = M_{KI}(Q_0) + (\frac{\partial M_{KI}}{\partial Q})_0 (Q - Q_0) \tag{1-11}$$

Substituting Eq. (1-11) with the vibronic functions into Eq. (1-9), and recognizing the $E_K - E_I = h\omega_{KI}$, we obtain an expression of $\alpha_{\sigma\rho}$ as a sum of two terms

$$\begin{aligned}\alpha_{\sigma\rho} = &\sum_{K\neq I}\sum_{k}[\frac{M^{\sigma}_{KI}(Q_0)M^{\rho}_{KI}(Q_0)}{\hbar(\omega_{KI}-\omega)} + \frac{M^{\sigma}_{KI}(Q_0)M^{\rho}_{KI}(Q_0)}{\hbar(\omega_{KI}+\omega)}]\langle i|k\rangle\langle k|f\rangle \\ &+\sum_{K\neq I}\sum_{k} M^{\rho}_{KI}(Q_0)[\frac{\partial M^{\rho}_{KI}}{\partial Q}]_0[\frac{\langle f|Q|k\rangle\langle k|i\rangle + \langle f|k\rangle\langle k|Q|i\rangle}{\hbar(\omega_{KI}-\omega)} \\ &+\frac{\langle f|Q|k\rangle\langle k|i\rangle + \langle f|k\rangle\langle k|Q|i\rangle}{\hbar(\omega_{KI}+\omega)}]\end{aligned} \tag{1-12}$$

where *i* and *f* represent initial and final vibrational levels of the ground electronic state I_e, while *k* represents vibrational levels of excited electronic states K_e. Matrix elements of the type $\langle k|i\rangle$ correspond to Franck-Condon overlap integrals.

In normal Raman scattering, the frequency of the incident light is considerably less than that needed to induce an optically allowed transition. That is $\omega_{KI} >> \omega$, and the denominator in all terms of Eq. (1-12) may be considered constant. Since $\sum|k\rangle\langle k| = 1$, Eq. (1-12) becomes:

$$\alpha_{\sigma\rho} = \frac{2\omega_{KI}}{\hbar(\omega_{KI}^2 - \omega^2)} \sum_{K \neq I} [M_{KI}^{\rho}(Q_0) M_{KI}^{\sigma}(Q_0) \langle i|f\rangle + M_{KI}^{\rho}(Q_0)(\frac{\partial M_{KI}^{\sigma}}{\partial Q})_0 \langle f|Q|i\rangle] \quad (1\text{-}13)$$

The first term in Eq. (1-13) gives Rayleigh scattering, since in the same electronic state, $\langle i|f\rangle = \delta_{if}$. In the harmonic oscillator approximation, the second term gives Raman scattering only when $f = i \pm 1$. Therefore, the normal Raman spectra are largely confined to fundamental frequencies. Usually the first term is considerably larger than the second term, since for allowed transitions, M_{KG}, the electronic transition moment, is much larger than $\frac{\partial M_{KG}}{\partial Q}$, the derivative of an electronic dipole moment. This is the reason that normal Raman scattering is much weaker than Rayleigh scattering. Experimentally it is found that the Raman intensity is often approximately three orders of magnitude less than Rayleigh intensity.

Immediately, we see from Eq. (1-13) that when ω is near the energy of an allowed molecular transition, $\omega \approx \omega_{KI}$, the denominator is not a constant and becomes smaller. This approaches a resonance condition. In this case, Franck-Condon overlap factors are not zero, because the vibrational levels involved

belong to different electronic states, and are therefore, not orthogonal. In the usual notation $\alpha = A + B + C$, the first term A in Eq. (1-12) is much larger than second and third terms B and C, since we have a rapidly converging Taylor series in which $\langle i|k\rangle\langle k|f\rangle$ is not small. Thus it is reasonable to expect a considerable increase in intensity. We have:

$$A = \hbar^{-1} \sum_{K_e} M_{KI}^{\rho}(Q_0) M_{KI}^{\sigma}(Q_0) \{ \sum_{k} [\frac{\langle i|k\rangle\langle k|f\rangle}{(\omega_{KI} - \omega + i\Gamma)} + \frac{\langle i|k\rangle\langle k|f\rangle}{(\omega_{KI} + \omega + i\Gamma)}] \} \quad (1\text{-}14)$$

Where $\Gamma = \Delta\omega_{KI} = (2\tau)^{-1}$, is the line width due to the uncertainty principle. The total scattering intensity is

$$I = \frac{8\pi(\omega \pm \omega_{IF})^4 I_L}{9c^4\hbar^2} K_E \sum_{\rho,\sigma} [M_{KI}^{\rho}(Q_0) M_{KI}^{\sigma}(Q_0)]^2 \frac{|\langle i|k\rangle\langle k|f\rangle|}{(\omega_{KI} \pm \omega)^2 + \Gamma^2} \quad (1\text{-}15)$$

From the equation, we can see that the scattered intensity will depend on which particular excited state is in resonance with the exciting light. So the resonance Raman spectra will change with the excitation frequency. Also in RRS, the selection rule obtained in NR no longer holds due to the intrusion of only one chosen excited state. Consequently, we can expect rich overtone transitions and considerable increase in intensity.

However, two other processes compete with the resonance effect, and both of these occur with higher probability than RRS. One process is the non-radiative

pathway. In this case, the molecule returns to the lower electronic state by dissipating the energy of photon as heat. The second process is fluorescence, and resonance Raman spectra often coincide with the fluorescence spectra. In the case of most biological molecules, the resonance Raman spectrum may be obscured by the fluorescence emission. Avoiding the intense fluorescence by shifting the excitation frequency out of the resonance range gives a weaker normal Raman spectrum.

One of the advantages of SERS is that the fluorescence can be quenched sufficiently by the roughened metal surface, while SERS gives much stronger Raman intensity than normal Raman scattering or even RRS in some cases.

1.4 Surface Enhanced Raman Scattering

The first report of an anomalously intense Raman signal from pyridine adsorbed on a silver electrode under potentiostatic electrochemical control was published in 1974 [21]. The authors initially thought that the oxidation-reduction cycles applied to a silver electrode had significantly increased the surface area of the electrode so that a well-defined Raman spectrum of pyridine could be obtained. It was soon pointed out by Jeanmaire and Van Duyne,[22] and Albrecht and Creighton [23] that only a single ORC was necessary to produce an intense Raman spectrum and that the Raman signal was enhanced by at least five to six orders of magnitude over that of an isolated molecule in the bulk solution. These early reports initiated a new research area of Raman spectroscopy, which was

called surface enhanced Raman scattering (SERS). During the last 25 years, an interest has been aroused to study SERS both as a fundamental phenomenon and as a new technique. Now it is well known that the SERS effect has been observed at many types of interfaces [36-39], such as the metal/gas, colloid/liquid, and solid/solid Interfaces. SERS active substrates include roughened coinage metals [25-29] and some alkali and transition metals [30-31], such as Ni, Ti, and Al. Among them, Ag shows the most significant enhancement. Enhancement factors of up to 10^6 are found at electrodes for species that do not give RR scattering in solution, while species that show RR scattering in solution show a combined enhancement factor of 10^8 to 10^{10} on the surface. Also SERS characteristics change with the applied potential, polarization property of the excitation light, incident light angles, etc. These results offer the encouraging prospect that the SERS technique might be a valuable *in-situ* method for exploring the interaction of metal surfaces and the adsorbates. Ag is an electrode with high hydrogen overpotential, and Au is noble metal with a large, useful potential range, and both of them are general-purpose working electrodes in electrochemistry, which makes SERS particularly useful in electrochemical studies.

Many experimental details of the SERS phenomenon have been elucidated and many theoretical models have been proposed to explain the enhancement. For examples, SERS effect has been described as (1) a resonance Raman scattering process [40-42], (2) a reflection modulation effect [43-44], and (3) an electron-hole pair excitation [45-47]. Many of the models have similar features. For the pretreated electrochemical interface, it has been widely accepted that two

main mechanisms operate: (1) an electromagnetic enhancement related to the enhancement of the oscillating electric field of the exciting light by larger scale metal surface structures, and (2) a charge transfer resonance Raman type enhancement related to atomic-scale structures. The combination of two mechanisms gives up to a 10^6 order of magnitude enhancement for the Raman signal.

The overall enhanced scattering intensity of an individual molecule in SERS by these two mechanisms can be defined by the following:

$$I_{SERS} = [8\pi(\omega_o + \omega_{IF})^4 / 9c^4] \cdot K_E I_L L^2(\omega_0) L^2(\omega_{IF}) \sum_{\rho,\sigma} |\alpha_{\rho\sigma}|^2 \quad (1\text{-}16)$$

where ω_0 is the incident laser angular frequency, ω_{IF} is a Raman-shifted angular frequency, I_L is the intensity of laser radiation, $L^2(\omega_0)$ and $L^2(\omega_{IF})$ are the electromagnetic enhancement factors, and $\sum_{\sigma,\rho} |\alpha_{\sigma\rho}|^2$ is the charge transfer enhancement factor. In this equation, we suppose that the molecule distribution factor on a metal surface is uniform in order to simplify the SERS enhancement model.

(1) Electromagnetic enhancement (EM)

The electromagnetic enhancement can be described in terms of $L^2(\omega_0)L^2(\omega_{IF})$. $L^2(\omega_0)$ is the so called dipolar surface plasmon (DSP) enhancement and $L^2(\omega_{IF})$ is called the antenna enhancement. In order to simplify the illustration of the electromagnetic enhancement mechanism, we only consider the SERS enhancement for spherical particles as an example.

(1-1) The localized dipolar surface plasmon enhancement

One source of the electromagnetic enhancement comes from the interaction of the uniform excitation field E_0 with the metallic particle. The metallic particle has a high conductivity, which is expressed by its internal dielectric function ϵ and it is surrounded by a homogeneous medium of dielectric function of ϵ_0. Both dielectric functions depend on the frequency of the oscillating radiation $\epsilon = \epsilon(\omega)$. At the long wavelength approximation, $\lambda >> 20a$, where a is the radius of the spherical metal particle, and λ is the wavelength of the radiation, the electrostatic potential outside the sphere is [39]

$$\Phi = -E_0 r\cos\theta + g(\frac{a^3}{r^2})E_0\cos\theta \qquad (1\text{-}17)$$

With

$$g = \frac{\varepsilon_i(\omega_0) - \varepsilon_0}{\varepsilon_i(\omega_0) + 2\varepsilon_0} \qquad (1\text{-}18)$$

Two terms contribute to the potential outside the sphere; one from the excitation light (first term) and the other from the field of an electric dipole located at the center of the sphere with polarizability ga^3 oriented in the direction of the excitation field (second term). The excitation field polarizes the metal sphere so that there develop surface charge of opposite sign on either side of the sphere which alternate with frequency ω_0 as the electric field of the excitation light changes sign. This mode is called a localized dipolar surface plasmon.

The electric field outside the metal particle in the radial direction is $E_n = -\frac{\partial \Phi}{\partial r}$. We have

$$\bar{E}_n = \left\langle E_n^2 \right\rangle^{\frac{1}{2}} = (\frac{1}{3})^{\frac{1}{2}} E_0[1 + 2g(\frac{a}{r})^3] \qquad (1\text{-}19)$$

Therefore, an induced molecular dipole, μ, oriented perpendicular to the sphere surface will be enhanced because the field normal component has an additional term E_n. This DSP enhancement is described as

$$\frac{E_n^2}{E_0^2} = L_n^2(\omega_0) \qquad (1\text{-}20)$$

(1-2) The Antenna enhancement

A further electromagnetic enhancement factor the so-called Antenna effect is caused by the oscillating molecular dipole of the adsorbed molecule inducing a dipole in the metal sphere. Thus, the metal sphere acts as an antenna for the near field of the oscillating molecular dipole, and the emitted Raman radiation from the molecule at frequency ω_{IF} is then enhanced by the presence of the metal particle. The Antenna effect, to a good approximation, has the same form as DSP effect, $L^2(\omega_0)$. However, the frequency of the light is now the Stokes-shifted (Raman) frequency ω_{IF} giving $L^2(\omega_{IF})$. The frequency is manifested in the dielectric function, which becomes

$$g_0 = \frac{\varepsilon(\omega_{IF}) - \varepsilon_0}{\varepsilon(\omega_{IF}) + 2\varepsilon_0} \qquad (1\text{-}21)$$

For a molecule adsorbed on the surface of a metal sphere (r=a), with its vibrational mode oriented normal to the surface, the total electromagnetic enhancement is

$$g_0 = \frac{1}{9}(1+2g)^2(1+2g_0)^2 \qquad (1\text{-}22)$$

For Equation (1-18), when $\varepsilon_i(\omega_0) = -2\varepsilon_0$, the value of g becomes infinite, which would maximize $L^2(\omega_0)L^2(\omega_{IF})$. This situation will occur at a given excitation frequency ω_0; thus the system may be turned into resonance by changing the excitation frequency to ω_0. However, the dielectric functions are complex variables, so that a zero in the denominator of g giving an infinite enhancement, is not possible since ε should be expressed as $\varepsilon = \varepsilon_1 + i\,\varepsilon_2$. But, certain resonance enhancement conditions can be reached.

Experimental values for ε_1 and ε_2 can be found for Ag, Au and other metals at optical frequencies [48-49]. For example, for water at optical frequencies, ε_0=1.77, and the resonance condition is ε_1=-2, ε_0=-3.54, which occurs for Ag at 382nm. The imaginary component ε_2 is fairly constant and for Ag is approximately 0.3 in the 300 to 500nm region, according to the data of Johnson and Christy [49]. This value gives a $L^2(\omega_0)L^2(\omega_{IF})$ of 1.7×10^5 for Ag at 382nm, with the molecule oriented perpendicular to the surface. The theoretical calculation matches experimental data quite reasonably.

(2) Charge Transfer Enhancement

The term $\sum_{\sigma,\rho}|\alpha_{\sigma\rho}|^2$ in Eq. (1-16) represents the charge transfer enhancement factor, which arises from the interaction between the adsorbed molecule and surface adatoms of the metal [50-53] when the molecule is chemisorbed or physisorbed on the metal surface.

In contrast to polyatomic molecules that usually have discrete electronic and vibrational energy levels, metal often have several bands of energy levels. Valence electrons in the metal form a conduction band, which spreads out through the entire metal. The conduction band is usually not completely filled with electrons. The highest filled level of this band is called the Fermi level, E_F. In Ag and certain other metals, the conduction bands are derived from the 4*s* and 4*p* atomic orbitals. In an electrode immersed in an electrolyte solution, variation of applied potential V may add or remove electrons from the conduction band, thus changing the Fermi level.

In the charge transfer model, we can consider the molecule and metal system as a whole and assume that the Fermi level of the metal lies between the molecular ground state and one of the excited states of the molecule. There are two charge-transfer types: molecule to metal, and metal to molecule. In a metal to molecule charge transfer, the process can be described [19] as: (1) a metallic electron in an *sp*-conduction band absorbs a photon, the electron is promoted to the vacant sp-band above the Fermi level, leaving a hole below the Fermi level in the filled *sp*-band, (2) the electron either tunnels to a temporary negative molecular complex or crosses over to an excited state of the molecule-metal system, which is the charge transfer acceptor level of the chemisorbed

molecules, (3) the electron returns to the metal, recombines with the hole, and reradiates a Raman-shifted photon, (4) the molecule is left in the excited vibrational state. The charge transfer resonance energy is the difference between the adatom surface state level and the charge transfer acceptor level. A similar set of steps can be used to describe the molecule-to-metal charge transfer process: (1) A ground-state electron of the chemisorbed molecule absorbs a photon and it is vertically excited; (2) it either tunnels to the vacant level above the Fermi level of the metal, forming a temporary positive molecule complex, or crosses over to the lowest unoccupied level of the adatom surface state of the coupled molecule-adatom system;(3) the electron returns to the molecular ground electronic state and in the process reradiates a Raman-shifted photon; (4) the chemiadsorbed molecule is left in an excited vibrational state. The charge transfer energy is the difference between the molecular ground state and the Fermi level in a weakly coupled molecule-metal system, or between the HOMO and the LUMO of a more strongly coupled molecule-adatom complex.

Given the general equation α=A+B+C, as we have in Eq. (1-12) with an off-resonance excitation, if we consider in term A those states in which either K or I is actually a metal state, we might expect resonant contributions to the Raman intensity.

For molecule-to-metal charge transfer, $|k\rangle = |M\rangle$, we have

$$A_f = 2\hbar^{-1}\sum_{M_e} M^{\rho}_{MI}(Q_0)M^{\sigma}_{MI}(Q_0)\langle i|k\rangle\langle k|f\rangle\frac{\omega_{MI}+\omega_f}{(\omega_{MI}+\omega_f)^2-\omega^2} \qquad (1\text{-}23)$$

For metal-to-molecule charge transfer, $|I\rangle = |M\rangle$, we have

$$A_k = 2\hbar^{-1}\sum_{M_e} M^{\rho}_{KM}(Q_0)M^{\sigma}_{KM}(Q_0)\langle i|k\rangle\langle k|f\rangle\frac{\omega_{KM}+\omega_f}{(\omega_{KM}+\omega_f)^2-\omega^2} \qquad (1\text{-}24)$$

This charge transfer mechanism explains very well the resonance excitation and resonance potential dependence. The resonance maximum occurs at E_K-($E_{F(0)}$+eV)= $h\omega$ for metal-to-molecule charge transfer, and at ($E_{F(0)}$+eV)-E_I = $h\omega$ for molecule-to-metal charge transfer, and the electrode potential can be used to tune the Fermi level to match the resonance excitation. A negative shift of the potential will raise the Fermi level, and in metal-to-molecule charge transfer, a compensating shift to the lower energy of the excitation frequency will be required to reach resonance, while a shift to the higher resonance frequency is observed in molecule-to-metal charge transfer model for a negative shift in potential. A theoretical calculation shows that the predicted intensity vs. voltage profile fits the experimental curves quite well in the SERS study of piperidine and pyridine [50]. A detailed quantum mechanic charge-transfer theory was given by Lombardi et.al [54]. Three terms A, B, and C contribute to the SERS polarizability. The A term represents Franck-Condon coupling, while the B and C terms represent the transition from the ground state of the adsorbed molecule to the metal Fermi level and the transition from the metal Fermi level to an excited state of the molecule, respectively.

From the charge transfer theory we can see that the enhancement mechanisms of RRS and SERS are similar in terms of resonant charge transfer transitions. However SERS is different from RR in some aspects. We expect intense overtones in RR, and the totally symmetric vibrations are usually enhanced. In SERS, very few observations of overtones have been reported.

Also non-totally symmetric vibrations are often as intense as totally symmetric ones. Those experimental facts are all supported by the charge-transfer theory.

1.5 A Brief Overview of SERS Applications

Since the use of the laser as an excitation source and the discovery of SERS effect, SERS has become an important analytical technique for obtaining structural information for molecules on metal electrode. SERS had been applied in many interesting systems, such as biomolecucles, Langmuir-Blodgett films, electrochemical adsorption/desorption, and reaction kinetics, catalysis and molecule sensors [55-62]. Recently development of SERS research has been moving into more practical areas, such as immunuassay [63], medicine[64], thin-layer chromatography[65], and chemical sensors and biosensors[66].

SERS is particular conducive to study interactions between biological molecules with metal surfaces, which may be related to real physiological process. SERS or the combination of surface-enhanced Raman with Resonance Raman (SERRS) enhancement has permitted one to observe the vibrational spectra of the heme chromophore in highly dilute solutions of myglobin [67-68] and cytochrome c [69]. The vibrational information revealed the central metal oxidation states, spin states, and other conformational information. This type of structural information was not available in conventional electrochemical experiments. Flavins and flavoproteins are another class of molecules, which have been successfully studied with SERS techniques [71-74]. The different redox forms, ionic

forms, their adsorption sites as well as orientations on metal electrodes have been well interpreted by SERS spectra in electrochemical environments.

New developments in SERS with applications to biomolecules have been concerned with electron transfer process between molecules with Ag or Au electrodes with bifunctional surface modifier such as 4-pyridylthiol and 11-undecanoic acid [75]. For cytochrome c, it has been demonstrated that modification of the metal surface with organic and inorganic species serves to preserve the native structure of the protein in the adsorbed state. As a result, a reversible electrochemical response is obtained. The electron transfer process can be followed by monitoring the change in the oxidation sensitive bands of the heme in the SERS spectrum as a function of potential.

In certain cases, SERS or SERRS can achieve very low detection limits comparable to those for fluorescence spectroscopy. The very low detection limit makes SERS or SERRS a method to approach single molecule detection. The experiment has been carried out to measure the SERRS of rhodamine 6G at femto-molar concentration in sliver colloidal solution [70], as few as 60 molecules are detected.

With the development of optical multichannel analyzer (OMA) coupled with photodiode array detection technique, the time resolved surface enhanced Raman Spectroscopy (TRSERS) technique has been developed as an *in-situ* monitoring method of surface dynamic processes such as electrode reactions, surface diffusions, adsorption/desorption, and photon or potential induced surface reaction kinetics.

Initially TRSERS was applied to study slow dynamic process at ms level, such as adsorption/desorption [76], growth or aggregation of Ag particles [77] and surface photochemical reactions [78]. The SERS signal obtained during a cyclic voltammetry (CV) run provide real time, *in-situ*, and molecular specific information of adsorbed molecules, which makes it possible to identify transient chemical species. More recently, TRSERS has been successfully used to examine short time resolved surface dynamic studies with μs and ns time resolution. Our laboratory has reported time dependent SERS spectra of radical species formed by photochemical or electrochemical reaction on the SERS active substrates [71-74,79], which include p-nitrobenzoic acid, 4-cyanopyridine, 4-pyridine carboxaldehyde, 3-hydroxyflavone and flavin mononucleitide (FMN). An example of a photochemical reaction that has been studied with TRSERS is the FMN molecule. FMN is a coenzyme, which plays an important role in redox enzyme systems. It has also been used as a reagent to produce a highly oxidizing excited state redox species in a photogalvanic cell that utilizes solar energy to oxidize organic material at an illuminated electrode and reduces H^+ to H_2 at the dark electrode. The direct photoinduced charge transfer from adsorbed FMN to a Ag electrode has been observed by Zhang et al. in our laboratory, using a ns pulse laser pump and CW laser probe TRSERS system. Two short-lived intermediates at 75ns and 775ns were identified as the enol and keto forms of the photo-oxidized flavin monocation radical in aqueous and deuterated solution [74].

1.6 Objectives and Organization of this Dissertation

In the first chapter, a brief overview and introduction of basic Raman theory, Resonance Raman theory and SERS theory has been given. Also an overview of Raman applications has been discussed.

The second chapter will cover a detail explanation of Raman and SERS spectra acquisition techniques, including the description of the basic optics, dispersing system and detection system, as well as the sample pretreatment method.

Chapter 3 will present cyclic voltammetry (CV) results of lumazine on glassy carbon and silver electrodes in non-aqueous and aqueous solutions with supporting electrolytes. The CV of lumazine was carried out for different pH ranges. The result showed a one electron, one proton reduction was involved in the lumazine reduction on the electrode. Also the CV of adsorbed lumazine on a roughened Ag electrode was carried out in order to aid the SERS studies accomplished in chapter 4. The result shows that the electrode reaction of an adsorbed species was different from that of a species diffusing from bulk solution in some ways.

Chapter 4 will demonstrate characterization of surface species of the selected biological molecule, lumazine, and its interaction and electrochemical reaction on a silver electrode with the SERS technique. The NR and SERS results of lumazine, its pH dependence and voltage dependence will also be interpreted. Band assignment will be given based upon Raman, IR spectra, and

ab inito calculations. Redox states, orientation and adsorption sites of lumazine on the silver surface will be discussed.

In chapter 5, a study of the SERS dependence of 2-mercaptopyridine and piperidine will be discussed quantitatively. 2-mercaptopyridine molecules are directly bonded with Ag via a chemical reaction, while piperidine molecules are physiorbed on Ag electrode via their lone pair electrons on the N atom, thus presenting different SERS intensity vs. potential profiles. The effect of electrode potential on the orientation of molecules will be interpreted.

References

(1) Advances in Catalysis; D. D. Eley, H. Pines and P. B. Weisz, Eds.; Academic Press, Inc.; Orlando, **1985**

(2) J Kijenski and A. Baiker; Catalysis Today, **1989**, 5, pp1-107

(3) Laser-Controlled Chemical Processing of Surfaces, Materials Research Society Symposia Proceedings, V29; A. W. Johnson, D. J. Ehrlich and H. R. Schlossberg, Eds.; North Holland, New York, **1984**

(4) S. R. Morrison; Electrochemistry at Semiconductor and Oxidized Metal Electrodes; Plenum Press, New York, **1980**

(5) Advances in Corrosion Science and Technology, Vol. 7; M. G. Fontana Chapman and Hall, London, **1985**

(6) G. Wranglen; An Introduction to Corrosion and Protection of Metals; Vol. 28; F. Mansfeld, Ed.; Marcel Dekker, New York, **1987**

(7) X. L. Zhou and J. M. White; Surf. Sci., **1988**, 194, 438

(8) X. Y. Zhu, S. Akhter, M. E. Castro and J. M. White; Surf. Sci., **1988**, 195, L145

(9) Low Energy Electron Diffraction: Experiment, Theory and Surface Structure Determination; Springer Series in Surface Sciences, Vol. 6; M. A. Van Hove, W. H. Weinberg, C. M. Chan, Eds., Springer-Verlag, **1986**, Berlin, New York, 1986 (LEED).

(10) J. Dericbourg; Surf. Sci., **1992**, 269/270, 1157

(11) Scanning Tunneling Microscopy 1: Springer Series in Surface Sciences, Vol. 20; D. Anselmetti, et. al. Eds., Springer-Verlag, Berlin, 1986, Berlin, New York, **1986**

(12) G. Bracco, M. Canepa, P. Cantini, F. Fossa, L. Mattera, S. Terreni and D. Truffelli; Surf. Sci., **1992**, 269/270, 61

(13) A, Ausmees, M. Elango, A. Kikas, E. Nommiste and A. Saar; Surf. Sci., **1992**, 269/270, 583

(14) H. Ibach, M. Balden, D. Bruchmann and S. Lehwald; Surf. Sci., **1992**, 269/270, 94

(15) Vibrational Spectroscopies for Adsorbed Species, ACS Symposium Series, 137; A. T. Bell and M. L. Hair, Eds.; American Society; Washington. D. C., **1980**

(16) A. Smekal, Naturwiss, **1928**, 11, 873

(17) C. V. Raman and K. S. Krishnan; Nature, 1928, 121, 501

(18) M. Fleischmann and I. R. Hill; in 'Raman Spectroscopy'; Palph. E. White, J. O'M. Bockris (eds); Comprehensive Treatise of Electrochemistry, Vol.8, Plenum Press, **1984**, New York and London, pp373-432

(19) R. L. Birke and J. R. Lombardi; 'Surface-Enhanced Raman Scattering', in J. R. Gale (ed.), Spectroelectrochemistry: Theory and Practice, Plenum Press, Mew York, **1988**, pp263-348

(20) A. C. Albrecht; J. Chem. Phys., **1961**, 34, 1476

(21) M. Fleischman, P. J. Hendra and A. J. McQuillan; J. Chem. Phys. Letter, **1974**, 26, 163

(22) D. L. Jeanmaire and R. P. VanDuyne; J. Electroanal. Chem., **1977**, 84, 1-20

(23) M.G. Albrecht and J. A. Creighton; J. Am. Chem. Soc.; **1977**, 99, 5215

(24) R. P. Van Duyne; in 'Chemical and Biochemical Applications of Lasers'; C. B.Moore Ed.; Academic Press, New York, **1979**, Vol.4, pp101-184

(25) R. L. Paul. A. J. McQuilan, P. J. Hendra, and M. Fleischman; J. Electroanal. Chem., **1975**, 66, 248

(26) M. L. A. Temperini, H. C. Chagas, and O. Sala; Chem. Phys. Letters; **1981**, 79(1), 75

(27) J. R. Lombardi, and R. L. Birke; Surf. Sci.; **1980**, 95, 1259

(28) M. Fleischman, I. R. Hill, and G. Sundholm; J. Electroanal. Chem., **1983**, 157(2), 259

(29) M. Fleischman, I. R. Hill, and G. Sundholm; J. Electroanal. Chem., **1983**, 157(1), 153

(30) L. –W. H. Leung, M. J. Weaver, J. Sm. Chem. Soc.; **1987**, 109, 5113

(31) M. Fleischmann, Z. Q. Tian, L. J. Li; J. Electroanal. Chem.; **1987**, 217, 397

(32) Jia Xu, 'Surface-enhanced Raman Spectroscopy on Electrodes: Enhancement Mechanisms and Application to the studies of Flavin Molecules" PH.D thesis, 1987, The City University of New York

(33) T. M. Davine, in 'Electrochemical and Optical Techniques for the Study and Monitoring of Metallic Corrosion', M. G. S. Ferroira and C. A. Melendres (eds). Kluwer Academic Publishers, **1991**, 389-437

(34) J. A. Creighron, M. G. Albrecht, R. E. Hester, and J. A. D. Matthew; Chem. Phys. Letters, **1978**, 55, 55

(35) D. L. Jeanmaire, and R. P. Van Duyne; J. Electroanal. Chem., **1977**, 84, 1

(36) R. R. Smardzewski, R. J. Coltion, and J. S. Murday; Chem. Phys. Lett., **1979**, 68(1), 53

(37) J. E. Rowe, C. V. Shank, D. A. Zwemer, and C. A. Murray; Phys. Rev. Lett., **1980**, 44(26), 1770

(38) H. Seki, and R. Philpott; J. Chem. Phys., **1980**, 73(10), 5376

(39) J. D. Jackson, Classical Electrodynamics, 2nd Edition, John Wiley and Sons, New York, **1975**, p50

(40) S. Efrima, and H. Metiu; J. Chem. Phys. **1979**, 70, 1602, 2297, 1939

(41) F. W. King, R. P. Van Duyne, and G. C. Schatz; J. Chem. Phys.; **1978**, 69, 4472

(42) A. Otto; Surf. Sci.; **1978**, 75, L392

(43) A. Otto, in: Proc. Conf. On Vibrations in the Adsorbed Layer, Jülich, Germany, **1978**, p162

(44) S. L. McCall, and P. M. Platzman; Bull. Am. Phys. Soc. **1979**, 24, 340

(45) A. Otto, J. Timper, J. Billmann, G. Kovacs and I. Pockrand; Surf. Sci., **1980**, 92, L55

(46) R.K. Chang; 'Raman Spectroscopic Techniques in Interfacial Electrochemistry', in C. Gutierrez and C. Melendres (eds.), Spectroscopic and Diffraction Techniques in Interfacial Electrochemistry, Kluwer Academic Publishers, Netherlands, pp155-180

(47) J. A. Creighton; 'The Selection Rules for Surface-Enhanced Raman Spectroscopy', in R. J. H. Clark and R. E. Hester (eds.), Spectroscopy of Surfaces, Hohn Wiley and Sons Ltd., 1988, pp57-89

(48) P. B. Johnson and R. W. Christy; Phys. Rev., **1972**, B6, 4370

(49) H. J. Hagemann, W. Gudet, and C. Kunz; J. Opt. Soc. Am., **1975**, 65, 742

(50) R. L. Birke, and J. R. Lombardi; 'Surface Enhanced Raman Scattering', in J. R. Gale (ed.), Spectroelectrochemistry: Theory and Practice' Plenum Press, New York, **1988**, 263-348

(51) R. L. Birke, T. Lu, and J. R. Lombardi: 'Surface-enhanced Raman Spectroscopy', in R. Varmi and J. R. Selman (eds.), Techniques for the characterization of Electrodes and Electrochemical Process, John Wiley and Son, Inc., New York, **1992**, 211-277

(52) A. Otto, in 'Light Scattering in Solids III', (M. Cardona and G. Guntherodt. Eds.), Springer-Verlag, Heidelberg.

(53) G. J. Schulz, in 'Principles of Laser Plasmas" (George Bekefi, ed.), Wiley, New York, **1976**, 33

(54) John R. Lombardi, Ronald L. Birke, Tianhong Lu and Jia Xu; J. Chem. Phys., **1986**, 84(8), 4174

(55) E. Koglin and J. M. Sequaris; in 'Analytical Problems', Springer-Verlag, Berlin Heidelberg, New York, Tokyo, **1986**, Vol.134, pp1

(56) T. M. Cotton; in 'Surface and Interfacial Aspects of Biomedial Polymers', J. D. Andrade, (Ed.), Plenum Press, New York, **1985**, vol.2, pp161-187

(57) Y. J. Chen, G. M. Carter and S. K. Tripathy; Solid State Commun., **1985**, 54, 19

(58) R. Aroca and D. Battisti; Langmuir, 1990, 6, 250

(59) R. Aroca and U. Guhathakurta-Ghosh; J. Am. Chem. Soc., **1989**, 111, 7681

(60) J. H. Kim, T. M. Cotton, R. A. Uphaus and D.Mobius; J. Phys. Chem., **1989**, 93, 3713

(61) T. M. Cotton, R. A. Uphaus and D. Mobius; J. Phys. Chem., **1986**, 90, 6071

(62) M. Takahashi, M. Goto and M. Tto; J. Electroanal. Chem., **1989**, 93, 3753

(63) P. J. Tarcha, T. E. Rohr, J. J. Markese and T. Cotton; Surface Enhanced Raman Spectroscopy Immunoassay or Other Specific-Binding Assay, Eur. Pat. Appl. Ep587, 008, Mar., **1994**, US Appl. 944, 138, Sept., **1992**

(64) I. Nabiev, I. Chourpa and M. Manfait; J. Raman Spectrosc., **1994**, 25(1), 13

(65) S. L. Wright, K. J. Latas, A. N. Mortensen, E. A. Orr, J. V. Paukstelis, R. M. Hammaker and W. G. Fateley; Proc. SPIE-Int. Soc. Opt. Eng., **1993**, 1857

(66) T Vo-Dinh; in 'XVth International Conference on Raman Spectroscopy', edited by S. A. Asher and P. B. Stein, **1996**, pp1210

(67) Therese. M. Cotton, Steven G. Schultz, Richard P. Van Duyne; J. Am. Chem. Soc., **1980**, 102, 7960-7962

(68) James F. Rusling and Alaa-Eldin F. Nassar; J. Am. Chem. Soc., **1993**, 115, 11891-11897

(69) Lars H. Eng, Vicki Schlegel, Danli Wang, et al.; Langmuir **1996**, 12, 3055-3059

(70) Katrin Kneipp, Yang Wang, Ramachandra R. Dasari, and Michael S. Feld; Applied Spectroscopy, **1995**, 49(6), 780

(71) Ronald L. Birke, Chongtie Shi, Wei Zhang, and John R. Lombardi; J. Phys. Chem. B, **1998**, 102(41), 7983

(72) Chongtie Shi, Wei Zhang, Ronald L. Birke and John R. Lombardi; J. Electroanal. Chem., **1997**, 423, 67

(73) Chongtie Shi, Wei Zhang, John R. Lombardi and Ronald Birke; J. Phys. Chem., **1992**, 96(25), 10093

(74) Wei Zhang, Alberto Vivoni, John R. Lombardi, and Ronald L. Birke; J. Phys. Chem., **1995**, 99(34), 12846

(75) T.M. Cotton, G. Chumanov, M. Sibbald and J. Zheng; in 'XVth International Conference on Raman Spectroscopy', Edited by S. A. Asher and P. B. Stein, **1996**, pp28

(76) C. K. Chen, T. F. Heinz, D. Rcard and Y. R. Shen; Chem. Phys. Lett., **1981**, 83(3), 455

(77) k. Kneipp; J. Molec. Struct.; **1990**, 218, 357

(78) S. Sun, R. L. Birke and J. R. Lombardi; J. Phys. Chem.; **1988**, 92, 5965

(79) Ronald L. Birke and John R. Lombardi; Molecular Engineering, **1994**, 4, 277

CHAPTER 2 EXPERIMENTAL TECHNIQUES

2.1 Description of SERS Instrumentation

The basic elements of the SERS experimental setup used in this thesis are identical to those used in normal Raman or resonance Raman instruments, except for the special SERS cell. The SERS cell is an electrochemical cell, which contains a roughened Ag electrode surface with adsorbed molecules or ions, which are the scattering centers for the incident excitation light. A potentiostat coupled with a waveform generator are used to control the potential applied on the Ag electrode.

A block diagram of such a Raman spectrometer is shown in Figure 2.1. Detailed description is as follows:

1. Light source

The monochromatic radiation source is a continuous wave (CW) laser. Three laser instruments we used in this thesis are: an Argon laser (Spectra Physics Model 2020) for 488nm excitation line, a Krypton laser (Spectra Physics Model 2010) for 647.1nm excitation line, and a tunable Ti-Sapphire laser (600nm to 1100nm) (Spectra Physics Model 3900S), which needs to be pumped by the Argon laser. A 488nm or 647.1nm interference filter was placed in front of the Argon or Krypton laser output slit to eliminate unwanted lasing and plasma emission lines. For the Ti-Sapphire laser, a grating is used to eliminate the

plasma emission. For the SERS measurement the actual laser power illuminated on the electrode surface is ca. 40mW.

A collection lens with low f number is used to collect as much scattered light as possible, and the f number of the focusing lens should match that of the monochromator so as to optimize the optical system.

The electrochemical cell is a three-electrode system consisting of a 99.999% pure Ag working electrode, a platinum wire counter electrode, and a saturated calomel reference electrode (SCE). The cell geometry and electrode pretreatment we used will be discussed in the next section 2.2.

2. The Monochromator and Detection System

There are two monochromator and detection systems used in our experiments.

One is the conventional temporal scanning monochromator with a photomulitplier tube detector with which the spectrum is obtained by sequentially scanning a dispersive device, e.g., a grating, so that the spatially dispersed bands move across the exit slit of the monochromator linearly with time. A Spex Model 1401 scanning double monochromator is used to disperse Raman scattering light. A photomultiplier tube (PMT) serves as the detector. A thermoelectrical refrigerator chamber is housing the PMT. The temperature can be 40^0C below the ambient so as to minimize the dark current. The PMT operates with a photon counting mode. The output anode pulses of the PMT are fed to a low noise amplifier whose output then goes to a pulse-height discriminator. The discriminator level is properly adjusted in order to pick up the

largest number of signal pulses while rejecting dark current pulses. The pulses from the discriminator are counted by a digital counter (lab PC+), which is interfaced with a PC computer. The spectrum is then saved and displayed on the computer.

The advantages of this optical system are its high spectral resolution (a resolution of $2cm^{-1}$ is used for ordinary experiment, but it can be set as low as $0.2cm^{-1}$), broad spectral range ($100\sim4000cm^{-1}$), very sensitive detection, as well as high signal to noise ratio. The disadvantage is that the resolution limits the scan rate. For our instrument, the appropriate scan rate is 50 cm^{-1}/s. It takes 20min to scan a range of $1000cm^{-1}$.

The other combination is a single monochromator (Spex 500) coupled with a charge-coupled device (CCD) array detector. A notch filter is placed in front of entrance slit to eliminate the intense Rayleigh band at the excitation frequency of the laser, as well as stray light. Liquid nitrogen is used to lower the CCD detector temperature down to 140K to minimize the thermal noise. The CCD detector and monochromator are interfaced with the computer, so that the instrument operation and spectra acquisition are all controlled with software SpectraMax 32. The exposure time is usually a few seconds to a few minutes depends on the intensity of the SERS signal. A certain amount of scans can be accumulated to increase the signal to noise ratio. The use of array detectors, e.g., CCD, photodiode array (PDA), and charge injection device (CID), not only has the advantage of fast recording of a single spectrum but also allows successive spectra to be recorded as a function of time for time-resolved studies.

2.2 SERS Cell and Ag Electrode Pretreatment

The electrochemical setup is a three-electrode cell consisting of a working electrode, an inert counter electrode, and a reference electrode. The working electrode is constructed from a 99.99% pure Ag wire, which is embedded in a Teflon cylinder. For aqueous electrolyte solutions, the counter electrode is a platinum wire and the reference electrode is a saturated calomel electrode (SCE).

A two-compartment SERS cell, which we used with 90^0 scattering geometry, is illustrated in Figure 2.2. The two compartments are separated by a ground glass frit. If a deleterious species is produced at the counter electrode, it could be separated from the working and reference electrode. The working compartment is very small and holds as small as 1mL of sample for taking SERS spectra. Both the optically flat window and the silver electrode were made at a 45^0 angle to facilitate the 90^0 scattering angle with the laser beam. In this case, the electrode can be positioned as close to the window as possible (a few millimeters) to minimize the adsorption, fluorescence emission, and normal Raman signal and other interference from solution.

The design of this cell also allows us to bubble inert gas (Ar or N_2) before and during the experiment to remove oxygen from the system and prevent oxygen re-dissolving.

As we discussed in chapter 1, both EM and CT enhancements required a certain degrees of surface roughness. There have been many effective pretreatment methods reported. Among them are electrodeposition, chemical etching, chemical deposition, and an oxidation-reduction cycle (ORC), as well as others. In this thesis, we have employed an ORC to create a SERS-active electrode surface. The pretreatment process roughens the electrode, producing sites of large-scale roughness (hemispherical nodules 25 to 500nm in diameter) and molecular-scale roughness (possibly adatoms or adatom clusters). The large-scale roughness features have been associated with the EM mechanism and the adatom sites with the CT mechanism.

The pretreatment can be accomplished in the electrolyte with or without the molecules of interest, which we call "*in-situ*" or "*ex-situ*" pretreatment, respectively. The *ex-situ* method usually can avoid the complexation of silver and molecule. Also it can be used when the molecule will undergo reduction or oxidation during the ORC. Both of the methods usually give identical spectra in most cases, while the *in-situ* method gives more intense SERS spectra.

Also the pretreatment can be done in the presence and absence of laser light. An additional enhancement of 10-fold was observed with laser illumination during pretreatment. The effect of the laser illumination seems to be the photoreduction of the silver halide layer, producing Ag nuclei growth sites for formation of Ag microsturctures during the reduction stage of the ORC. With pretreatment in the dark, about 10% intensity reproducibility can be obtained with SERS bands, while the pretreatment under laser light gives worse reproducibility.

The electrochemical instrumentation necessary for activating the Ag surface and providing potential control include a potentiostat (EG&G PARC Model 173) and a waveform generator (EG&G PARC Model 175). The latter is capable of generating a potential pulse and a triangular waveform on top of an initial potential.

Usually the electrode was first polished with a finely divided alumina slurry (0.3 ~ 0.05μm), cleaned with high purely deionzed and distilled water, and ultra-sonicated to remove any adhering alumina, and then transferred into the electrochemical cell, where it is subjected to the ORC pretreatment. The initial potential is set negative to the onset of Ag oxidation, and the electrode potential is swept or stepped to a potential where Ag oxidation occurs. Then the potential is swept or stepped back to a potential to allow the reduction of Ag. Strong molecule adsorption and/or silver-metal complexation occur during the process. The reduction potential is critical, which is usually related to the Ag deposition rate and then the surface roughness and uniformity. For different supporting electrolytes, a cyclic voltammetry scan is usually needed to determine the oxidation and reduction potential of Ag in the particular electrolyte. Also the pretreatment should avoid causing the reduction or oxidation of investigated species. An *ex-situ* pretreatment is needed if necessary. The dwell time (ca. 0.5 to 10s) is usually based on trials. For those fluorescence molecules, which are strongly adsorbed on the Ag electrode after an ORC pretreatment, the electrode is then washed with deionized water to remove unadsorbed molecules, and the spectra are taken with supporting electrolyte only in SERS cell.

In a 0.1M KCl electrolyte, a double potential step sequence of –0.1V to 0.25V and back to –0.1 V versus SCE, with a dwell time of 1 to 5s at 0.25V gives strong SERS spectra between 0.0V to –0.9V on Ag. One ORC produces a silver surface, which usually yields intense SERS spectra. The amount of charge passed seems to affect the intensity of the SERS scattering. If more than 50mC cm^{-2} is applied, the intensity of the SERS signal has been found to decrease in some systems.

Usually the SERS spectra of organic molecules are identical in any halide, sulfate or nitrate electrolyte. But the intensity varies with the different choices of supporting electrolyte. When the sample molecule is a weakly adsorbed neutral molecule (e.g. piperidine) or cation, an electrolyte is used containing an anion, which can form a precipitate with the Ag ion produced by the oxidation of the electrode, e.g., KCl. In this case the sample molecule is co-adsorbed with the anion and a precipitate film is formed on the Ag electrode surface by oxidation of electrode, which can then be reduced back to a roughened surface with metallic nodules by potential reversal. When the sample molecule is strongly adsorbed species (e.g. lumazine and flavin), it has been shown experimentally that SO_4^{2-} makes a good electrolyte anion because it is only weakly adsorbed, so that the anion of the electrolyte does not displace the sample species from the Ag surface after the ORC. In this case, a concentration gradient of Ag ion is reduced to form the roughened SERS-active surface. The selection of electrolyte and the ORC conditions are usually based on trial.

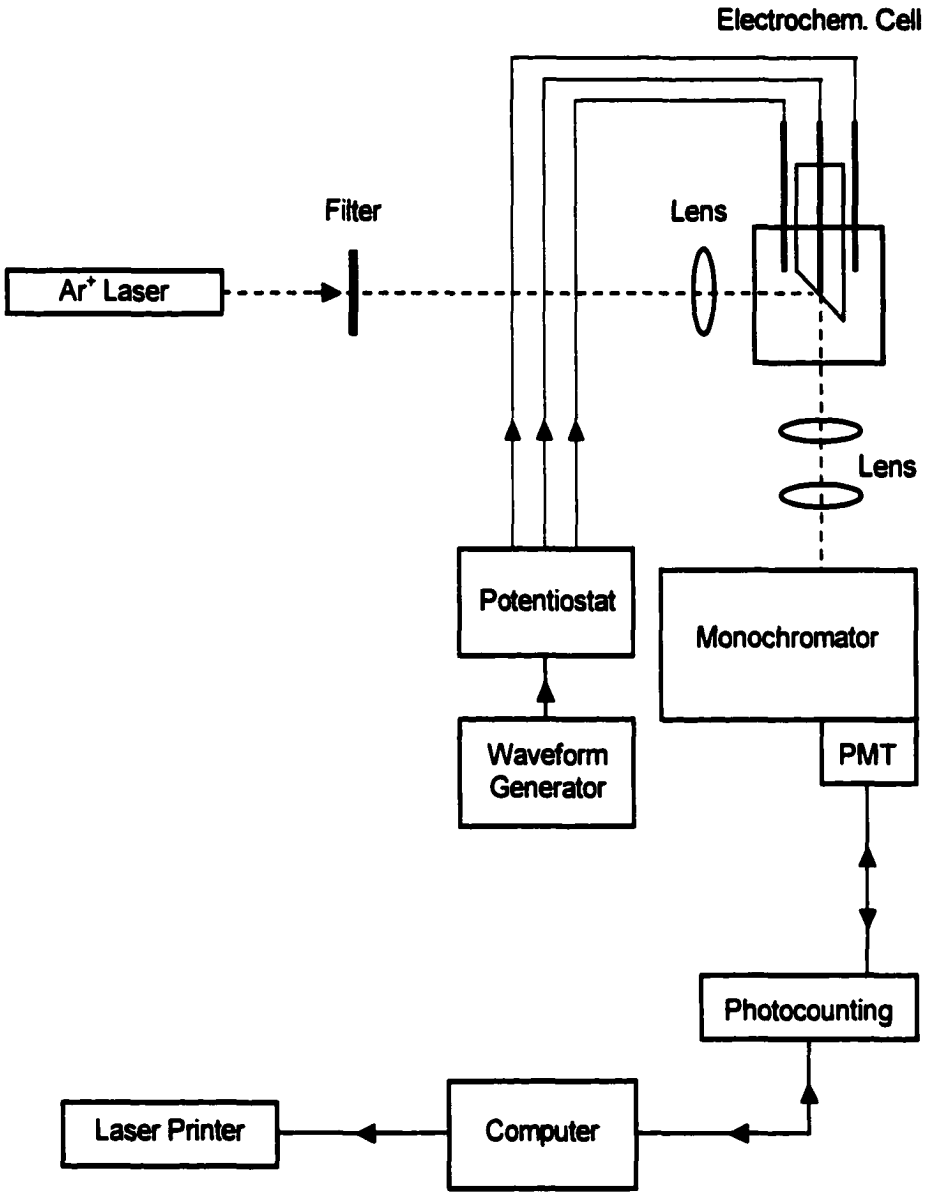

Figure 2.1 Raman Instrumentation

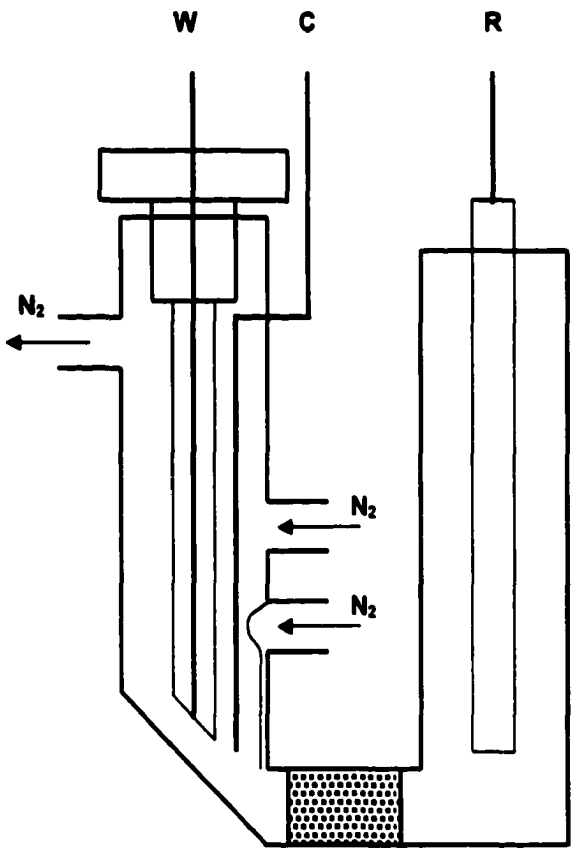

Figure 2.2 Micro SERS Cell with 90° Collection Geometry
W: Working electrode
C: Counter electrode
R: Reference electrode

CHAPTER 3 ELECTROCHEMISTRY STUDY OF LUMAZINE

3.1 Introduction

Lumazine is a naturally occurring molecule that belongs to a group of biologically significant compounds called pteridines. Pteridines (also called pterins) are bicyclic molecules composed of fused pyrimidine and pyrazine ring nitrogen heterocyclic compounds that are found as the core structures of folic acid and flavin molecules. Lumazine forms part of the skeleton of flavins. Also the half of the lumazine structure containing the two ring carbonyls represents the structure of the nucleic base uracil. The structures and numbering of lumazine, uracil and flavin are shown in Figure 3.1.

Investigations of the interaction between metals and pteridines have attracted great attention[1-3], owing to their capability to undergo either one- or two-electron transfer reactions through their potentially metal-chelating α-carbonylpyrazine moiety. The lumazine molecule is similar to the flavin molecule and can serve as electron transfer coenzymes in many organisms. Its core structures function as (a) cofactors for enzymes involved in hydroxylation, (b) methyl transfer, (c) redox mediatiors, (d) pigments for the eyes and wings of certain insects, and (e) cofactors in luminescence proteins. The capability of pterins to act as enzyme cofactors depends significantly on their oxidation/reduction states and on their overall redox chemistry[7-9].

Lumazine is structurally related to flavin molecules, which have been the subject of previous electrochemistry and surface-enhance Raman scattering studies in our laboratory[4-6]. Lumazine and flavin are not only structurally related, but they are also associated in the same enzymatic systems where electron transfer processes occur. An example of such an enzyme system is found in photobacterium luciferase (a glowing bacteria.) This system is used for the process of bioluminescence, where LUM accepts an electron from a flavin molecule. These bioluminescent bacteria are often symbiotically associated with a species of fish, the light serving a biological function for the host. Based on fluorescence studies, it has been suggested that the bound ligand in LUM protein from photobacterium be mostly exposed to the solvent. The details of the mechanism of chemical-to-photochemical conversion are not known. If long-range electron energy transfer takes place, then the correct orientation of the LUM ring with respect to the donor is a critical factor. If such a mechanism requires orbital overlap (e.g., in electron exchange, then both orientation and proximity to the source of chemical energy would have to be under control.

In order to understand the metal-pterin cofactor interactions in living systems, several research efforts[8,9,11,19-21] have been made on the synthesis and structure of metal-lumazine complexes, their UV-vis adsorption spectra. Also FT-IR, RR, electrochemistry and theoretical calculations have been carried out on lumazine.

Lumazine can undergo one-electron reduction in water solution and forms free radicals. One-electron reduction induced by pulse radiolysis and CF_3COOH

radical was carried out in water solution and has been examined by optical spectra and ESR[25]. The estimated reduction potential was determined to be –0.8V vs. SCE. A series of radical forms of lumazine were found within different pH ranges based upon the their different absorption spectra. Four lumazine radical cations and anions may exist in solution. The lumazine redox system and occurrence of the lumazine species as a function of pH and redox state are suggested in Figure 3.2.

However only a limited number of cyclic voltammetry studies of lumazine and other pterins have been reported. Previous electrochemistry and spectroscopy study showed that the flavin molecule is reduced either in a single-step two-electron process or a two-step one-electron process depending on pH range. As a molecule structurally similar to flavin, we expect that there should be a further reduction from the lumazine radical semiquinone to the fully reduced lumazine.

We performed cyclic voltammetry in aqueous buffer solution in the pH range of 5 to 11, and in non-aqueous solution. Also we examined the number of electron transferred via bulk electrolysis coulometry to verify the one electron one proton reduction of lumazine in aqueous solution.

3.2 Experimental Section

Cyclic voltammetry (CV) experiments were performed using a CH Instruments model 660 electrochemical workstation with an electrolyte solution of

0.1M K_2SO_4 in deionized distilled water and with a solute (lumazine) concentration in the millimolar range. The pH of the solution was controlled by adjusting with acid or base or by using a buffer system that consists of sodium hydroxide and potassium dihydrogen phosphate buffer solution (PBS). The test solution was deaerated by nitrogen bubbling for 20 minutes prior each measurement. A glassy carbon or Ag working electrode was used to obtain the voltammograms of lumazine versus a Ag/AgCl (saturated KCl) reference electrode with a Pt wire as counter electrode. It should be noted that there is a less than 0.04V difference between the Ag/AgCl reference electrode used in electrochemistry studies and the saturated calomel electrode (SCE) used in SERS studies.

Bulk electrolysis coulometry was carried out in 1mM lumazine in PBS buffer solutions in different pH ranges. The electrodes used in the coulometry were a Hg pool as working electrode, a Pt wire served as count electrode and a Ag/AgCl (saturated KCl) as reference electrode.

3.3 Results and Discussion

The cyclic voltammogram of lumazine on a glassy carbon electrode in non-aqueous (DMF) solvent with 0.1M tetrabutylammonium hexafluorophosphate as supporting electrolyte is shown in Figure 3.3. There are two well-separated reduction peaks located at –1.22V and –1.97V. On the reverse scan, the first oxidation peak at ca. –1.75V is not well defined. The second oxidation peak

appears at –0.76V. Experiments show that this peak is coupled to the reduction peak at –1.22V. A similar CV curve was also obtained on a Ag electrode.

Figure 3.4 shows a cyclic voltammogram of 3mM lumazine in 0.1M phosphate buffer solution at pH=6.8 at a glassy carbon electrode initiated at 0.0V versus Ag/AgCl and scanned first toward negative potentials, reversed in a positive direction and then finally in the negative potential direction. In aqueous solution, one reduction peak at –0.83V versus the Ag/AgCl reference electrode is observed. On the reverse scan, the oxidation peaks are found at 0.08V and 0.54V. A similar result was also obtained on a Ag electrode.

In the pH range of 5 to 11, a plot of log peak current vs. log scan rate (10mV/s ~ 500mV/s) for the first reduction peak gives a slope of 0.5 on both working electrodes, indicating that the reduction wave is diffusion controlled. A controlled potential electrolysis coulometry experiment was performed with 3mM of lumazine in pH 7 and pH 11 buffer solutions. From the total Q measured, a one-electron transfer process is confirmed.

The oxidized forms of lumazine (LH_2) have pK_as of ~3, 7.96, and ~12.64, as shown in Figure 3.2. A pKa of 7.9 is assigned to (3)NH, located between the carbonyl groups. Its one-electron reduction forms, the reduced semiquinone forms, have pK_as of ~2.9, ~8.6 and ~12.6. Figure 3.5 and Figure 3.6 present the plots of peak potential (E_p) versus pH on glassy carbon and silver electrodes. On either silver or glassy carbon electrodes, the reduction peak potential versus pH between 5~7 gives a slope of ca. 60mV/pH, which shows the process involves a 1 H^+ + 1e transfer, with the electron-transfer process forming the lumazine

semiquinone radical species. The reduction potential of LH_2 on the silver electrode is about the same as that on glassy carbon electrode at the same pH. For example, at pH=6.8, the peak potentials (E_p) are –0.83V and –0.81V for glassy carbon electrode and silver electrode, respectively. However, when the solution pH gets higher than 8 to 11 and LH^- is the dominant species in bulk solution, the potential difference on the silver and glassy carbon electrodes becomes significant. A broader reduction peak appears on the glassy carbon electrode compared to a sharper reduction peak, which appears on the silver electrode as shown in Figure 3.7 and Figure 3.8. In this pH range, ΔE_p/pH is ca. 118mV/pH on glassy carbon electrode and only ca. 31mV/pH on silver electrode. The changes in slope of ΔE_p/pH occur at pH values that corresponding to the acid dissociation constants of the reduced and oxidized forms of lumazine, i.e. 7.96 and ~8.6. Similar slope changes were found with other pteridine compounds[15].

At pH > 8 it appears that the negative charged lumazine LH^- molecules have a strong affinity to the Ag electrode surface. The adsorbed LH^- may undergo one electron reduction without the participation of protons. This may be the reason that its ΔE_p/pH slope is much smaller than on the glassy carbon electrode. On the glassy carbon electrode, ΔE_p/pH is ca. 118mV/pH, and the following electrode reaction is suggested:

$$2H^+ + LH^- + e \rightarrow LH_3\cdot$$

On the reversed scan, up to three oxidation peaks were found in the pH range investigated. The number of oxidation peaks, their peak potentials and currents greatly depend on the scan rate and pH. Three typical cyclic voltammetry curves were obtained.

Figure 3.9 to Figure 3.11 show the voltammgrams of lumazine at three different pH values on the glassy carbon electrode as a function of scan rates. At pH = 5.49 (Figure 3.9), two oxidation peaks (II and III) were found at 0.70V and 0.14V at low scan rate (between 20mV/s and 200 mV/s). An additional peak (I) at –0.50V was observed at the highest scan rate (500mV/s). The magnitude of peak current for each oxidation peak depends on the scan rate. It is suggested that the electrode process involve a following reaction step. The reduction product, $LH_3\bullet$, which gives oxidation peak I at the highest scan rate, is an unstable species at lower scan rates. Comparing the peak currents for oxidation peak II and peak III, we can find that the peak current increases with increasing scan rate for peak II, and the peak current is independent of scan rate for peak III. The peak current ratio of peak III to peak II increases with decrease of the scan rate. It is suggested that the substance that gives rise to oxidation peak II is further consumed by another homogeneous reaction, in which the product correspond to oxidation peak III.

Within the pH 7.4 to 8.6 range, as illustrated in Figure 3.10 which is at pH = 8.09, one main oxidation peak is found at all scan rates at –0.6 V. Also two smaller peaks are observed at 0.0V and 0.5V. In this range, there is equilibrium between the reduction products $LH_3\bullet$ and $LH_2\bullet^-$, since the pK_a is around 8.6 for

the semiquinone. The LH_3• could undergo further reaction, which could give the two more positive oxidation peaks.

At pH = 8.93 (Figure 3.11), one reduction and one oxidation peak were found for both high and low scan rates. At this pH, Lumazine is in form of LH^-. Accordingly, the reduction product would be LH_2^-•, which has no further chemical reaction. Further experiments are needed to identify the species from the following reaction of LH_3• species.

As we discussed above, similar to other pterins[26], lumazine shows irreversible electrochemistry on the electrodes due to chemical irreversibility of the following reactions. Recently, many attempts have been made to accomplish reversible one-electron reduction of pterins via the synthesis of metal-pterin complex. A successful example is the Ir complex of dimethyl lumazine which exhibits a largely reversible one-electron reduction, in contrast to the irreversible process of dimethyllumazine.

In our case, the electrochemistry of lumazine is quite complicated on silver electrodes when the lumazine diffuse to the electrode surface from the bulk solution. However, for adsorbed lumazine on the silver electrode through an oxidation and reduction cycle the CV curve without bulk lumazine is much more reversible. This roughened electrode system was prepared by roughening the silver electrode in 3mM lumazine solution and then transferred into a cell with buffer solution only. During the reduction-oxidation cycle, lumazine can be adsorbed or a silver-lumazine complex formed on the electrode surface. Figure 3.12 shows CV curves of adsorbed species in a supporting electrolyte at pH =

6.8 and pH=10.0 which is free of lumazine in the bulk solution. A reduction peak is found at –0.93V with a companion oxidation peak at -0.83V in both pH conditions. The fact that the peak potentials are independent of pH suggests that there is no proton involved the electrode reaction. The reduction and oxidation waves decay to baseline, which indicates that they are adsorption waves.

3.4 Conclusions

In general, the following points can be summarized based upon the electrochemistry presented herein:

Lumazine molecules undergo a one-electron and one -proton reduction in neutral aqueous solution. Similar to other pterin derivatives, it displays irreversible electrochemical behavior due to following chemical reactions. The reduction products vary with the solution pH value. The neutral lumazine radical is unstable in aqueous solution and can undergo further chemical reactions. However, when only an adsorbed species is involved the electrode process shows quasi-reversible one electron transfer without coupled proton transfer.

References

(1) Abelleira, A.; Galang, R. D.; Clarke, M. J., Inorg. Chem. **1990**, 29, 633-639

(2) Ladenstein, R.; Ritsert, K.; Huber, R.; Richter, G.; Bacher, A., Eur. J. Biochem. **1994**, 223, 1007-1017.

(3) O'Kane, D. J.; Lee, J., Biochemistry, **1985**, 24, 1467-1475.

(4) Xu, Jia; Birke, R. L.; Lombardi, J. R., J. Am. Chem. Soc. **1987**, 109, 5645.

(5) Wei, Zhang; Vivoni, A.; Lombardi, R. J.; Birke, R. L., J. Phys. Chem. **1995**, 99, 12846-12857.

(6) Shi, Chongti, Zhang, Wei, Lombardi, J. R.; Birke, R. L., J. Phys. Chem. **1992**, 96, 10093-10096.

(7) Burgmayer, S. J.; Nieter, Inorg. Chem. **1988**, 27, 4059-4065.

(8) Goodgame, M.; Schmidt, Inorg. Chim. Acta **1979**, 36, 151-154.

(9) Lehnen, J.; White, B. M.; Kendric, M. J., Inorg. Chim. Acta **1990**, 167, 257-259.

(10) Heilman, O.; Hornung, F. M.; Kaim, W.; Fiedler, J., J. Chem. Soc., Faraday Trans. **1996**, 92, 4233-4238.

(11) Lee, J.; Wang, Yanyun; Gibson, B., Biochemistry **1991**, 30, 6825-6835.

(12) O'Kane, D. J.; Lee, J., Biochemistry **1984**, 24, 1484-1488.

(13) Visser, A. J. W. G.; Lee, J., Biochemistry **1980**, 19, 4366-4372.

(14) Lee, J.; O'Kane, D. J.; Visser, A. J. W. G., Biochemistry **1985**, 24, 1476-1483.

(15) Glenn Dryhurst, Electrochemistry of Biological Molecules **1977**

(16) Foresman, J. B.; Frisch, A. Exploring Chemistry with Electronic Structure Methods, 2nd ed., Gaussian: Pittsburgh, PA, 1995-96.

(17) Nishina, Y.; Kitagawa, T.; Shiga, K.; Horiike, K.; Matsumura, Y.; Watari, H.; Yamano, T. J. Biochem. (Tokyo) **1978**, 84, 925-932.

(18) Kitagawa, T.; Nishina, Y.; Kyogoku, Y.; Yamano, T.; Ohishi, N.; Takai-suzuki, A.; Yagi, K. Biochemistry **1979**, 18 (9), 1804-1808.

(19) Vervoort, J.; O'Kane, D. J.; Carreira, L. A.; Lee, J. Identification of a Lumazine protein from Photobacterium Leignathi by Coherent Anti-strokes Raman Spectroscopy. Photochem. Photobiol. **1993**, 37 (no. 1), 117-119.

(20) Irwin, Richard M.; Visser, A. J. W. G.; Lee, John; Carreira, Lionel A. Protein-Ligand Interactions in Lumazine Protein and in Desulfovibrio Flavodoxins from Resonance Coherent Anti-Strokes Raman Spectroscopy. Biochemistry **1980**, 19, 4639-4446.

(21) Brutovsky, B.; Ulicny, J.; Miskovsky, P.; Lisy, V.; Chinsky, L. Resonance Raman Spectra of Selected Pterin Molecules. Genetic Algorithms Approach to Force Field Scaling. J. Raman Spectrosc. **1998**, 29, 833-839

(22) Norrestam, R.; Stensland, B.; Soderberg, E. The Crystal and Molecular Structure of Lumazine Hydrate. Acta Crystallog., B **1972**, 28, 659.

(23) Cotton, F. A.; Wilkinson, G. Advanced Inorganic Chemistry, 4th ed.; Wiley & Sons: New York, 1980, p 969.

(24) Benecky, M.; Yu, T.-J.; Watters, K. L.; McFarland: Metal-Flavin Complexation A resonance Raman Investigation. Biochim. Biphys. Acta **1980**, 627, 197.

(25) P. N. Moorthy and E. Hayon; J. Phys. Chem., **1975**, 79 (11).

(26) Inorganica Chimica Acta, **1979**, Vol. 36, 151-154.

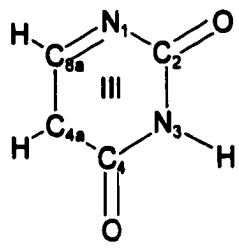

uracil

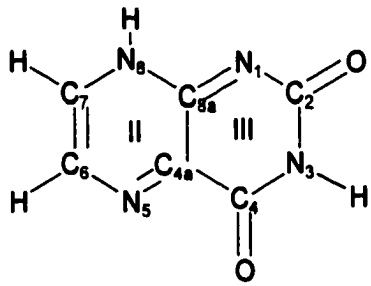

lumazine

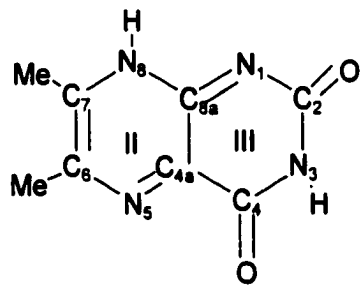

dimethyl-lumazine

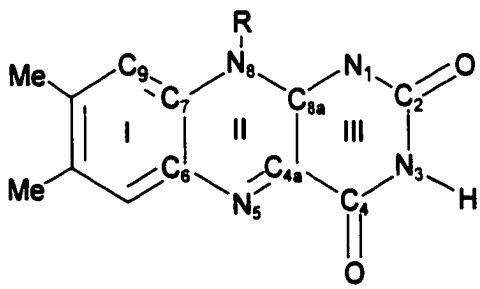

R=H: riboflavin
R=CH3: Lumiflavin
R=CH2-CH(OH)-CH(OH)-CH(OH)-CH2(H2PO4): flavin mononuleotide (FMN)

Figure 3.1 Lumazine and related molecule structures

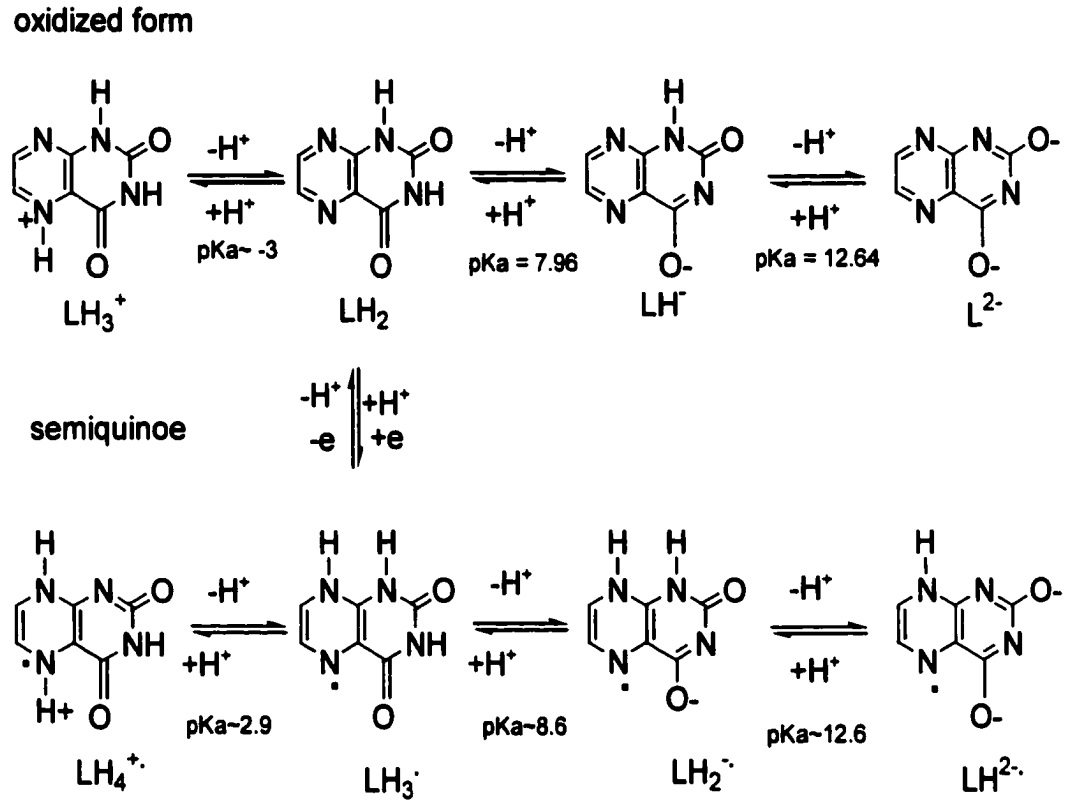

Figure 3.2 Lumazine redox system and the occurrence of the lumazine species as a function of pH and redox states in aqueous solution *(adapted from P. N. Moorthy and E. Hayon.[25])*

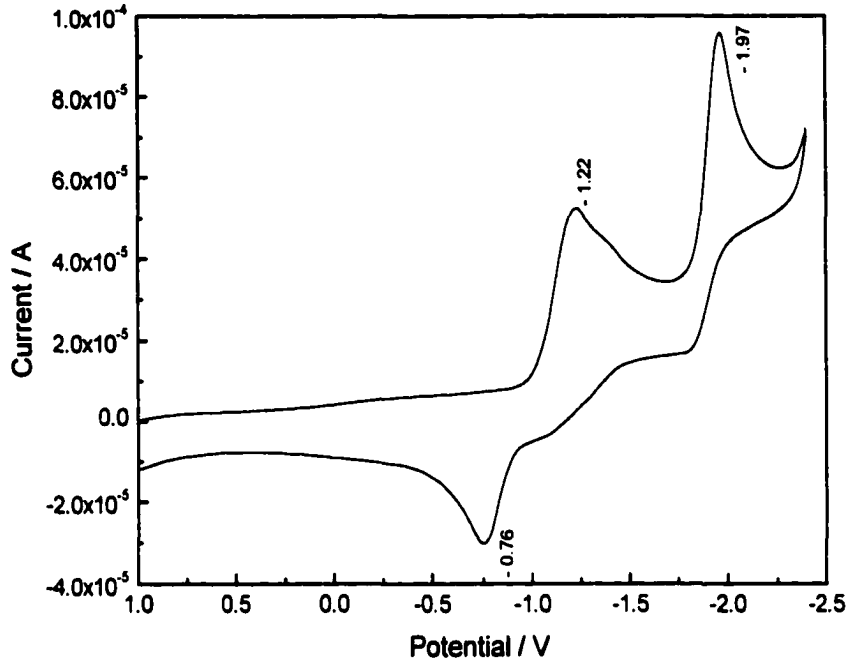

Figure 3. 3 CV curve of lumazine on glassy carbon electrode in DMF solution, scan rate: 100mV/s

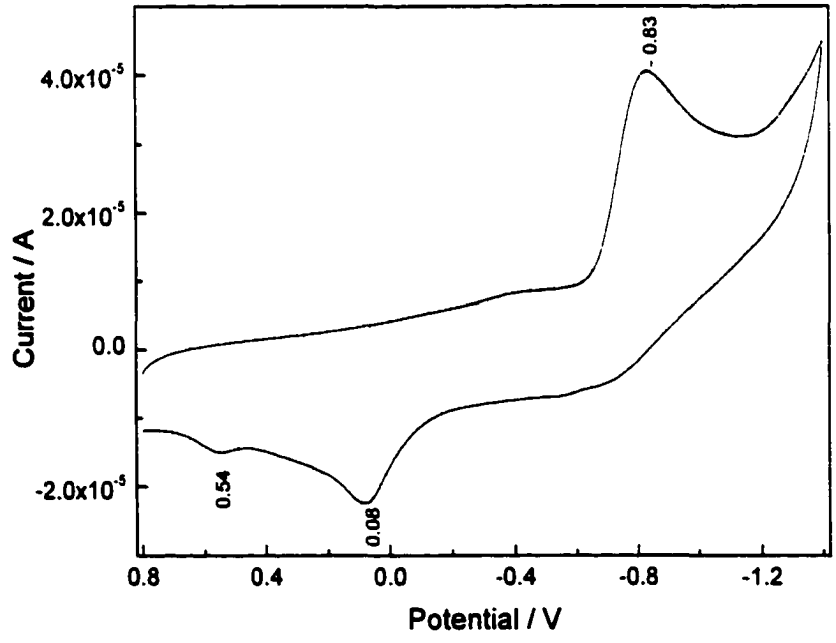

Figure 3.4 CV curve of 3mM lumazine in 0.1M PBS buffer solution, pH=6.8, glassy carbon electrode, scan rate: 100mV/s

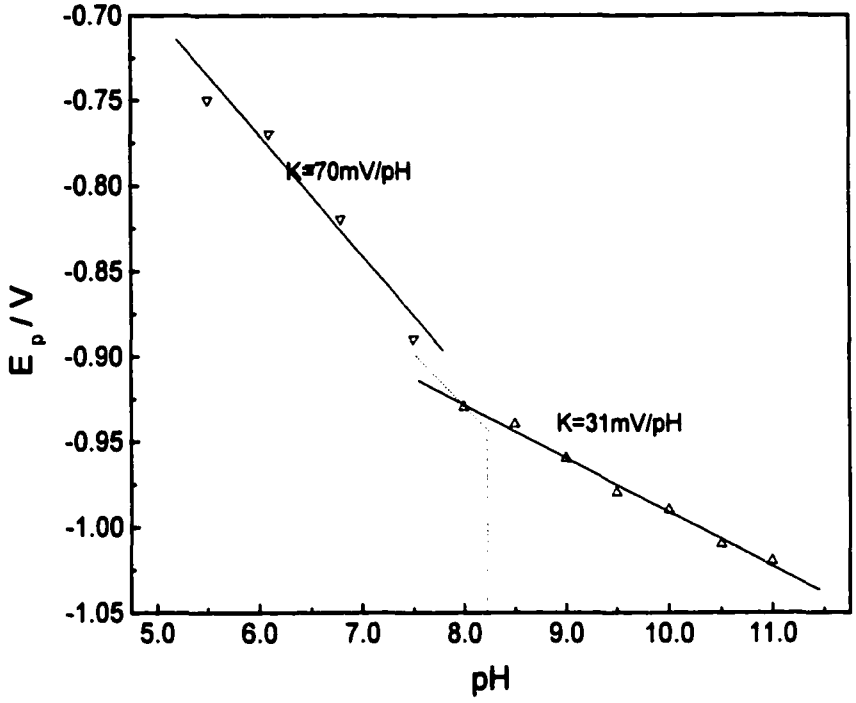

Figure 3.5 Variation of peak potential (E_p) with pH for lumazine reduction wave on Ag electrode

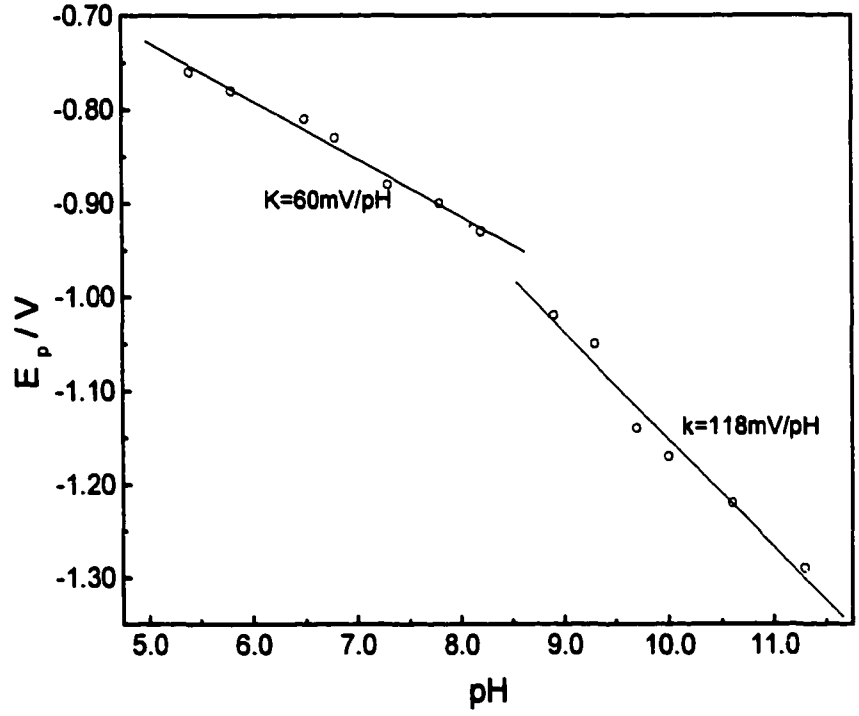

Figure 3.6 Variation of peak potential (E_p) with pH for lumazine reduction wave on glassy carbon electrode

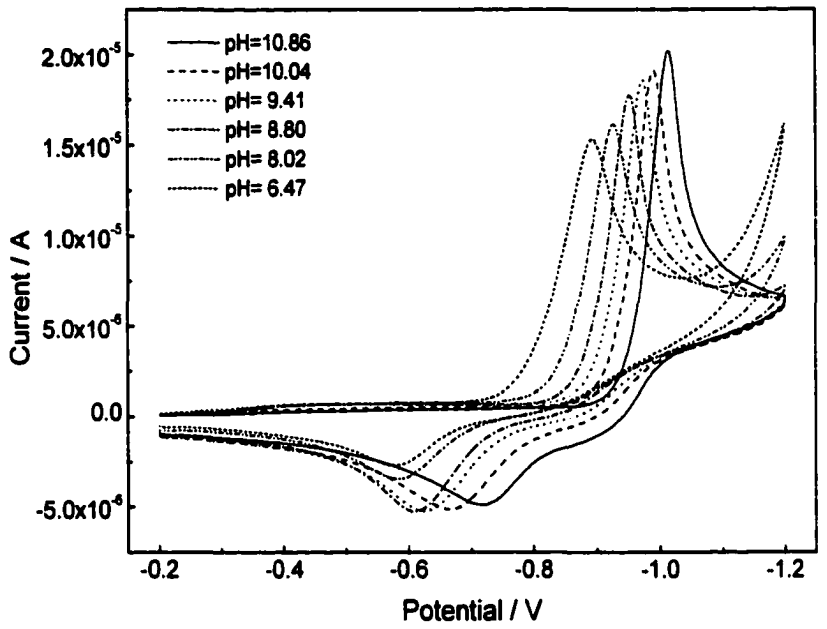

Figure 3.7 CV curves of lumazine on Ag electrode at different pH, scan rate: 100mV/s

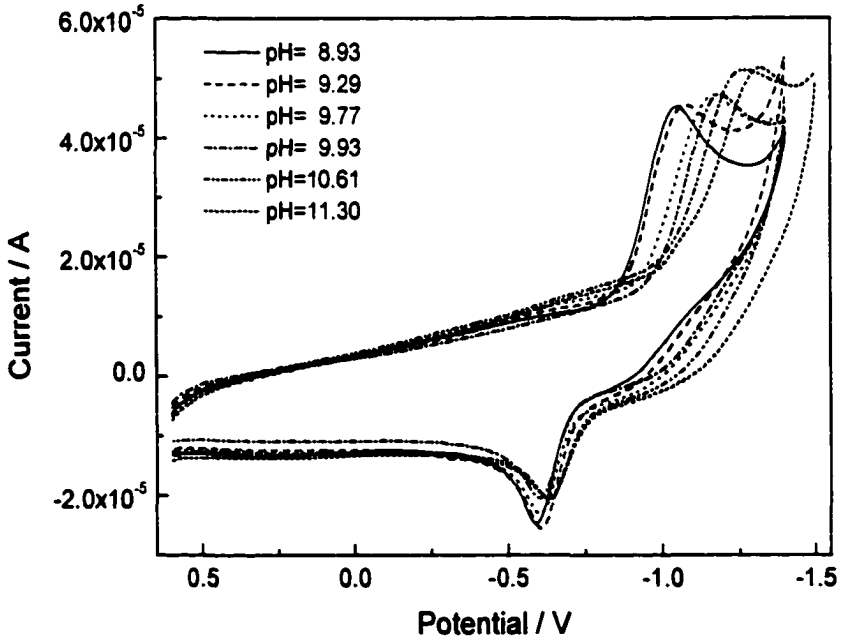

Figure 3.8 CV curves of lumazine on glassy carbon electrode at different pH, scan rate: 100mV/s

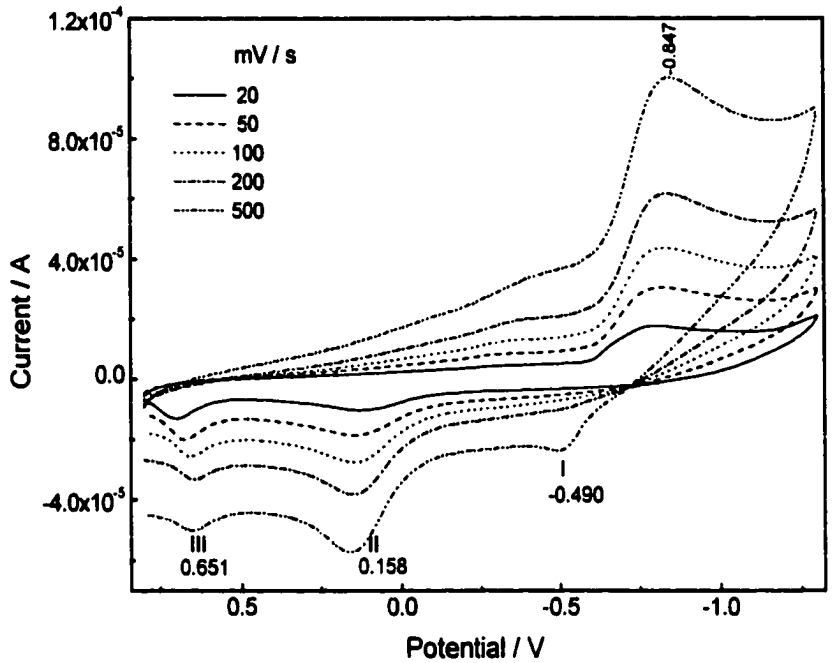

Figure 3.9 CV curves of lumazine on glassy carbon electrode, pH = 5.49. scan rate: 20. 50. 100. 200. 500mV/s

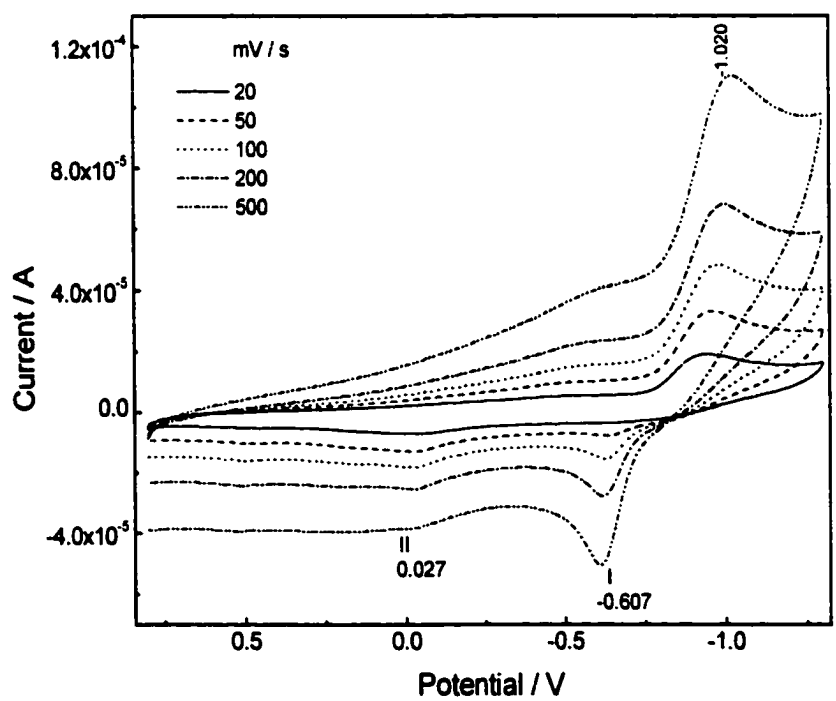

Figure 3.10 CV curves of lumazine on glassy carbon electrode, pH = 8.09, scan rate: 20, 50, 100, 200, 500mV/s

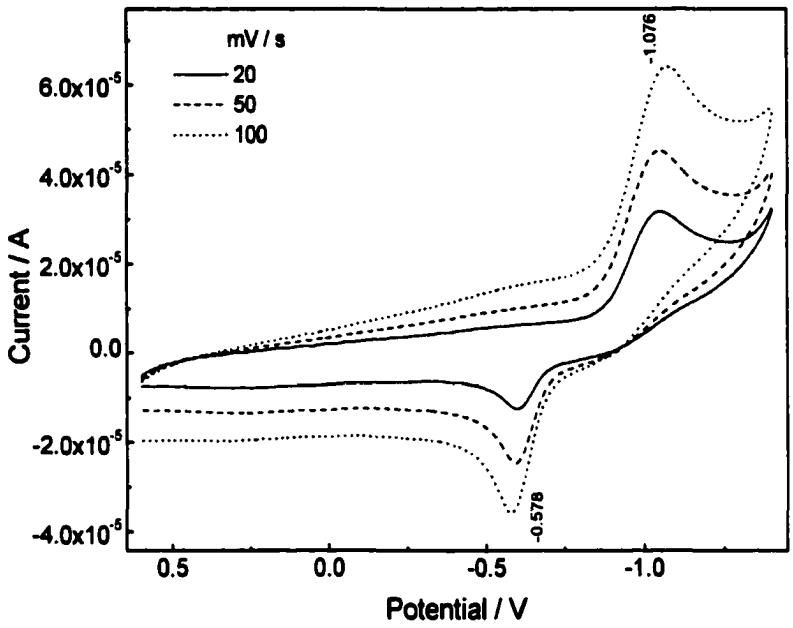

Figure 3.11 CV curves of lumazine on glassy carbon electrode, pH = 8.93, scan rate: 20, 50, 100mV/s

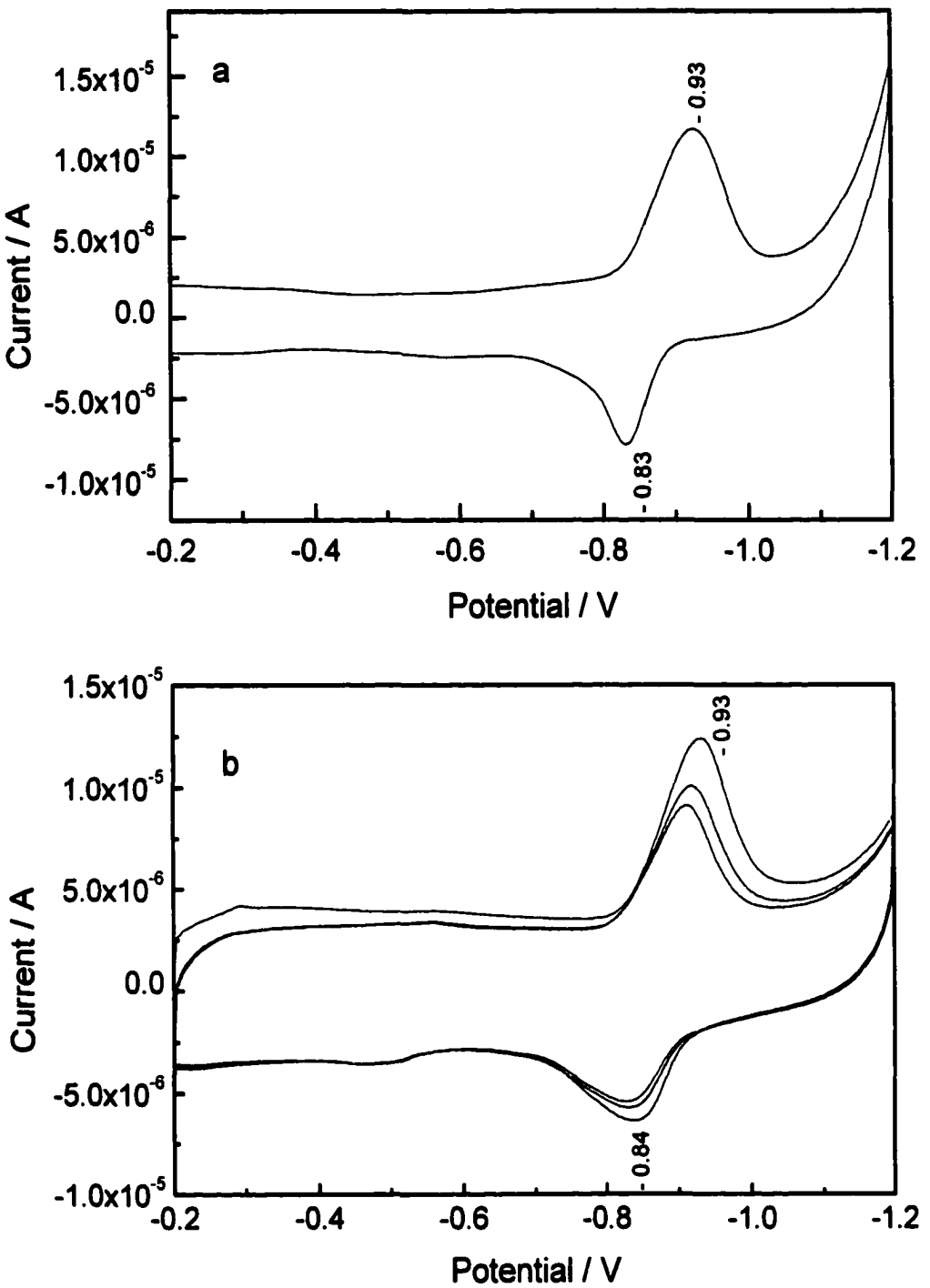

Figure 3.12 CV curves of adsorbed lumazine on Ag electrode after an ORC, in (a) pH=10.0 and (b) pH=6.8 buffer solutions, scan rate: 100mV/s

CHAPTER 4 A SURFACE-ENHANCED RAMAN AND AB INITIO STUDY OF SPECTRA OF LUMAZINE MOLECULES

4.1 Introduction

The lumazine (LUM) molecule is structurally related to flavin molecules, which have been the subject of previous surface-enhanced Raman scattering (SERS) studies in our laboratory. [4-6] It has been shown that SERS is an ideal technique to investigate aromatic and nitrogen-containing molecules because of the strong enhancement of this type of molecules on the Ag electrode. Our interest in lumazine arises from its being a simpler molecule than the isoalloxazines, which makes the investigation of its vibrational structure with ab initio calculations much easier. Also it makes a useful model compound for the study of the binding of molecules with multiple binding sites to a metal surface. We have used ab initio calculations in comparing spectra of different molecular forms of LUM and in interpreting SERS spectra in terms of the molecular structure of the molecules at the metal surface. Metal pteridine complexes[7, 8] are related to the LUM molecule on the electrode surface in SERS, and the FTIR spectra and electrochemistry of these compounds have been studied[7-10].

The normal Raman (NR) of LUM is hindered by severe interference from luminescence. In SERS, the fluorescence is quenched when molecules are adsorbed at a given electrode potential on a silver electrode surface[15] while the

Raman intensity is enhanced, making it ideal for studies on various biological species that usually contain a chromophore group. Another useful technique for discriminating against fluorescence has been coherent anti-Stokes Raman spectroscopy (CARS). There has been a CARS study published on 6,7-dimethyl-8-ribityllumazine by itself and in a flavoprotein enviroment.[19, 20] Also, recently there has been a UV resonance Raman scattering (RRS) measurement of the simple LUM Raman spectra.[21] This spectrum was excited at 257 nm, which also lowers the fluorescence background, and the result is very similar to our SERS spectrum.

Our earlier work with SERS spectra of flavins showed that the ribityl group did not affect the bands of the ring portion of the flavin, and we expected the same behavior for LUM. Thus, we were puzzled as to why the SERS and RRS spectra of simple LUM were so different from the CARS spectrum of the dimethyl-ribytllumazine form. Because of this disagreement, we have further investigated the Raman and infrared (IR) vibrational spectra of LUM and used normal mode ab initio calculations to elucidate the difference in the SERS spectra of LUM, [2,4(3*H*,8*H*)-pterdinedione] and the CARS spectra of the dimethyl-ribytllumazine form.[19-20] We find a different vibrational structure because only a few of the dimethyllumazine (DML) bands appear in the CARS spectrum. We also compare our ab initio molecular orbital calculations of the Raman spectrum of LUM with the semi-empirical calculations of LUM by Brutovsky et al.[21] The calculations indicate that almost all of the Raman bands of DML that should overlap with Raman bands of LUM do not appear in the CARS spectra.

Finally, the Raman frequency calculations aid in the analysis of the LUM geometry at the silver (Ag) surface. This analysis indicates that there is a lateral (dimeric) interaction of LUM molecules on the metal surface.

4.2 Experimental Section

Lumazine (2,4-pteridinedione [487-21-8], LUM) and riboflavin were purchased from Sigma Chemical Company and used as received. Reagent grade Na_2SO_4, K_2SO_4 and KCl served as supporting electrolytes. Electrolyte solutions for SERS studies were prepared with deionized distilled water and sodium sulfate (Na_2SO_4) at 0.1 M concentration and deaerated by nitrogen bubbling for 20min. The pH was regulated by the addition of H_2SO_4 and/or NaOH. The solutions of LUM or riboflavin were made up in the millimolar range (mM) in the electrolyte solution.

The electrochemical cell for SERS studies was composed of a Ag (99.999%) working electrode, a saturated calomel electrode (SCE) reference, and a platinum counter electrode. For LUM, the Ag working electrode was pretreated in presence of 2 mM LUM in 0.1 M Na_2SO_4 or K_2SO_4 solution, with an oxidation-reduction cycle of 2-5 s. The ORC pretreatment was accomplished in the presence of LUM molecules by applying a double potential step from –0.30V to +0.55V for 5s and then stepping back to –0.30V. For riboflavin, the working electrode was also pretreated in a similar manner, with a redox cycle of 1s. The redox cycle applied for riboflavin was from -0.5 to +0.5 V. The pretreated Ag working electrode was then rinsed with deionized water to wash out unadsorbed

molecules, and transferred into the Raman cell, which contained only the supporting electrolyte solution to eliminate the solution fluorescence.

The SERS experimental setup was described in chapter 2. The 488 nm line of a Ar^+ laser and 647.1nm line of a Kr^+ laser was used for SERS experiments with about 40 mW power on the roughened Ag electrode surface. Both excitation lines are off resonance lines. No significant difference in spectral features was observed by using two different excitation lines. The 730-760 nm line of a Ti-sapphire laser (Spectra-Physics model 3900S, driven with model 2020) was used for NRS experiments on a pressed lumazine solid powder. The spectra of the molecules were obtained at a 90^0 collection angle with a Spex model 1401 double monochromator (resolution ca. $4cm^{-1}$) and a PMT detector, or a Spex model 500 single monorchromator with a CCD detector. A Nicolet model FTIR spectrometer was used with KBr pellets for Fourier transform infrared (FTIR) measurements.

Normal mode calculations were carried out with standard force constants determined by a Gaussian 94[22] calculation of the ground-state wave function. The Gaussian 94 program was used to compute harmonic vibrational frequencies of the LUM molecules in C_s symmetry that resulted from interatomic motion. Geometric optimizations were carried out at the same level of the theory as used for the frequency calculations and all converged to the default values of Gaussian 94. However, these are local minima because of the symmetry constraint. The frequencies are dependent on the second derivative of the energy with respect to atomic structure,[16] and, for the most part, the calculations

were based on a single determinant Hartree-Fock ab initio method with 3-21G(d) and 6-31G(d) basis sets. For comparison, a calculation was made with the B3LYP exchange functional of density functional theory (DFT). Scalings of the vibrational modes were made with the scaling factors in reference 16 rounded to two significant figures because of the approximate nature of the theoretical results. The normal modes were then assigned by visualization with Spartan[23] in terms of the bond stretches and/or bends that make the major contributions to the potential energy distribution (PED).

4.3 Results and Discussion

4.3.1 A comparison of Raman spectra of lumazine

Figure 4.1 showed the Raman spectra of solid lumazine at 756nm and 736nm excitation along with the SERS spectrum at –0.6V vs. SCE. The solid Raman spectrum with 756nm excitation showed unenhanced broad Raman bands; the spectrum with 736nm excitation has a few sharp bands, which exhibit some resonance features. A comparison of the three spectra shows agreement in some bands, while the SERS has most strong and rich spectra. Only a few bands, 670, 686, 1280, and 1720cm^{-1}, are enhanced in RR. Those bands are expected to be total symmetric vibrations according to RR enhancement selection rule.

In Figure 4.2 we present a comparison of the SERS spectrum of LUM at -0.4 V with that of the FTIR spectrum, with an insert of the CARS spectrum of 6,7-

dimethyl-8-ribityllumazine.[19-20] The measured wavenumbers are listed in the columns of Table 4.1. It can be seen (Figure 4.2 and Table 4.1) that except for the expected differences in relative intensities, there is good agreement between the SERS and FTIR spectra. In addition, the SERS, NRS, and ultraviolet resonance Raman spectroscopy (UV RRS) spectra of LUM show very good agreement for most of the bands in both wavenumber and intensity (Table 4.1). Figure 4.3 is a comparison of the SERS spectra of LUM and riboflavin, both at -0.4 V versus SCE. Also listed in Table 1 are the SERS and IR results obtained with riboflavin.[4,17,18]

For comparison we included the CARS spectrum of DML as an insert in Figure 4.2 and list the measured lines in Table 1, column 4. We would have expected that the results of the CARS experiment and the SERS and RRS results would agree for most bands in frequency, because they are all Raman techniques. Note, however, the disparities. Only four bands are observed in the CARS spectrum, and only two (at 1238 and 1584 cm^{-1}) are close to a SERS or RRS line. Undoubtedly, the SERS results represent an accurate spectrum of LUM because of the almost complete agreement with the FTIR, NRS, and RRS results. However, as we shall see, the vibrational spectra of DML and LUM are consistent with the calculations to be presented.

4.3.2 The *ab inito* calculation and SERS band assignments

Table 4. 2 shows a comparison of the normal mode wavenumbers of LUM calculated by various quantum mechanical computational methods. The first two

columns of Table 4.2 show the calculations of Brutovsky et al.,[21] where the semiempirical AM1 method was used to find harmonic force constants for LUM in the 2,4(1*H*,3*H*)-pterdinedione form. These force constants were then optimized by using an optimization algorithm on the experimental data to find scale factors for the force constants. The two columns represent different scale factors; however, they do not appear to differ significantly from each other.

We used a higher level theoretical approach with the Gaussian 94 program and employed the Hartree-Fock self-consistent field (SCF) and DFT nonlocal (B3LYP) methods at the 3-21G(d) and 6-31G(d) basis set levels. One useful feature of the Hartree-Fock computational method is that it gives intensities as well as normal-mode frequencies and assignments. Because some of the protons on the ring nitrogens are labile, columns 3 and 4 in Table 2 show the results at the RHF/3-21G(d) level for the (1*H*, 3*H*) and (3*H*, 8*H*) tautomers of LUM. Brutovsky et al.[21] made their calculation for the (1*H*, 3*H*) tautomer; however, the (3*H*, 8*H*) tautomer is closer in structure to biologically significant molecules, which have a substitution at the 8N position. Calculations at the RHF/ 3-21G and B3LYP/6-31G levels show that the (1*H*, 3*H*) tautomer is slightly more stable than the (3*H*, 8*H*) tautomer because the absolute energies are -593.7592 and -600.5397 Hartrees for the former compound and -593.7219 and -600.5110 Hartrees for the latter compound, at the RHF and B3LYP levels, respectively. However, all of the other calculations were done for the (3*H*, 8*H*) tautomer because the results for the (3*H*, 8*H*) form fits the experimental data better both in terms of wavenumber and intensity match and because of its biological

relevance. For most bands there is little difference between the RHF/3-21G(d) and RHF/6-31G(d) calculations. The strongest band in the SERS spectrum at 1286 cm^{-1} shows up as the most intense band at 1275 and 1310 cm^{-1} in the calculations at the RHF/3-21G and RHF/6-31G(d) levels, respectively. All calculations of frequencies with the Hartree-Fock method have been scaled by 0.90 to take into account the neglect of electron correlation. Such a scaling is not made (usually 0.994) for the DFT B3LYP/6-31G(d) calculation and the agreement is quite good between the scaled Hartree-Fock and the unscaled DFT results, as seen in Table 4.2. Considering that the Ag surface affects the SERS bands and that the aqueous solvent affects both the SERS and RRS bands, the agreement between the calculated and experimental results is quite good. This agreement gives one confidence in the normal mode assignments given in Table 3 which come from the ab initio computations and differ somewhat from the AM1 semiempirical assignments.

Table 4.3 shows a comparison of the calculated Raman vibrational frequencies and assignments for LUM and DML [6,7-dimethyl-2,4(3*H*,8*H*)-pterdinedione] along with the SERS (-0.6 V) and CARS bands of the molecules. The calculations show that the Raman spectra of these molecules should have a large number of bands in common except for those modes that have a strong component of the methyl motion. Thus, DML has such modes, with methyl contributions at 994, 1038, 1264, 1359, 1456,1465, 1469, and 1481 cm^{-1}, and five methyl C-H vibrations, from 2899 to 2978 cm^{-1}, which have no counterpart in

LUM. On the other hand, there are 23 calculated DML modes that are quite close in frequency to calculated LUM modes.

The simplicity of the CARS spectrum of DML in comparison with that of flavin was interpreted as the result of the loss of the benzene ring I (Figure 3.1) from the flavin isoalloxazine ring.[20] However, our calculations and measurements show that the Raman spectra of both LUM and DML should have a band structure just as rich as those of flavins (Figure 4-3). Only four of the normal modes of DML show up in the CARS spectrum, and two of these modes, at 1264 and 1359 cm^{-1}, do not have a counterpart in the SERS or RRS spectra of LUM. The band at 1264 cm^{-1} is assigned to a mode that has strong stretching vibrations of C_6N_5 and N_8C_{8a} in ring II and N_1C_2 and N_3C_4 in ring III, as well as the C_7C_{10} stretch involving a methyl group. The band at 1359 cm^{-1} is assigned to a mode that has strong stretching vibrations of C_7N_8, N_8C_{8a}, and C_6C_7 in ring II, a $C_{8a}C_{4a}$ stretch, as well as C_7C_{10} and C_6C_9 stretches involving the methyl groups. Irvin et al.[20] attribute this mode to ring III motions of C_4-C_{4a}-C_{8a}, which really does not describe the mode well. The highest frequency band in the CARS spectrum is at 1584 cm^{-1}, and the mode assigned for this vibration based on our ab initio calculations involves ring motion in the linkage C_7-C_6-N_5-C_{4a}-C_{8a}-N_1, with some C_2=O contribution. The experimental evidence of this mode involving the N_5-C_{4a}-C_{8a}-N_1 linkage with some C_2=O vibration mixed in, given in the paper of Irwin et al.,[20] agrees well with our calculation.

The strongest band in the SERS spectrum at 1286 cm^{-1} is matched with a strong band in the NRS spectrum of the solid at 1280 cm^{-1} as well as a band at

1304 cm^{-1} in the RRS spectrum, all of which agree well with the calculated mode at 1310 cm^{-1} that shows strong ring III vibrations. The RRS band at 1740 cm^{-1} does not appear in the SERS or NRS spectra; however, a band at 1714 cm^{-1} is found. We assign the RRS band at 1740 cm^{-1} to a coupled out-of-phase C_2=O and C_4=O carbonyl vibration that appears at higher frequency in the calculations (1810, 1823 cm^{-1}), Table 4.3, but that are most likely lowered in solution by solvation effects. The SERS band at 1714 cm^{-1}, which is matched with a band at 1718 cm^{-1} in the NRS of the solid, is assigned to coupled carbonyl vibrations. In the solid state, a sheet structure has been determined by single-crystal X-ray diffraction[24] that shows hydrogen-bounded LUM dimers, where the LUM molecules in the dimer are not symmetry related and where the dimers on the molecular plane are held together by water molecules. We postulate at the Ag surface as well as in the solid that the carbonyl stretching vibration is lowered from the RRS solution frequency by hydrogen bonding between the N_3-H group of one LUM molecule and the C_2=O group of another.

4.3.3 The proposed orientation and adsorption sites of LUM on a Ag electrode

It is worthwhile noting some other interesting features of the SERS spectra of LUM in Figure 4.5. Note the doublet bands that appear at 688 and 698 cm^{-1} in Figure 4.5. The 688 cm^{-1} band is an A' mode involving an in-plane ring vibration (Table 4.3) and appears in both the SERS and RRS spectra of LUM. On the other hand, the higher frequency band at 698 cm^{-1} band is an A' ' nontotally

symmetric out-of-plane ring torsion (Table 4.3) and is not resonance Raman active only appearing in the SERS and NRS spectra. Other A' ' nontotally symmetric out-of-plane ring torsion modes also appear in the SERS (-0.6 V) spectrum at 525 and 812 cm^{-1}. According to the surface selection rules of SERS, in-plane vibrations are enhanced if the molecule is oriented with its molecular plane normal to the surface and out-of-plane modes are enhanced if the molecule is oriented with its molecular plane parallel to the surface. Because the bands in the doublet are of both types, the majority of molecules should be adsorbed with their molecular plane at an angle to the surface. Figure 4.7 shows that the 688 cm^{-1} mode with the in-plane vibrations grows with respect to the out-of-plane mode of the doublet as the potential is made more negative, indicating that the molecules are becoming oriented more toward the normal with this potential change. This SERS electromagnetic effect enhances a number of in-plane modes so that they are observed in the SERS spectrum but not in the RRS spectrum. For example, bands at 942, 1232, and 1398 cm^{-1} appear in the SERS spectrum but not in the RRS spectrum (Table 4.1). These bands involve the C_2-N_1 stretch with an $_{zz}$ polarizability component that would be enhanced by the proximity of the surface and an electromagnetic field of the exciting light normal to the surface.

In addition to the very strong band at ca. 1286 cm^{-1}, other bands in the spectrum with medium to strong intensity appear at 942, 1090, 1184,1234, 1320, 1526, and 1714 cm^{-1} (Figure 4.6). These bands all correspond closely to the calculated modes with the strongest intensities in the spectrum (Table 4.3)

except for the band at 1526 cm^{-1}, which is 36cm^{-1} lower than the calculated mode at 1562 cm^{-1}, the second most intense band in the calculated spectrum. Furthermore, there is another band at 1568 cm^{-1}, which is weak in the SERS spectrum and decreases with voltage (Figure 4.4), and is near the calculated mode at 1562 cm^{-1}. However, we have assigned the band at 1526 cm^{-1} to the calculated mode at 1562 cm^{-1} and the band at 1568 cm^{-1} to the calculated mode at 1626 cm^{-1}. As will be discussed later, these bands are assumed to be lowered from the calculated frequencies by the surface-molecule binding interaction.

One important concern in SERS studies is to account for the possible influence of the proximity of the molecule to a metal surface. Generally, where comparisons between NRS or RRS spectra and SERS spectra can be made, it is found that the surface has only a slight influence on the observed vibrational frequencies and more serious effects on the relative intensities of Raman lines. If possible, however, it is of value to determine the geometry of attachment to the surface. If the molecule is attached to the surface through one of the C=O or N atoms (or possible combination thereof), the molecular plane is perpendicular to the surface. On the contrary, if the attachment is through the electrons, we might infer that the molecular plane is parallel to the surface. Modes that vibrate perpendicular to the surface are usually enhanced more than those that vibrate parallel to the surface. We have presented evidence that the molecules bind with their molecular plane at an angle to the surface, so we instead examine the various C=O and N sites as possibilities. To this end, we compare our results with the IR spectrum of the Co metal complex[7] $Co(LUM)_2(H_2O)_3$. These results

are listed in Table 4.4, along with selected lines of the free solution LUM IR spectrum and our surface Raman lines.

In Table 4.4, note first the LUM IR lines at 1698 and 1720 cm^{-1}, which are attributed to vibrations of the C=O stretch. The ab initio calculation shows that both vibrations are coupled out-of-phase C_2=O and C_4=O stretches, with the C_2=O stretch being stronger for the lower frequency mode and the C_4=O for the higher frequency mode. However, the X-ray diffraction results on the Co complex clearly indicate that the metal is chelated through the N_5 and C_4=O ligand. The IR spectrum shows the C=O stretch in the Co complex shifts downward, as expected, to 1652 cm^{-1}. In the SERS spectrum, a single band is observed at 1707 cm^{-1}, which is close to the RRS band at 1714 cm^{-1}, but is assigned to a downshifted coupled C=O stretch component as is also found in the NRS of the solid. The band at 1740 cm^{-1} in the RRS spectrum is also assigned to the pure coupled C=O stretching vibration. If the SERS 1707 cm^{-1} band has been shifted down in frequency, it could indicate that the molecule might be attached to the surface by a chelate bond through the N_5 and the C_4=O ligand at a Ag adion site. However, we have attributed the downshift of the 1700 cm^{-1} to nonbonding surface interactions and a dimer H-bonding interaction in the surface layer. In fact, we might not expect chelate bonding for a Ag surface site on theoretical grounds because the Ag^+ ion typically forms linear complexes. This type of complexation is because of hybridization of the filled $4d_z^2$ orbital with a close lying vacant 5s orbital.[25] On the other hand, Ag^+ has been shown to form a one-to-one complex with flavin mononucleotide (FMN), with proposed N_5 binding to

Ag^+ and ionic binding of the oxygen on a C_4-O phenoxide to Ag^+ [26]. The latter does not appear to be the case on the surface, because some low-frequency SERS bands of LUM involving the C_4=O vibration are not shifted down from the comparable RRS bands. Such SERS bands are found at 564 and 688 cm^{-1} (Table 4.3). Furthermore, if such a surface structure is formed, one would expect the C_4=O bond to lose double-bond character and the C_4-N_3 bond to gain double-bond character, resulting in an upshift in frequency of a mode containing a C_4N_3 stretch, such as the band at 1232 cm^{-1}. Such a shift is not observed. Thus, there is no strong evidence for a chelate-type interaction between the Ag surface and the LUM molecule.

In the IR spectra, such a shift is observed; that is, there is an increase in the C_4N_3 stretch from 1218 cm^{-1} in the solution IR spectrum to 1230 cm^{-1} in the complex IR spectrum and, similarly, an increase of the N_5-C_{4a}-C_{8a}-N_8 stretch from 1277 cm^{-1} in the solution IR spectrum to 1290 cm^{-1} in the complex IR spectrum. Once again, these increases are expected when consideration is made of the charge redistribution to the ring expected for a metal attachment, as in the Co or Ag complex. In the SERS, the latter band is only at 1288 cm^{-1}, shifted to lower frequency from the solution RRS band at 1304 cm^{-1}. A similar analysis pertains to the 1390 cm^{-1} shift from the solution IR spectrum to 1415 cm^{-1} in the complex IR spectrum. This vibration corresponds to the C_{4a}-N_5-C_6 stretch, which is also expected to increase on increasing electron density in the ring. Here, the SERS line is at 1398 cm^{-1}, which is closer to the solution IR result.

These results indicate that it is unlikely that the molecule is attached to the surface through the N_5 and C_4=O ligands of the molecule. Note, however, the band at ca. 1568 cm^{-1} is downshifted in the SERS spectrum from 1590 cm^{-1} in the RRS spectrum, is not reported in the solution IR spectrum, but is also observed in the Co complex IR spectrum. In fact, the bands at 1526 and 1568 cm^{-1} are close to frequencies in the metal complex spectrum. These bands both involve the C_{8a}-N_1 and C_{4a}-N_5 stretches according to our assignments. Thus, a bonding interaction of the Ag surface site with LUM at the 1N and/or 5N position would tend to shift these bands down in frequency. We take these facts to indicate that the mode of attachment to the surface is through the 1N or 5N lone pair in a structure involving LUM dimers at the Ag surface.

The potential dependence of the SERS spectrum is shown in Figure 4.4. Most bands shift only slightly, at every pH studied, when the potential at which each spectrum is obtained is changed from -0.1 to -0.7 V (versus SCE). However, in Figure 4.7, we see that there are a few bands that show a potential dependency. For example, at pH 6.8, on going from 0.0 to -0.3 V, the mode at ca. 1700 cm^{-1} shifts from 1718 down to 1707 cm^{-1}. The broad band at ca. 200 cm^{-1}, which we believe is due to Ag surface-molecule vibrations, shifts to lower frequency as the potential is made more negative and is almost gone at -0.75 V. Furthermore, it is clear that the ca. 686 cm^{-1} in-plane vibration in the doublet grows relative to the ca. 700 cm^{-1} out-of-plane vibration. At potentials between 0.0 and -0.3 V, these bands have the same relative intensity and, if we assume they have the same SERS enhancement, then the tilt angle to the surface is ca.

45 degrees. Between -0.6 and -0.75 V, the relative intensity ratio of the bands at 700 and 686 cm^{-1} (I_{out} /I_{in} = 0.71) gives a tilt angle of ca. 50 degrees according to the formula $1/(1 + I_{out}/I_{in}) = \sin^2\theta$.

The CV result of adsorbed LUM shows that no electrochemical reactions take place when the potential is more positive than –0.90V. As the pH for each experiment was changed from basic to acidic (from pH 8 to 4), the band at ca. 1700 cm^{-1} (involving the C=O stretch) decreases in intensity and finally shifts to a shoulder at ca. 1630 cm^{-1} at pH 3.0. Figure 4.5 shows the SERS spectrum of LUM at pH 3.0 and -0.4 V. In addition to the loss of the band at 1700 cm^{-1}, several other changes are observed in the spectrum; for examples, an increased relative intensity for the out-of-plane 523 cm^{-1} vibration, a decrease in the relative intensity ratio for the 682/698 cm^{-1} doublet, and a downshift of the 1398 cm^{-1} band to 1390 cm^{-1}. The most likely cause for these changes is that C=O is protonated and/or that the molecule reorients in some way. From the change in the intensity ratio of the doublet and the increase in the 523 cm^{-1} band we conclude that the adsorbed molecules are tilting to a more flat orientation. Both the 1700 and 1398 cm^{-1} bands involve a component with C=O motion that could be lowered by protonation. Thus, a protonation is consistent with the reorientation, the band shifts, and the previous conclusion that the C=O bond is not strongly involved in attachment of the molecule to the surface.

4.3.4 Observation of SERS spectra of reduced LUM radical

When we used 647.1nm excitation with CCD detector, we were able to monitor the reduction of LUM on silver electrode and obtain the spectra of the reduced LUM radical species at potential more negative than –0.9V. Figure 4.6 shows SERS of lumazine at -0.6V vs. SCE with 488nm and 647.1nm excitation. In SERS with 647.1nm excitation, new shoulders at 715 and 1194cm^{-1} appear since the CCD detector has better resolution for red light than blue light. A pair of C=O vibration peaks are seen at 1697 and 1709cm^{-1}, instead of one peak at 1714cm^{-1}. Also the peaks at 1526 and 1568cm^{-1} merged to 1562cm^{-1} with 647.1nm. However, there is no major difference in two spectra. The relative intensity of each peak showed slight differences, and the frequency of each peak shifted less than 5cm^{-1} for most peaks.

As indicated by CV, adsorbed lumazine is reduced at potentials negative to E_p = -0.93V. Figure 4.7 shows the SERS of LUM at –0.7V, -0.90V and –0.93V where the electro-reduction takes place. At –0.90V, the band at 603cm^{-1} disappears, new bands at 648, 1569 cm^{-1} are observed, and some band shifts also can be observed. When the voltage is shifted to –0.93V, a complete disappearance of band at 603cm^{-1} takes place . We can assume this is the spectrum of pure lumazine radical. The spectra below 1000cm^{-1} were enhanced. An increase in intensity of out-plane/in plane ratio indicated that the molecules continue to orient more perpendicular to the silver surface sites. At more negative potential (-0.95V) the intensity of the spectra became very weak due to the loss of SERS active sites and the desorption of the molecules from electrode.

4.3.5 Observation of second layer of lumazine adsorbed on a Ag electrode

The SERS spectra of LUM previously were taken without lumazine in the supporting electrolyte. Figure 4.8 showed the SERS of LUM at –0.1V with and without $1x10^{-4}$M lumazine in the supporting electrolyte at –0.1V vs. SCE with 647.1nm excitation wavelength. For the spectrum containing bulk lumazine (Figure 4.8B), Raman bands after 1800 cm^{-1} are hindered by the fluorescence interference. We still can see two C=O vibration frequencies at 1694 and 1707cm^{-1} overlapped on the fluorescence band. The SERS feature exhibited significant changes in terms of relative intensity. The intensities of ring A' vibrations at 1564, 1488, 1233, 1322, and 1185cm^{-1} increased, with respect to 1286cm^{-1}, the most intense band in the spectrum free of bulk lumazine. The bands at 578, 712 and 1185cm^{-1}, which were shoulders in Figure 4.8A, now appear as peaks. And new bands appear at 351 and 806cm^{-1}. The change in SERS spectrum suggests that there is a second layer of molecules from solution interacting with the adsorbed molecules. As we discussed in Section 4.3.3, adsorbed lumazine molecules might interact as dimer on the electrode surface, as shown in Figure 4.9. It might be also possible that the second layer of LUM molecules from bulk solution interacts with the adsorbed layer. The 943cm^{-1} and 1393cm^{-1} bands, which were assigned to the N_1C_2 stretch and N_3C_2 moved to 951cm^{-1} and 1405cm^{-1}. If dimers are formed in a sheet structure in the second layer, there could be more electron density in these bonds causing an upshift in their frequencies.

4.4 Conclusions

By analysis of Raman spectra of lumazine and with the aid of ab inito calculations, we have proposed that lumazine is adsorbed on the Ag electrode via 1N or 5N atoms of the lumazine ring. The tilt angle is a function of potential, which changes from 45^0 (0.0 to –0.3V) to 50^0 (-0.6V to –0.7V). When bulk lumazine is present in the supporting electrolyte, the adsorbed lumazine layer interacted with the molecules in the solution as a dimer via hydrogen bonding. It is proposed that the spectrum of reduced lumazine semiquinone was observed when the potential was set more negative than –0.9V.

References

(1) Abelleira, A.; Galang, R. D.; Clarke, M. J. Synthesis and Electrochemistry of Pterins Coordinated to Tetraammineruthenium (II) (Inorg. Chem. **1990**, 29, 633-639).

(2) Ladenstein, R.; Ritsert, K.; Huber, R.; Richter, G.; Bacher, A. The Lumazine Synthase/Riboflavin Synthase complex of Bacillus Subtilis X-ray Structure Analysis of Hollow Reconstituted B-Subunit Capsids. Eur. J. Biochem. **1994**, 223, 1007-1017.

(3) O'Kane, D. J.; Lee, J. Chemical Characterization of Lumazine Protein from Photobacterium leignathi: Comparison with Lumazine Protein from Photobacterium. Biochemistry, **1985**, 24, 1467-1475.

(4) Xu, Jia; Birke, R. L.; Lombardi, J. R. Surface-Enhanced Raman Spectroscopy from Flavins Adsorbed on a Silver Electrode: Observation of the Unstable Semiquinone Intermediate. (J. Am. Chem. Soc. **1987**, 109, 5645.

(5) Wei, Zhang; Vivoni, A.; Lombardi, R. J.; Birke, R. L. Time Resolved SERS Study of Direct Photochemical Charge-Transfer Between FMN and a Silver Electrode. J. Phys. Chem. **1995**, 99, 12846-12857.

(6) Shi, Chongti, Zhang, Wei, Lombardi, J. R.; Birke, R. L. Nanosecond Time Scale Kinetics in the Flavin Mononucleotide on an Electrode Surface Using Time-Resolved Surface-Enhanced Raman Spectroscopy. J. Phys. Chem. **1992**, 96, 10093-10096.

(7) Burgmayer, S. J.; Nieter, Transition-Metal Pteridine Complexes. Preparation and Characterization of Cobalt (II) Pteridines. Inorg. Chem. **1988**, 27, 4059-4065

(8) Goodgame, M.; Schmidt, A. Metal Complexes of 2, 4-(1H,3H)-Pteridinedione. Inorg. Chim. Acta **1979**, 36, 151-154

(9) Lehnen, J.; White, B. M.; Kendric, M. J. Electrochemical Studies of Biologically Significant Pterin Compounds. Inorg. Chim. Acta **1990**, 167, 257-259

(10) Heilman, O.; Hornung, F. M.; Kaim, W.; Fiedler, J. Structure, EPR, UV-VIS and IR Spectroelectrochemistry of Reversibly Reducible Compounds $[(C_5Me_5)IrCl(L)](PF_6)$, L = 1,3-dimethyllumazine or 1,3-dimethylalloxazine. J. Chem. Soc., Faraday Trans. **1996**, 92, 4233-4238

(11) Lee, J.; Wang, Yanyun; Gibson, B. Electronic Excitation Transfer in the Complex of Lumazine Protein with Bacterial Bioluminescence Intermediates. Biochemistry **1991**, 30, 6825-6835

(12) O'Kane, D. J.; Lee, J. Physical Characterization of Lumazine Proteins from Photobacterium. Biochemistry **1984**, 24, 1484-1488

(13) Visser, A. J. W. G.; Lee, J. Lumazine Protein from the Bioluminescent Bacterium Photobacterium phosphoreum. A Fluorescence Study of the Protein-Ligand Equilibrium. Biochemistry **1980**, 19, 4366-4372

(14) Lee, J.; O'Kane, D. J.; Visser, A. J. W. G. Spectral Properties and Function of Two Lumazine Proteins from Photobacterium. Biochemistry **1985**, 24, 1476-1483

(15) Birke, R. L.; Lombardi, J. R. In Spectroelectrochemistry: Theory and Practice; Gale, James R., Ed.; Plenum: New York, 1988.

(16) Foresman, J. B.; Frisch, A. Exploring Chemistry with Electronic Structure Methods, 2nd ed., Gaussian: Pittsburgh, PA, 1995-96.

(17) Nishina, Y.; Kitagawa, T.; Shiga, K.; Horiike, K.; Matsumura, Y.; Watari, H.; Yamano, T. J. Biochem. (Tokyo) **1978**, 84, 925-932

(18) Kitagawa, T.; Nishina, Y.; Kyogoku, Y.; Yamano, T.; Ohishi, N.; Takai-suzuki, A.; Yagi, K. Biochemistry **1979**, 18 (9), 1804-1808

(19) Vervoort, J.; O'Kane, D. J.; Carreira, L. A.; Lee, J. Identification of a Lumazine protein from Photobacterium Leignathi by Coherent Anti-strokes Raman Spectroscopy. Photochem. Photobiol. **1993**, 37 (no. 1), 117-119

(20) Irwin, Richard M.; Visser, A. J. W. G.; Lee, John; Carreira, Lionel A. Protein-Ligand Interactions in Lumazine Protein and in Desulfovibrio Flavodoxins from Resonance Coherent Anti-Strokes Raman Spectroscopy. Biochemistry **1980**, 19, 4639-4446

(21) Brutovsky, B.; Ulicny, J.; Miskovsky, P.; Lisy, V.; Chinsky, L. Resonance Raman Spectra of Selected Pterin Molecules. Genetic Algorithms Approach to Force Field Scaling. J. Raman Spectrosc. **1998**, 29, 833-839

(22) Frisch, M. J.; Trucks, G. W.; Schlegel, H. B.; Gill, P. M. W.; Johnson, B. G.; Foresman, J. B.; Robb, M. A.; Cheeseman, J. R.; Keith, T.; Peterssons, G. A.; Montomery, J. A.; Raghavachari, K.; Al-Laham, M. A.; Zakrzewski, V. G.; Oritz, J. V.; Foresman, J. B.; Ciosłowski, J.; Stefanov, B. B.; Nanayakkara, A.; Challacombe, M.; Peng, C. Y.; Ayala, P. Y.; Chen, W.; Wong, M. W.; Andres, J. L.; Replogle, E. S.; Gomperts, R.; Martin, R. L.; Fox, D. J.; Binkley, J. S.; Defrees, D. J.; Baker, J.; Stewart, J. J. P.; Head-Gordan, J.; Gonzalez, C.; Pople, J. A. Gaussian-94, Rev. D.1; Gaussian: Pittsburgh, PA 1995.

(23) Spartan 5.0; Wavefunction: Irvine, CA, 1997.

(24) Norrestam, R.; Stensland, B.; Soderberg, E. The Crystal and Molecular Structure of Lumazine Hydrate. Acta Crystallog., B **1972**, 28, 659

(25) Cotton, F. A.; Wilkinson, G. Advanced Inorganic Chemistry, 4th ed.; Wiley & Sons: New York, 1980, p 969.

(26) Benecky, M.; Yu, T.-J.; Watters, K. L.; McFarland: Metal-Flavin Complexation A resonance Raman Investigation. Biochim. Biphys. Acta **1980**, 627, 197

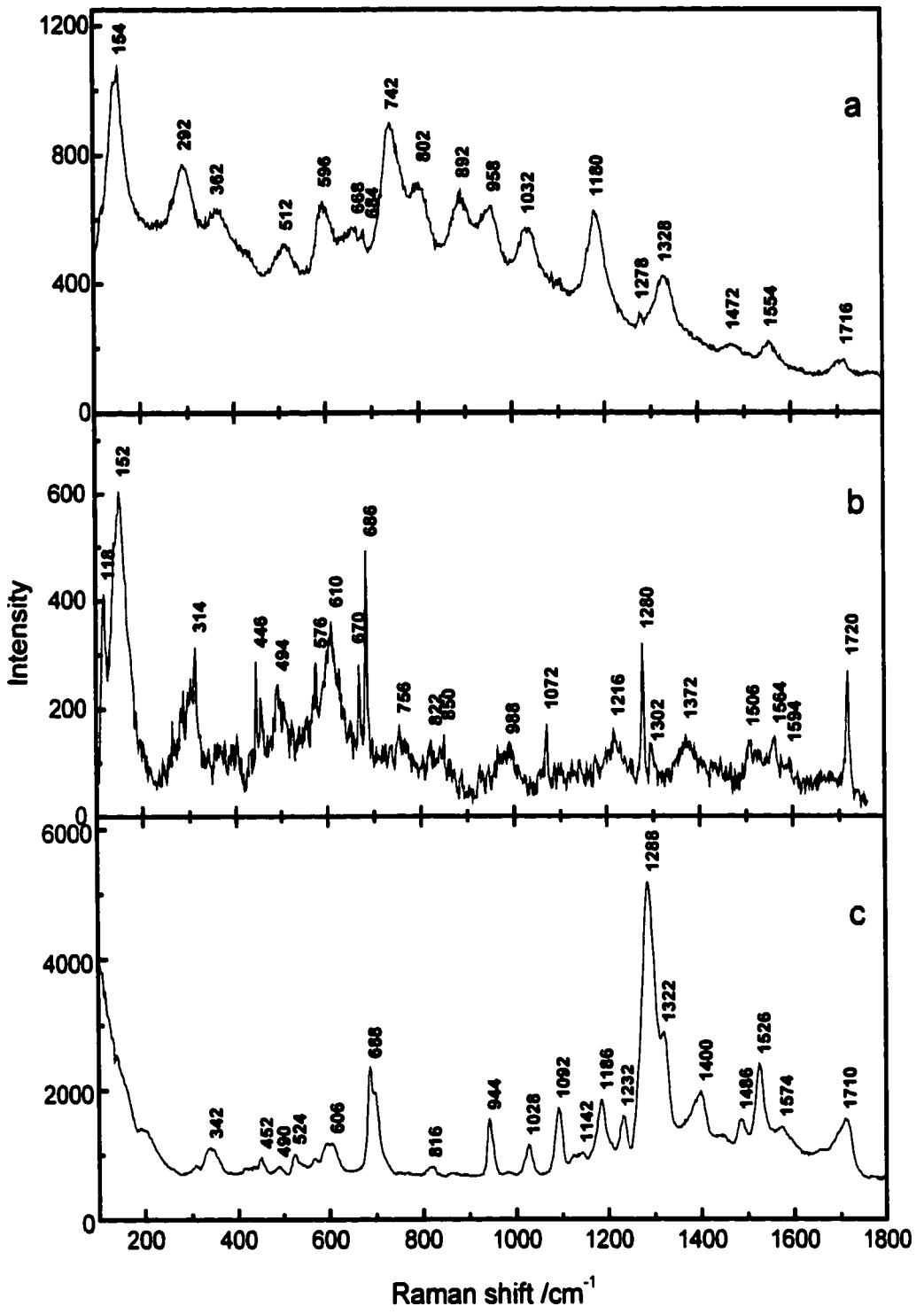

Figure 4.1 (a) NR of solid lumazine with 756nm excitation, (b) NR of solid lumazine with 736nm excitation, (c) SERS of lumazine at –0.6V vs. SCE with 488nm excitation

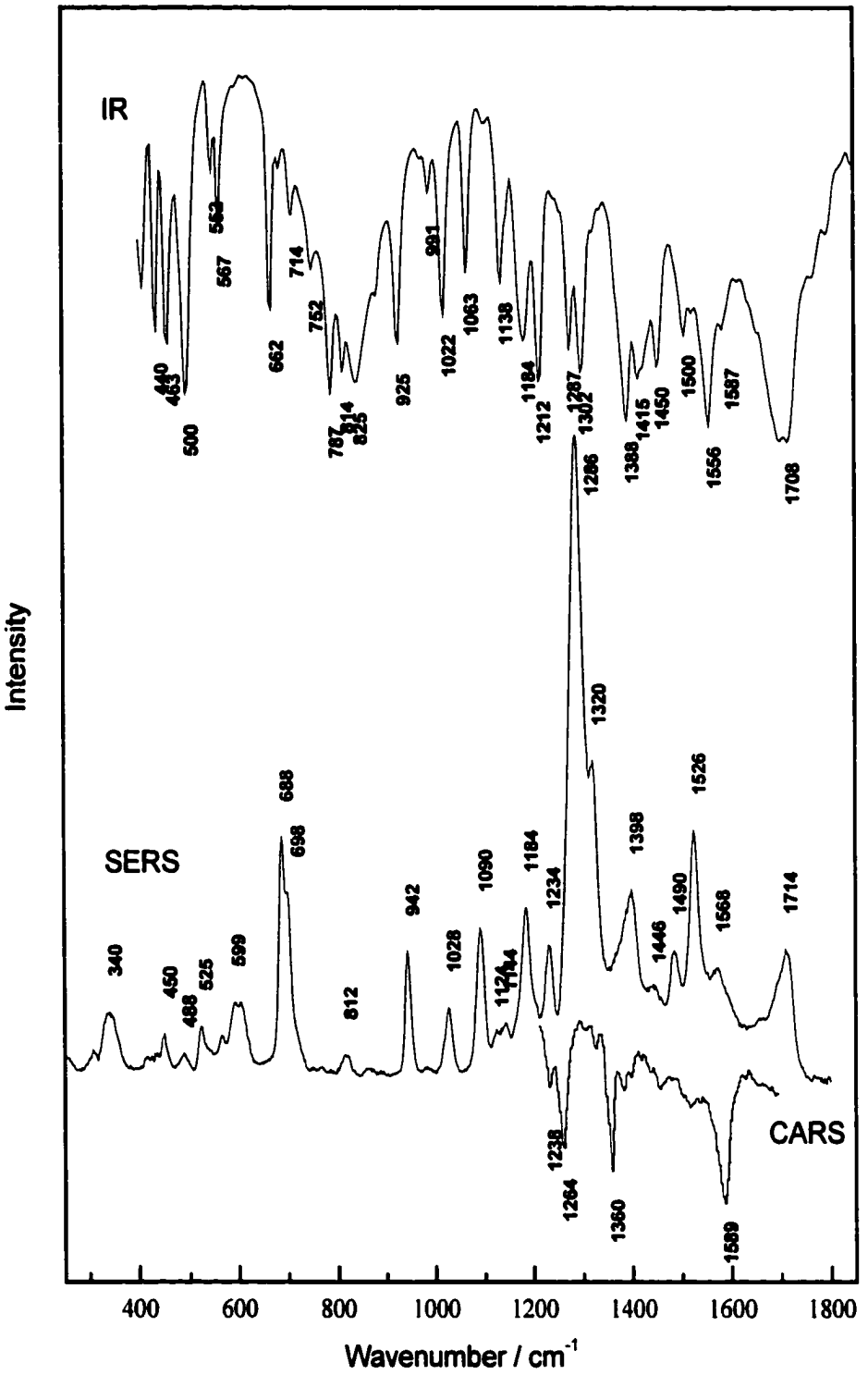

Figure 4.2 Comparison of the (1) the FTIR of lumazine in a KBr pellet, (2) the SERS of lumazine at Ag electrode, and (3) the CARS of dimethyllumazine (from ref. 20)

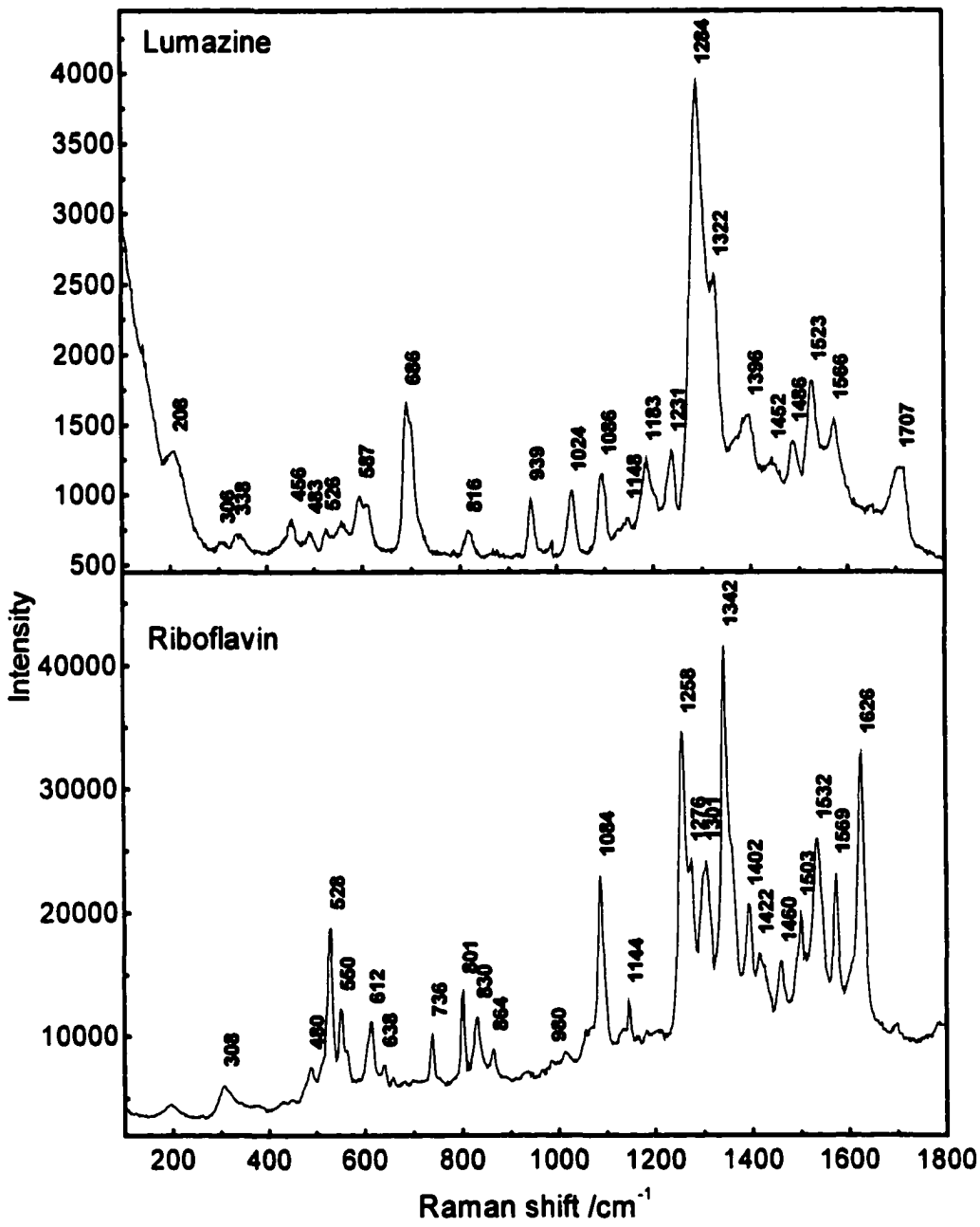

Figure 4.3 Comparison of the SERS of lumazine and riboflavin at –0.4V versus SCE and at pH=6.0, 488nm excitation

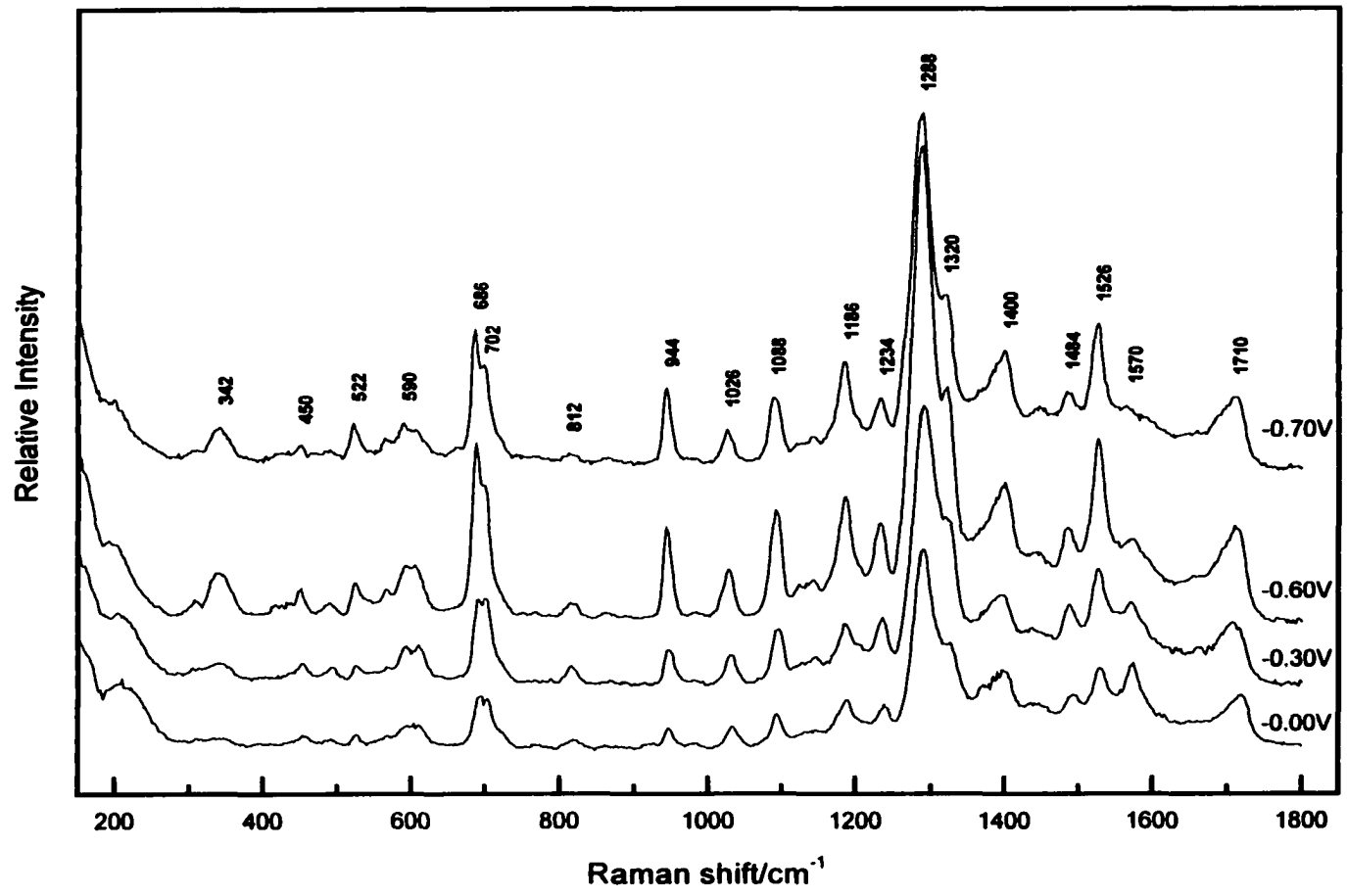

Figure 4. 4 SERS of lumazine at different potential vs. SCE with 488nm excitation in 0.1N Na_2SO_4 electrolyte

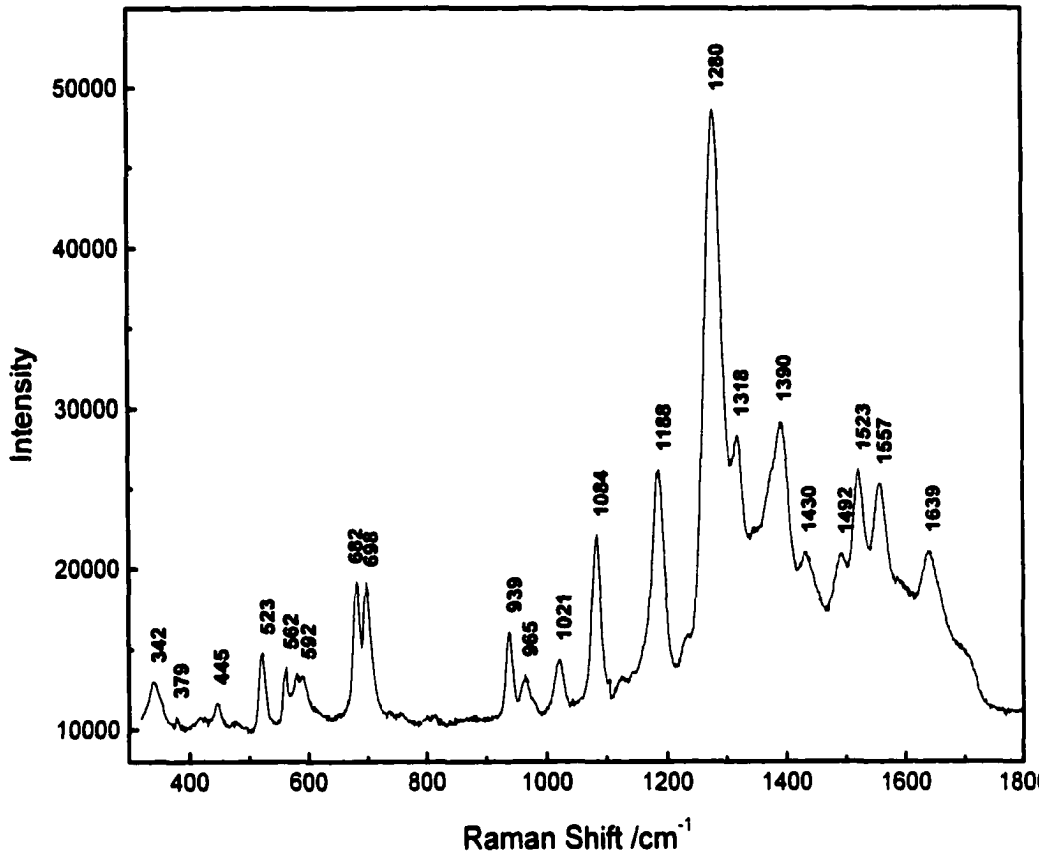

Figure 4.5 SERS of lumazine at –0.4V vs. SCE in 0.1N Na_2SO_4, pH=3, 488nm excitation

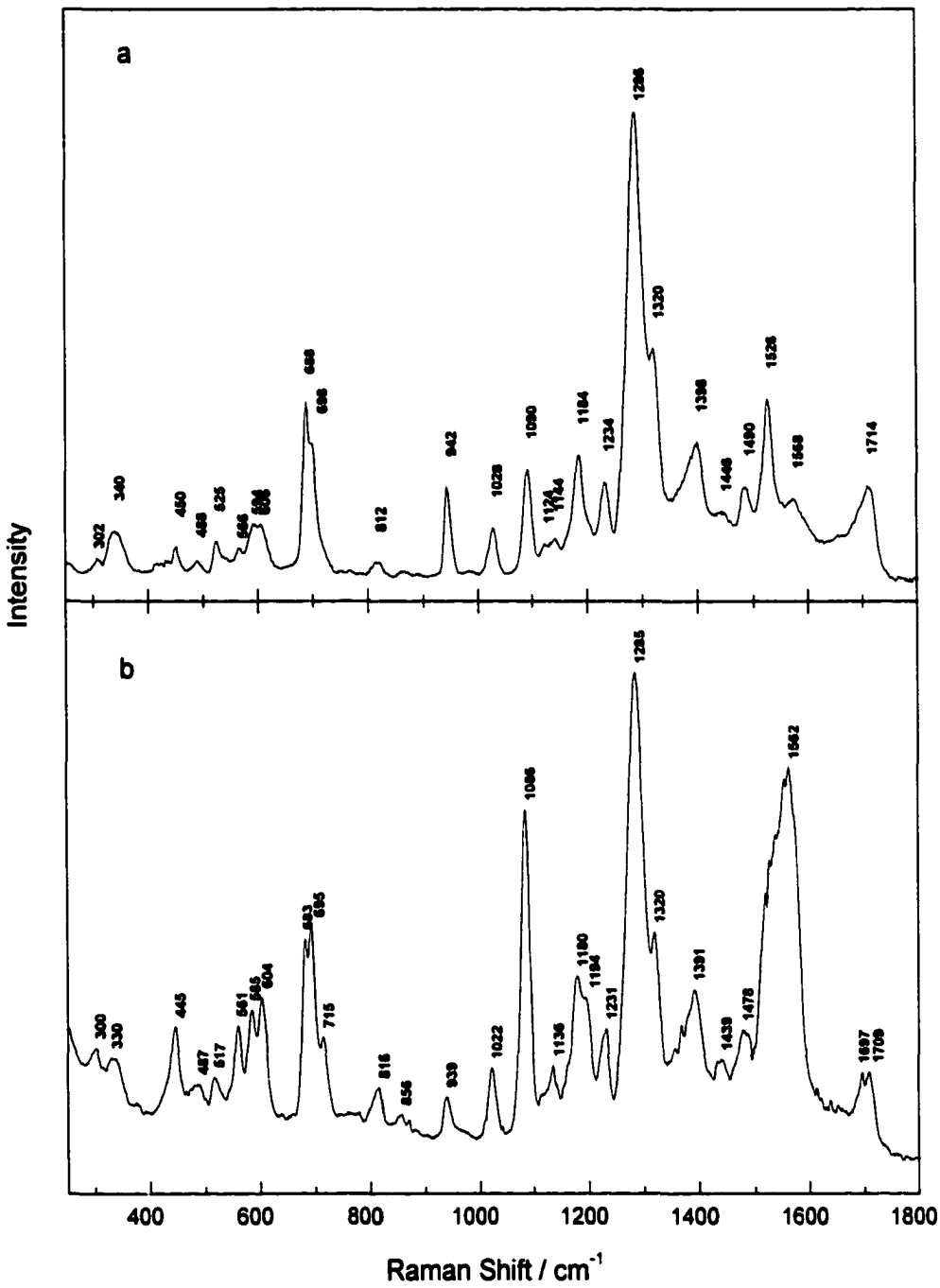

Figure 4.6 SERS of lumazine at –0.6V vs. SCE (a) 488nm excitation (b) 647.1nm excitation wavelength

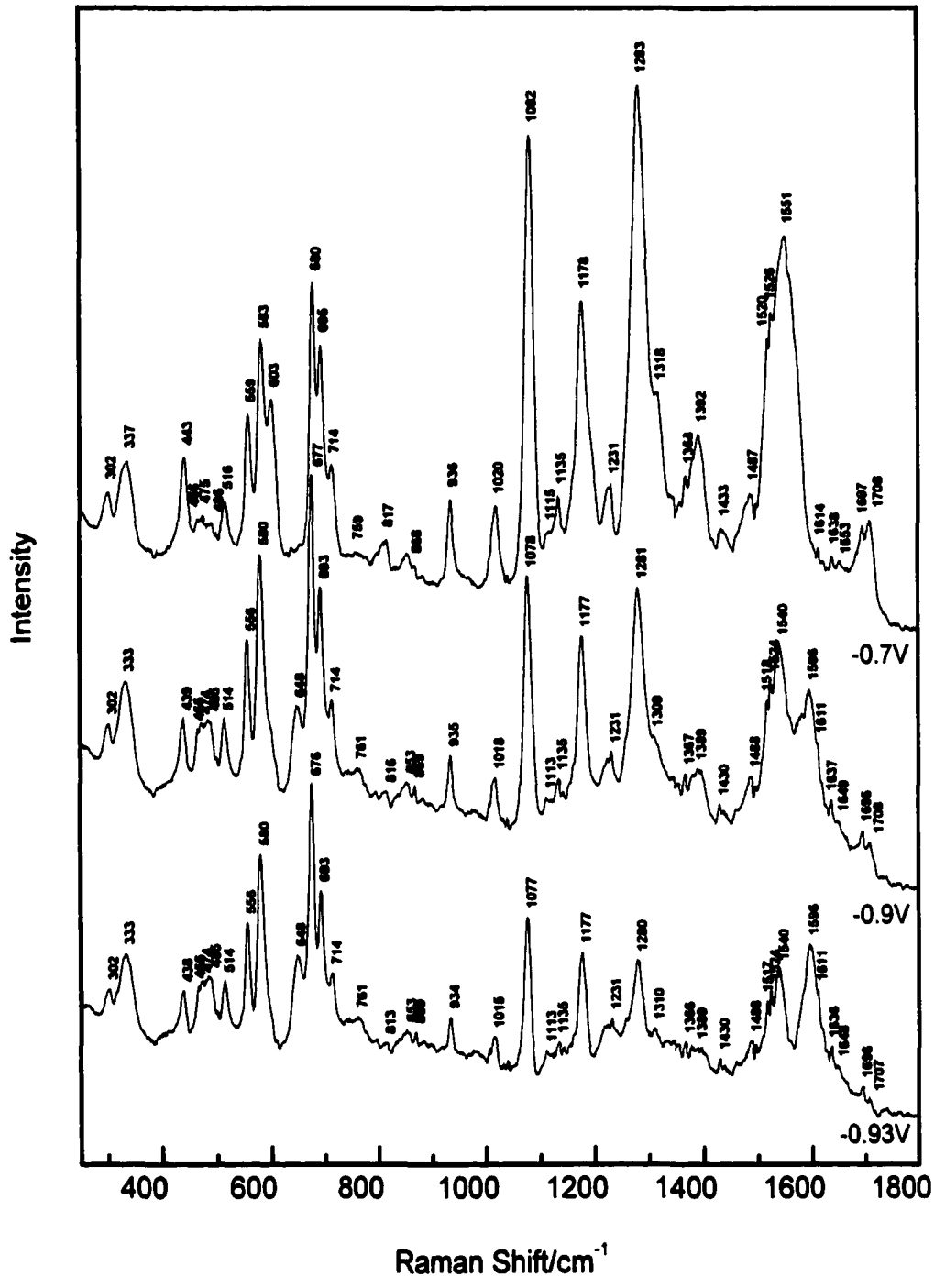

Figure 4.7 SERS spectra change with applied potentials, 647.1nm excitation

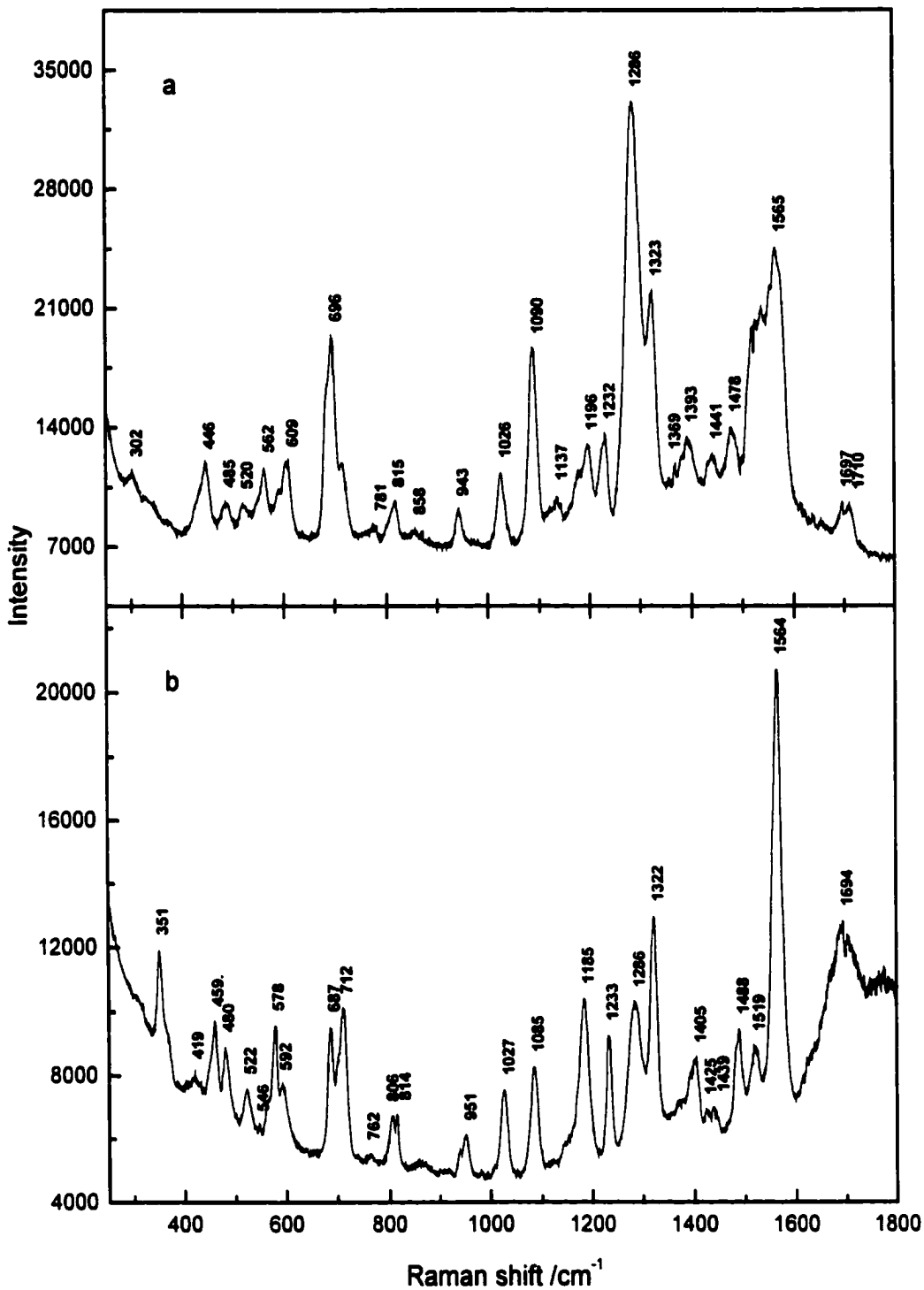

Figure 4.8 SERS at –0.1V vs. SCE (a) without lumazine present in solution, (b) with lumazine present in solution, 647.1nm excitation

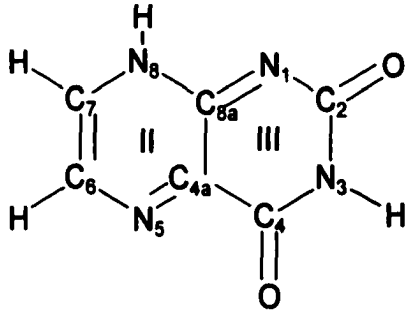

(8H, 3H) tautomer

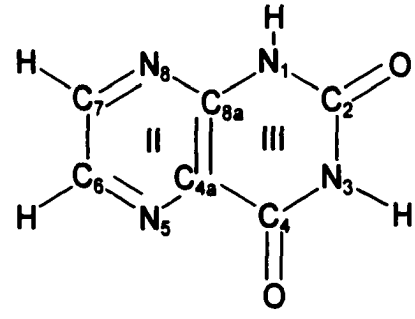

(1H, 3H) tautomer

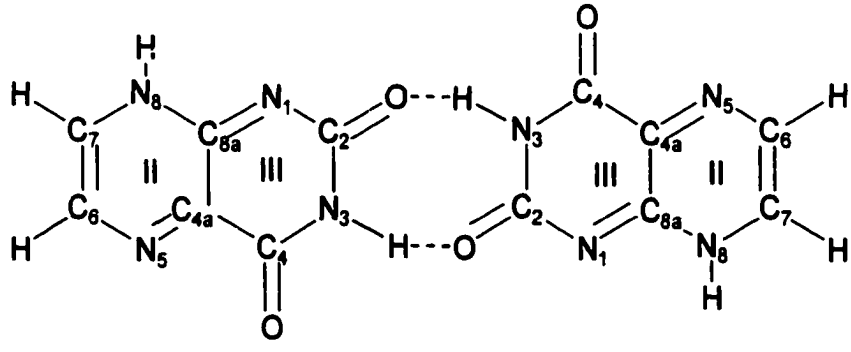

Dimer

Figure 4.9 Lumazine tautomer and dimer structures

Table 4.1 Wavenumbers (cm^{-1}) of Lumazine and Riboflavin for Various Vibrational Spectroscopic Methods

SERS[a] (lumazine)	FTIR (lumazine)	NRS[b] (lumazine)	CARS[20] (DM lumazine)	RRS[21] (lumazine)	SERS (riboflavin)	IR (riboflavin)
306(w)		312 (ms)			414	388
456 (w)		448 (m)			462	437
483 (w)	500 (m)	490 (m)		495 (w)	480	503
526(w)				528	522	
587 (w)		588 (mw)		560 (w)	538	563
					612	604
686 (s)		670 (m)				627
688 (s)	662 (m)	684 (vs)		685 (vs)	736	735
816 (vw)	787 (m)	812 (w)		820 (w)	801	785
	825 (m)				830	824
					864	865
939 (m)	925 (m)					
		972 (w)			980	
1024 (m)	1012 (m)			1016 (vw)*		
1086 (m)	1063 (w)	1070 (m)		1068 (s)	1084	1081
1183 (m)	1184(w)			1184 (m)	1144	
	1212 (w)	1202 (m)				1206
1231 (w)			1238 (w)		1232	
			1264 (s)		1258	
1284 (vs)	1287 (m)	1280 (s)		1304 (s)		1272
1322 (s)	1312 (m)				1301	
		1354 (m)	1359 (s)		1342	1346
1396 (m)	1388 (w)				1402	1396
					1422	1425
1452 (vw)	1450 (m)	1458 (vw)		1459 (vw)	1460	1461
1486 (w)	1500 (w)				1503	
1523 (m)					1518 (sh)	1532
	1556 (s)	1558 (w)				1552
1566 (m)	1587 (w)		1584 (s)	1590 (s)	1569	1583
					1626	1621
1707 (m)	1708 (s)	1718 (s)			1714 (m)	
					1740 (m)	

[a] SERS spectra measured at -0.4 V versus SCE and at pH 6.0.[b] The NRS spectrum is of the solid.

Table 4. 2 Comparison of Band Wavenumbers (cm^{-1}) in the Raman Spectrum of Lumazine for Various Calculation Methods.

AM1[a]	AM1[a]	RHF/3-21G[b]	RHF/3-21G[c]	RHF/6-31G[c]	B3LYP/6-31G[d]	SERS[e]	RRS
423	425	448(5)	446(8)	439(9)	425	456(w)	
494	482	495(8)	460(8)	470(11)	486	483(w)	495(w)
556	547	551(7)	540(6)	538(5)	552	587(w)	560(w)
660	634	649(6)	625(7)	622(7)	644		
691	688	687(9)	660(3)	662(2)	678	686(s)	685(s)
742	733	713(5)	763(7)	765(6)	731		
836	835	815(1)	864(4)	804(7)	829	816(w)	820(w)
961	958	970(1)	970(6)	962(1)	942	939(m)	
986	990	1039(9)	1040(24)	1063(14)	991	1024(m)	
1068	1060	1065(9)	1081(9)	1100(17)	1101	1086(m)	1068(s)
1140	1134	1135(16)	1150(11)	1150(11)			
1191	1178	1191(3)	1169(20)	1192(67)	1195	1183(m)	1184(m)
1228	1208	1254(26)	1222(41)	1233(24)	1212	1231(m)	
1305	1273	1273(6)	1275(142)	1310(250)	1334	1284(vs)	1304(s)
1338	1315		1295(23)	1341(41)	1363	1322(m)	
	1424	1418(6)	1398(28)	1409(8)	1411	1396(w)	
		1428(5)	1413(12)	1416(21)	1438	1452(vw)	1459(vw)
1459	1453	1486(11)	1467(14)	1485(18)	1518	1486(w)	1518(sh)
1504	1537	1557(60)	1530(101)	1562(121)	1561	1523(w)	
1591	1606	1569(19)	1608(27)	1626(42)	1635	1566(m)	1590(s)
1647	1646		1642(77)	1680(52)		1707(m)	1714(m)
1716	1711	1760(8)	1754(30)	1810(45)	1812		
1738	1738	1768(45)	1778(67)	1823(47)	1820		1740(m)

[a] Lumazine as 2,4(1*H*,3*H*)-pterdinedione from ref 21; Raman activity not calculated; the first and second columns differ only in a scale factor set (ref 21).[b] Lumazine as 2,4(1*H*,3*H*)-pterdinedione; results scaled by 0.90; Raman activity.[c] Lumazine as 2,4(3*H*,8*H*)-pterdinedione; results scaled by 0.90; Raman activity.[d] Lumazine as 2,4(3*H*,8*H*)-pterdinedione; no scaling; Raman activity not calculated with the density function theory.[e] SERS spectra measured at -0.4 V versus SCE and at pH 6.0 (Figure 6).

Table 4. 3 Assignments for Lumazine and Dimethyl lumazine Bands from RHF/6-31G(d) Calculations[a]

lumazine SERS[b]/calc[c]	assignment	dimethyl lumazine CARS/calc[c]	assignment
340(m)/381(1)	A' ' C_2O & C_4O in pl. wg: N_3H		
450(w)/439(9)	A' ring br.: C_2O, C_4O, C_6H,	423(7)	A' ring br.: N_3H
488(vw)/470(1)	A' ring br.: N_3H		
525(w)/521(5)	A' ring: out-of -pl. tors.	526(3)	A' ' ring br.: Me rks.
564(vw)/538(5)	A' ring br.: N_8H, C_6H, C_2O, C_4O		
599(m)/622(2)	A' ring br.: N_8H, C_2O	590(6)	A' ring: out-of pl. tors.
688(s)/662 (2)	A' ring rock: N_1C_2O, N_3C_4O, C_7H	648(9)	A' ring br.: N_8H
698(s)/703(2)/765 (6)	A' ' ring: out-of pl. tors.		
	A' ring br.: C_7N_8H, N_3H, C_6H, C_7H	736(4)	A' ring br: C_6C_9, C_7C_{10}
812(w)/804(7)	A' ' ring: out-of -pl. tors.	807(5)	A' ring: out-of pl. tors.
		837(11)	A' ring br.: N_3H, N_8H, C_2O, C_4O
942(ms)/962(1)	A' ring br.: N_1C_2, $C_2N_3C_2O$, N_3H	959(24)	A' ring br.: N_1C_2, C_2N_3, C_7N_8, N_3C_4O, C_6C_7, Me rks.
		994(22)	A' symm. ring br.: Me rks., C_2O, C_4O, Me rks.
1028(m)/1063(14)	A' ring: C_7N_8, C_6N_5, $N_8C_{8a}C_{4a}N_5$, C_2N_3, C_6H	1026(4)	A' ' ring: C_7N_8, C_2N_3, N_3H, N_8H, C_2O, C_4O
		1038(1)	A': Me out-of-plane twist,
1090(m)/1100(17)	A' ring: N_8C_{8a}, N_5C_6, $C_{8a}C_{4a}N_5$, C_4O	1094(1)	A' ' ring br.: N_1C_2O, C_4O, C_7C_{10}, Me rks.
1144(vw)/1150(11)	A' ring: C_7N_8, C_6N_5, $C_{4a}C_4$, C_7H, N_3H	1159(244)	A' ' ring br.: C_7N_8, C_6N_5, C_2N_3, N_5C_{4a}, N_8C_{8a}, Me rks.
1184(m)/1192(67)	A' ring II-III br.: C_6C_7, C_6N_5, N_8C_{8a}, C_2N_3,	1180(15)	A' ' ring br.: C_6C_9, C_7C_{10}
1234(m)/1234(24)	A' ring II-III: N_1C_2, N_3C_4, $C_6N_5N_1C_2O$, $C_{4a}C_4O$	1238(m)/1237(86)	A' ' ring br.: N_1C_2, N_3C_4
		1264(s)/1285(113)	A' ring br.: N_8C_{8a}, N_1C_2, N_5C_6, C_4N_3, OC_4N_8, C_7C_{10}, Me rk.
1286(vs)/1310 (250)	A' ring II-III: N_8C_{8a}, $C_{8a}C_{4a}$, C_7C_6, $C_{4a}N_5$, C_7H rk., C_2O rk.		
1320(m)/1341(41)	A' ring br.: C_7N_8, C_6N_5, $C_{4a}C_4C_{4a}C_4O$, N_1C_2O, N_3H	1341(1)	A' ' ring br.
		1359(s)/1369(129)	A' ' ring br.: C_7N_8, N_8C_{8a}, C_7C_6, C_7C_{10}, C_6C_9, N_1C_2, N_3C_4, $C_{8a}C_{4a}$, Me rk.
1398(w)/1409(8)	A' ring br.: C_4C_{4a}, C_2N_3, N_5C_6, N_1C_2, C_2O, C_4O	1410(8)	A' ring br.: C_2N_3, C_4N_3, N_1C_{8a}, C_4O, Me rk.
1446(vw)/1416(21)	A' ' ring br.: C_4N_3, C_2O, C_4O, N_3H rk.	1416(29)	A' ' ring br.: C_4N_3, C_2O, C_4O, Me rk.
		1456(25)	A': Me tws., C_2O, C_4O
		1465(12)	A' ' ring II-III br.: Me rk.

		1469(12)	A': Me rk.
		1481(8)	A': C_2O, N_3C_4O, Me rk.
1490 (w)/1485(18)	A' ring br.: C_7N_8, $C_{4a}C_4$, C_7H	1489(33)	A' ' ring br.: C_7N_8, $C_{4a}C_4$, C
1526(ms)/1562 (121)	A' ring br.: C_7C_6, $C_{4a}N_5$, N_5C_6, $C_{8a}N_1$, C_2O	1584(s)/1562(165)	A' ring br.: C_7C_6, N_5C_6, $C_{4a}N_5$, $C_{8a}N_1$, C_2O
1568(m)/1626(42)	A' ring br.: C_7C_6, $C_{8a}N_1$, N_8C_{8a}, N_8H rk.	1623(51)	A' ring br.: C_7C_6, $C_7N_8C_{8a}$, $C_{8a}N_1$, C_2O, C_4O, $C_6N_5C_{4a}$, C_7C_{10}
1680(52)	A' ring br.: C_7C_6, N_5C_{4a}, C_7N_8, $C_{8a}N_1$, C_2O, C_4O	1679(65)	A' ring br.: C_7C_6, N_8C_{8a}, N_5C_{4a}, C_2O, C_4O
1714(m)/1810(45)	A': C_2O, C_4O	1805(56)	A': C_2O, C_4O
1823(47)	A': C_2O, C_4O	1819(47)	A': C_4O, C_4O
		2899(127)	A': Me(C_9H)
3086(68)	A' asym.: C_7H, C_6H	2905(217)	A': Me($C_{10}H$)
3104(20)	A' sym.: C_7H, C_6H	2950(99)	A' ': Me(C_9H)
		2968	A' ': Me($C_{10}H$)
		2970	A': Me(C_9H), Me($C_{10}H$)
		2978	A': Me(C_9H), Me($C_{10}H$)
3453(62)	A': N_8H	3451(47)	A': N_8H
3461(92)	A': N_3H	3463(102)	A': N_3H

[a] Abbrevations: br., breathing; tors., torsion; rk., rock; tws., twist; wg., wag. Two atoms indicates stretch; three or more atoms is a bend.[b] SERS spectrum measured at -0.6 V versus SCE.[c] Modes that had an intensity <2.0 are not reported unless a band appears in the spectrum.

Table 4. 4 Comparison of the Vibrational Bands (cm^{-1}) of Lumazine and a Cobalt-Lumazine Complex

lumazine IR[a]	lumazine IR metal complex[a] $Co(LUM)_2(H_2O)_3$	lumazine SERS (-0.6 V)	lumazine RRS[b]	assignment
1063 (w)	1069 (m)	1090 (ms)	1068 (s)	N_8C_{8a}, $C_{4a}N_5$, N_5C_6
1137 (w)	1164 (m)	1184 (ms)	1184 (m)	C_6C_7, C_6N_5, N_8C_{8a}, C_2N_3
1218 (s)	1230 (vs)	1234 (m)		N_1C_2, N_3C_4
1277 (m)	1290 (vs)	1286 (vs)	1304 (s)	$C_{8a}C_{4a}$, N_8C_{8a}, $C_{4a}N_5$, C_6C_7
1300 (m)	1309 (vs)	1322 (s)		C_7N_8, C_6N_5, $C_{4a}C_4$
1390 (vs)	1415 (vs)	1398 (m)		$C_{4a}C_4$, C_2N_3, C_6N_5
	1501 (vs)	1490 (w)	1459 (vw)	C_7N_8, $C_{4a}C_4$
1554 (vs)		1526 (m)	1518 (sh)	C_6C_7, $C_{4a}N_5$, $C_{8a}N_1$
	1575 (vs)	1568 (mw)	1590 (s)	C_6C_7, $C_{8a}N_8$, $C_{8a}N_1$
	1620 (vs)			C=O
1698 (vs)	1652 (vs)	1714 (s)	1714 (m)	C_2=O, C_4=O
1720 (vs)			1740 (m)	C_2=O, C_4=O
3080				C_7H, C_6H
3170				NH
	3300 (vs)			NH

[a] Reference 7.[b] Reference 21.

CHAPTER 5 VOLTAGE DEPENDENCE STUDY OF SERS OF PIPERIDINE AND 2-MERCAPTOPYRIDINE ON A SILVER ELECTRODE

5.1 Introduction

As we discussed in chapter 1, there are two separate mechanisms involved in SERS effect: the electromagnetic mechanism and chemical mechanism. For the EM mechanism, there is no requirement of specific chemical bonds between the adsorbate and metal, and the enhancement factor for a single metal active site is up to 10^4. However, many molecules, which can interact with the metal surface via lone pair electrons, π aromatic rings, or other chemical bonding, display enhancement ratios up to 10^6. For the SERS of those molecules in an electrochemical environment, one of the most characteristic features is that the Raman signal of the molecules adsorbed on the electrode in absence of a redox process exhibits a bell shaped curve of intensity versus applied potential. Further theoretical studies showed that the SERS of these molecules could be interpreted in terms of a resonance shaped intensity profile as a function of applied potential.

Several groups first reported the SERS-voltage dependence. Jeanmaire and van Duyne showed that the Raman signal reaches a maximum at different applied electrode potentials, V_{max}, for different bands of pyridine adsorbed on a silver electrode. Furtak *et al.* [2-3] found that in an electrochemical cell, the voltage

at which the intensity reached a maximum varied linearly with the excitation frequency (ω). Similar results were obtained on CN^- and pyridine [5].

Charge transfer theory was then proposed [1-3] to explain the phenomenon. The theory treated the molecule and metal system as a whole; charge transfer transitions were possible both in ground state and excited states, which could explain the effect. It was suggested that the Fermi level of the metal is positioned between the molecular ground state and one or more of the excited states of the molecules, and that transitions from the Fermi level to the excited state or from the ground state to the Fermi level were involved.

Lombardi *et al.* [1] further proposed that the molecules could be divided into two classes: those for which V_{max} had a positive slope with ω and those for which the slope was negative with excitation frequency ω. Two types of charge transfer could be envisioned. Molecule to metal charge transfer, in which an electron is transferred from the highest occupied molecular orbital to the Fermi level of the metal is associated with a negative slope in V_{max} with ω. Conversely positive slopes are associated with transitions in which an electron is transferred from the Fermi level of the metal to the lowest unoccupied orbital in the molecule. A charge-transfer theory was then established.

The dependence of the SERS intensity on V is given by the following expression

$$I \propto |\alpha^{CT}|^2 \propto \{\ln|\omega^{CT}+\omega_i-\omega+i\Gamma|^2$$

where ω^{CT} is an energy frequency difference, which depends on applied voltage V, ω is the laser excitation frequency, and ω_i is a vibrational frequency which only

appears for polarizability components from the A term. A similar expression without ω_I comes from the B and C terms. The resonance comes when $\omega^{CT}=\omega_i-\omega$, which can be modulated by the voltage V.

However, many other possible factors may distort the resonance profile shape. One of the possible factors is that the active sites change as the voltage changes. Loss of active sites occurs at potentials negative to the point of zero charge (ca. –0.7V versus SCE on Ag) and will cause a loss in SERS intensity. Another consideration of how the SERS intensities could change with potential is that the surface concentration, Γ, might change with potential. However, it is suggested that a roughened SERS-active surface stabilize molecule adsorption. So Γ may be less affected by potential on a rough surface than on a smooth surface. Changes in orientation of surface molecules with potential have also been considered as another source of potential dependence of I versus V. Different vibration modes will show different I vs. V profile according to SERS surface selection rules. Therefore, a voltage dependence study of SERS spectra should provide us with information on molecule adsorption/desorption, surface reactions, bonding sites and molecule orientation, etc.

The SERS voltage dependence of piperidine and 2-mercaptopyridine (2-MP) was studied in this chapter. Adsorption of mercaptans on metal electrodes has been a focus of substantial research interests [8-10]. Because of the strong bonding between mercaptans and a silver or gold electrode, they are often used as electrode modifiers to enhance the charge transfer process between electrode and biomolecules. It is thus important to know the bonding site and orientation

change with the potential change. Piperidine and pyridine both contain nitrogen lone pairs, and they exhibit intense SERS due to the chemical effect. Unlike pyridine, which has a π-electron system, piperidine has a saturated electron configuration. Therefore, the only possible interaction site with metal electrode surface is via the lone-pair electrons on the N atom. These two molecules represent different degrees of bonding strength with a Ag electrode. Piperidine adsorbs on silver surface via physical adsorption, which can be shown by its SERS intensity as a function of bulk concentration. Thiols adsorbed on Ag or Au electrode via a real chemical bond, Ag-S. Therefore It would appear to be interesting to study the difference in SERS vs. electrode potential profiles for these two different types of adsorbed molecules.

5.2 Experimental Section

The experiment was carried out on a Spex 500 monochromator with a CCD detector. The laser, Raman spectrometer, electrochemical cell, electrodes, focusing arrangement, and electrochemical instrumentation have been introduced in chapter 2.

2-MP and reagent grade KCl were purchased from Sigma-Aldrich Chemical Inc. A $1x10^{-4}$ M 2-MP solution was prepared in ethanol. A silver electrode with a purity of 99.999% was polished prior to each experiment with fine grades of Alumna powders down to 0.05μm, and then was roughened in 0.1M KCl supporting electrolyte by an oxidation-reduction cycle (ORC). The ORC

was done by setting the applied potential of the working electrode at –1.25V to clean surface, followed by applying an oxidation step to 0.183 V vs. SCE for 10s, then jumping the potential back to 0.0V for 10s. The electrode was then immersed in the $1x10^{-4}$M 2-MP ethanol solution for 1hr. The electrode was rinsed with ethanol and distilled water sequentially, and then transferred into an electrochemical cell with 0.1M KCl supporting electrolyte. All solutions were made from AR-grade reagents and deionized distilled water. All electrode potentials quoted here are relative to the saturated calomel electrode (SCE).

Piperidine was purchased from Aldrich Chemical Co. and reagent grade KCl from Fisher Scientific Co. In the case of piperidine studies, first the electrode was polished with emery paper until bright, then was subjected to a chemical cleaning by submersion in a 50%/50% solution of H_2O_2 and NH_4OH for 10s, and finally washed with deionized and distilled water. Then the electrode was transferred to the Raman cell, which contained 0.05M piperidine and 0.1M KCl solution. The electrochemical pretreatment was done by setting the applied potential of the working electrode at –1.25V to clean the surface, followed by applying an oxidation step to 0.183 V vs. SCE for 10s, then jumping the potential back to 0.0V for 10s. Finally, the spectra were measured at a variety of different potentials from 0.0V to –1.0V.

A Kr^+ laser (Spectra Physics, Model 2020) at 647.1nm was used as an excitation source, with laser power about 50mW. A Spex 500 monochromator coupled with a 647.1nm notch filter to cut off laser light and stray light, and a multi-channel CCD detector was used to collect Raman spectra. The resolution is

ca. 2 cm^{-1}. It took approximately a 20s exposure time for each spectrum. Spectra from 0.0V to –1.0V vs. SCE were taken with one pretreatment with a step of –0.05V between each applied potential in order to construct the I vs. V curve. The laser light was blocked while the potential was changed and there was a few second intervals before the next spectrum was taken.

5.3 Results and Discussion

5.3.1 SERS of piperidine

Previous SERS studies of piperidine have been reported by a few research groups [6,7]. Significant changes in the SERS spectra with electrode potential for different vibration modes were reported by our laboratory in 1984[6]. The experiment was carried on a scanning spectrophotometer and the intensity vs. potential profiles were semi quantitative. With the use of a CCD detector, we were able to obtain a spectrum within a few seconds and the spectra ~ voltage relation can be measured quantitatively with one single pretreatment.

Figure 5.1 shows the SERS of piperidine at different electrode potentials versus SCE. The relative intensity of different peaks depends significantly on the applied potential. A detailed analysis and band assignment (Table 5.1) was given by Sanchez *et al.*[6]

Figure 5.2a to Figure 5.2c presented the overlays of the spectra taken in different Raman shift regions at different voltages (from bottom to top: -0.0V to –

0.90V, 0.05V interval) after one pretreatment. The spectra exhibit differences not only in Raman frequency but also in intensity. A possible reason is that the surface concentration changes with the voltage. However, the occurrence of some nearly isosbestic points at 450, 580, and 1350 cm^{-1} might suggest that the total surface concentration of the piperidine molecule is approximately the same over the entire potential range applied. When the potential was moved negative of –0.9V, those isosbestic points are lost, which suggests that surface molecule desorption occurs or the loss of active sites occurs. To simplify our consideration, we might exclude the concentration factor from our consideration in the range of –0.0V to –0.9V. Also the isosbestic points suggest that there are two species in equilibrium on the surface and their relative surface concentrations change with voltage. A cyclic voltammetry experiment[6] has shown that there is no electrode reaction involved in the range from 0.0V to –1.0V vs. SCE, and the spectra are reversible with change in potential. Instead of a redox couple existing on the surface, two structural piperidine isomers may be in equilibrium on the silver surface. As already noted in our previous work,[6] the two species might be an equatorial conformer and an axial conformer. The relative concentrations of two species thus might be a function of applied potential.

When the potential is more positive than –0.5V, one species is dominant, and there is no dramatic change in band distribution, except for a moderate intensity change as the potential is moved. When potential is moved more negative than -0.5V, bands at 432 and 1151cm^{-1} show a rapid growth, accompanied with the disappearance of bands 1054 and 1368cm^{-1}. In addition,

new bands at 625, 1283 and 1378cm^{-1} appear, which indicates the formation of another species.

Figure 5.3 shows the intensity vs. potential profiles for some of the bands. It was not surprising that the profiles do not show a single resonance shape. For some bands, two maxima are found at –0.2V and –0.8V. It is possible that different species are predominates at –0.2V and at –0.8V. Therefore, they may be on overlap of two resonance profiles.

5.3.2 SERS of 2-mercaptopyridine

2-mercaptopyridine (2-MP) is an interesting molecule to investigate by SERS since it contains several sites, which may function as ligands to the metal surface: i.e. a sulfur atom, a nitrogen atom, as well as the aromatic π system.

2-MP exists as a thione in neutral aqueous solution, the thiol form in basic solution or ethanol solution, and as the thione dimer in the solid state.

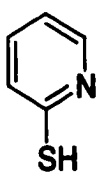

thiol

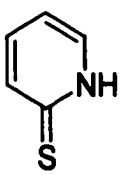

thione

The normal Raman of 2-MP at different pH values in aqueous solution has been investigated previously. Also the SERS of 2-MP with a Ag colloid was studied by Jung *et al* [10]. It was suggested that 2-MP chemisorbed on the metal surface mainly via a Ag-S bond, and that the nitrogen atom also plays a secondary role, i.e., the ring nitrogen could also bind to a surface Ag atom. The

orientation of 2-MP on the Ag electrode might be either flat or normal with respect to Ag surface depending on the surface coverage. We used the self-assembly method to form a monolayer of 2-MP on the roughened silver electrode. 2-MP binds to the surface upon breakage of the S-H bond and the formation of the Ag-S bond:

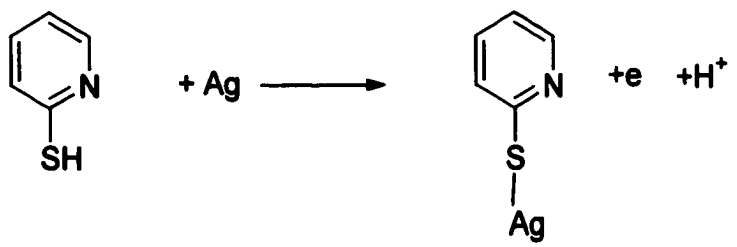

The advantage of SERS at a potential controlled electrode is that we can analyze any change in molecule orientation or change in binding site by monitoring the SERS bands with applied potential on the electrode, using the SERS selection rules.

Figure 5.4 showed the SERS of 2-MP monolayer on the silver electrode at –0.0V, -0.2V, -0.4V, -0.6V, -0.8V and –1.0V. The band assignments for the Ag electrode SERS are given in Table 5.2, according to the previous reference, and a comparison is made with the Ag colloid SERS.

From the table, we can see that the SERS taken on the electrode agrees closely with the SERS taken in the Ag colloid. The complete loss of the S-H stretching vibration, v(S-H), at 2570 cm^{-1} and the observation of a broad band at 190 cm^{-1} at potentials more negative than –1.0V confirms that 2-MP is adsorbed on the Ag electrode via its S atoms. This Ag-S vibration band is overlapped with surface Ag-Cl vibration band (ca. 220 cm^{-1}) at higher potentials. The intense 994cm^{-1} line represents aromatic ring breathing, which proves that the pyridine

ring is in the thiol form. It was also suggested that N probably also interact with the Ag surface since the molecule geometry is positioned for such an interaction. However there is no evidence for this assertion, since the Ag-N stretching frequency is in the range of surface Ag-Cl vibration. The use of other supporting electrolyte anions such as F^- or SO_4^{2-} did not show such intense spectra. Our experiments also show that the 2-MP film exhibited better stability against prolonged irradiation of laser light than thiol phenol (PhSH) film. Also a previous SERS study of 4-mercaptopyridine showed competition between Ag-S and Ag-N bonding. This might indicate that the N atom is involved in surface bonding interactions in 2-MP.

The frequency shift for each band is within ± 4cm^{-1} over the entire potential range. However, a significant intensity change vs. potential was observed. The relationship of the Raman intensity vs. applied potential for each band is shown in Figure 5.5a and Figure 5.5b. There are three types of profiles we obtained. Most bands, including 631 cm^{-1}, 994 cm^{-1} (ring breathing), 1044 cm^{-1} (C-H in plane bending), 1224 cm^{-1} and 1540 cm^{-1} (ring stretches) show a linear increase in intensity when the voltage is shifted from 0.0V to –1.0V. However, the band at 432 cm^{-1} showed an intensity decrease when the voltage was shifted negative. The 1077cm^{-1} (C-H bending/C-S stretching) and 1111 cm^{-1} (ring breathing/C-S stretching) show a maximum at –0.4 V and –0.3V, respectively. One might ask if the maximum is caused by a charge-transfer mechanism. However, a change of excitation laser wavelength from 647.1nm to 488nm did not change the position of the maximum, indicating that this is not a charge

transfer effect. On the other hand, the intensity change might be related to a molecular orientation change with the potential. The 432 cm^{-1} band contains a C-S bending mode and an out-of-plane ring deformation. According to SERS surface selection rule, if the pyridine ring is going from flat face-on orientation to a more normal one, the C-S bond also changes from flat to more normal with respect to the Ag surface. The SERS intensities of both C-S bending and out-of-plane ring deformation will decrease. Therefore, the negative potential shift results in a molecule orientation change from face-on to a more normal orientation. 1111 cm^{-1} band contains a ring breathing mode and a C-S stretching mode. When the molecule changes from a flat orientation to a more normal orientation, the breathing mode is expected to increase in intensity and C-S stretching mode is expected to decrease in intensity, a maximum is shown in the intensity vs. voltage profile.

The decrease in intensity for 432cm, 1077, 1111 cm^{-1} bands with potential is quite moderate compared to the dramatic increase of those in-plane and symmetric modes, which means that the orientation change is not the only factor contributing to the intensity. The potential dependency experiments show that the intensity at 631cm^{-1}, 994 cm^{-1}, 1044 cm^{-1}, and 1224 cm^{-1} bands increases linearly with a negative shift in potential before exhibiting an abnormal increase and then disappearing gradually at very negative potentials. Figure 5.6 shows the disappearance of SERS with time at 10s interval in pH=7 solution at –1.1V. The potential where the spectra disappeared is dependent on the pH of the supporting electrolyte. When the pH of supporting electrolyte changed from 3 to

12, the potential where the spectra disappeared changed from –0.8V to –1.3V. This is about a change of 56mV/pH. This might indicate that the cleavage of Ag-S bond occurs in one electron one proton reduction process, which is the reverse process for self-assembly process:

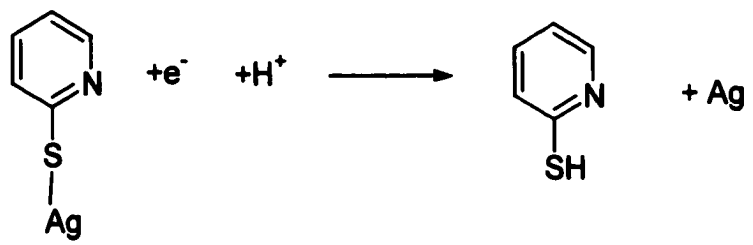

One interesting feature we have never found before is that for the SERS spectra of 2-MP directly bonded on a roughened electrode, the intensity increases at very negative potential until the species is reduced and the Ag-S bond is broken. This is different from the normal SERS voltage dependence, when a charge-transfer mechanism operates. It is possible that the resonance condition exists at much more negative potential which can not be observed because of the hydrogen evolution and/or desorption.

A similar phenomenon was also observed in the SERS of surfactants of Brij-35 and CTAB[13]. In the SERS of CTAB, there is an intensity maximum at ca. –0.5V, which was attributed to a resonant charge-transfer mechanism. However, when the potential is shifted to values more negative than –0.8V, the intensities of the C-H stretching bands increase dramatically until they reach a second maximum around –1.3V. When potential moves more negative than –1.3V, the SERS intensity decrease rapidly possibly due to the evolution of large amount of hydrogen gas, which destroys the surface. The large enhancement of the

intensity at second maximum might be attributed to the formation of adsorbed hydrogen.

Another interesting feature is that the SERS of the 2-MP monolayer showed a larger enhancement (about 5 times) than the SERS of piperidine. A possible reason is that the SERS intensity is proportional to the chemical bonding strength between adsorbate and metal. For N containing molecules, the interaction between molecule and metal is via adsorption or complexation, which is a weaker interaction compared to chemical bonding. A theoretical study[14] based upon the charge transfer theory suggested that the strength of chemical bonding between silver cluster and pyridine is related to Raman intensity. Another reason is that the self assembly process is actually a chemical reaction and a new molecule Ag-S-R exist on Ag electrode other than 2-MP. The addition of a Ag atom into the molecule will lead to a polarizability increase because of the large volume of the Ag atom.

Another observation that stands out is the small background in the SERS spectra of 2-MP, which remains almost the same at different potentials. For many SERS spectra, a potential dependent background continuum is exhibited, which has similar features to the SERS voltage dependence. The enhancement mechanism for the background was explained as a luminescence effect involving the metal bands.

5.4 Conclusions

1. Piperidine is adsorbed on the silver surface via N atom. From –0.0V to 0.9V, the surface concentration is nearly same on the electrode surface. The dramatic change of the SERS spectra with the potential is attributed to the two structural isomers of piperidine. The relative concentration of the two isomers is a function of potential applied. One species is dominant at potentials positive to –0.5V; the other species is dominant at potentials negative to –0.8V. Raman intensity vs. potential profiles for some of the bands exhibit two intensity maxima.

2. 2-Mercaptopyridine is adsorbed on the silver surface via Ag-S bonding forming a self-assembled monolayer. The C-S bond is tilted with respect to silver surface. When the applied potential moves to negative values, the C-S bond orients more towards the normal with respect to the Ag surface. 2-Mercaptopyridine exhibits a stronger enhancement on silver surface than piperidine. A possible reason is that the chemical bond formed with Ag-S is stronger than the weak adsorption between Ag and N, and the enhancement factor is related to the chemical bonding between adsorbate and metal through the polarizability of the molecule.

References

(1) Lombardi, R. L. Birke, Tianhong Lu and Jia Xu, J. Chem. Phys. **1986**, 84(8), 4174-4180

(2) T. E. Furtak and S. H. Macomber, Chem. Phys. Letters, **1983**, 95, 328

(3) T. E. Furtak and D. Roy, Phys. Rev. Lett, **1983**, 50, 1301

(4) S. Venkatersan, Gayle Erdheim, John R. Lombardi and Ronald L. Birke, Surface Science **1980**, 101, 387-398

(5) Otto, J. Electron Spectrosc. Relat. Phenom. **1982**, 44, 105

(6) Luis A. Sanchez, Ronald L. Birke, and John R. Lombardi, J. Phys. Chem. Vol. 88(9), 1984.

(7) Pemble, M.E. Ph.D. Thesis, University of Southampton, Southampton, England, 1980.

(8) Jean A, Baldwin, Blanka Vickova, Mark P. Andrews, and Ian S. Butler, Langmuir, **1997**, 13, 3744-3751

(9) Yoon Soo Pang, Hyun Jin Hwang, Myung Soo Kim, J. Mol. Struct. **1998**, 441, 63-67

(10) Hee Sook Jung, Kwan Kim, Myung Soo Kim, J. Mol. Struct. **1997**, 407, 139-147

(11) T. Sueoka, J. Inukai and M Ito, J. Electron Spectroscopy and Related Phenomena, **1993**,64/65, 263-270

(12) W. H. Li, B. W. Mao and Z. Q. Tian, J. Raman. Spectroscopy, **1995**, 26, 233-237

(13) Suncheng Sun, Ronald L. Birke and John R. Lombardi, J. Phys. Chem. **1990**, 94, 2005-2010

(14) Jun-Ho Chol and Hojing Kim, Bull. Korean Chem. Soc., 14(3), **1993**

Table 5.1 Band (cm^{-1}) Assignments for Piperidine [6]

NR[6] (in 0.1M KCl)	SERS (at –0.6V)	Vibrational Assignment
	302	
412	432	A' skel def
351	456	A'' skel def
	586	
814	809	A' skel str
	844	A' ext def $(CH_2)_r$
864	865	A'' skel str
1017	965	A' ext def $(CH_2)_r$
1035	1016	A' skel str
1054	1046	A'' ext def $(CH_2)_r$
1157	1151	A' ext def $(CH_2)_t$
1176	1176	A'' ext def $(CH_2)_t$
1269	1256	A'/A'' ext def $(CH_2)_t$
1294		A'/A'' ext def $(CH_2)_w$
1348	1348	A''
1449	1378	
1462	1446	A' CH_2 scissor

Table 5.2 Band (cm^{-1}) Assignments for 2-MP [8]

SERS (at -1.0V)	Ag colloid	Vibrational Assignment
432	435	A'' δ(C-S)/β(CCC)
481	485	
631	634	A'' γ(CCC)
715	720	A' ν(C-S)/ β(CC)
994	998	A' 1a (ring breathing)
1044	1048	A' 18a, β(CH)
1077	1084	A' 18b (CH) + ν(C-S)
1111	1117	A' 12a ring breathing + ν(C-S)
1224	1228	
1404	1411	A' 19a ν(C=C/C=N)
1540	1549	A' 8b ν(C=C)
1573	1579	A' 8a ν(C=C)

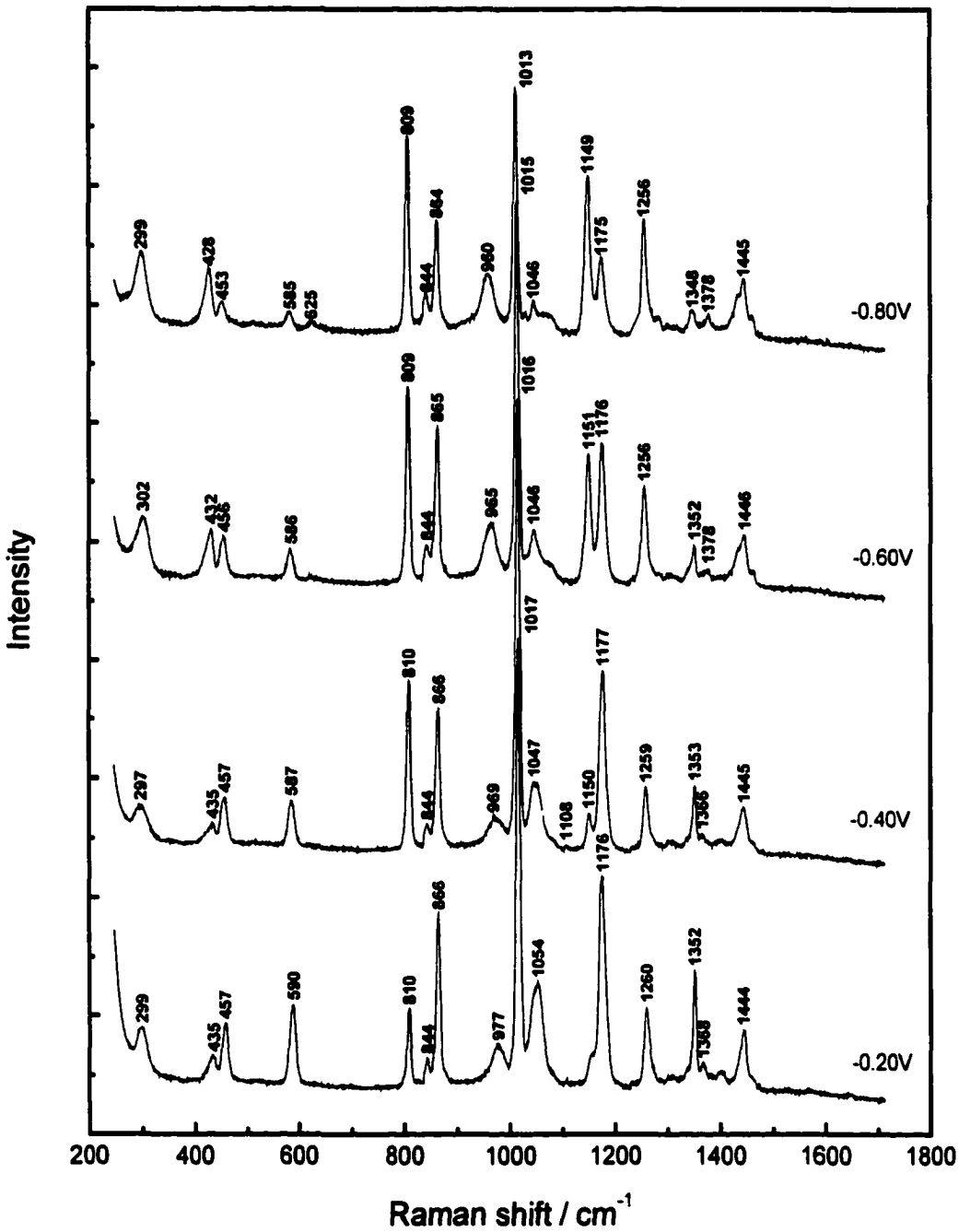

Figure 5.1 SERS of piperidine on Ag electrode, excitation: 647.1nm

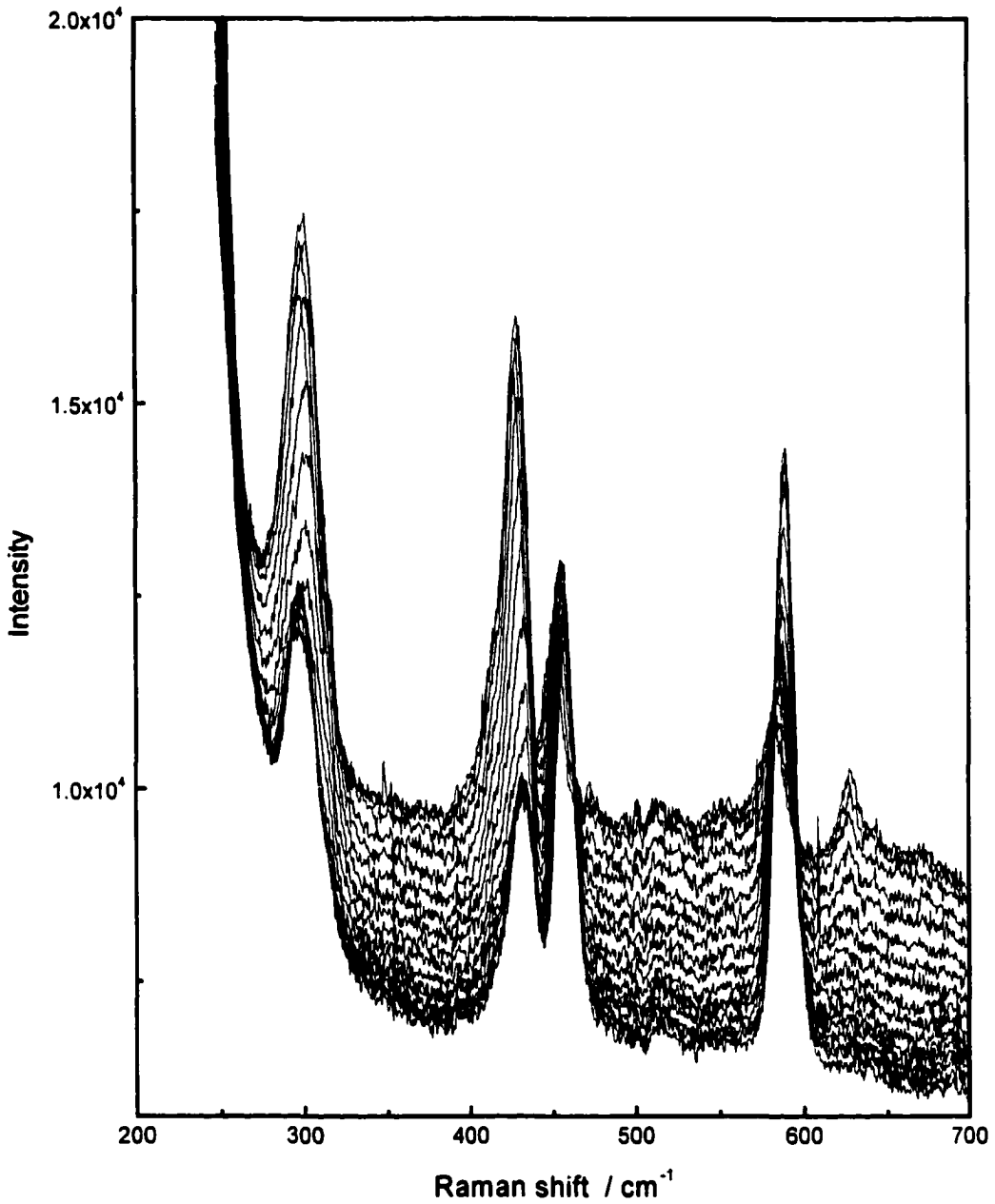

Figure 5.2a SERS of piperidine at different electrode potentials (from bottom to top: 0.0V to –0.90V, 0.05V interval)

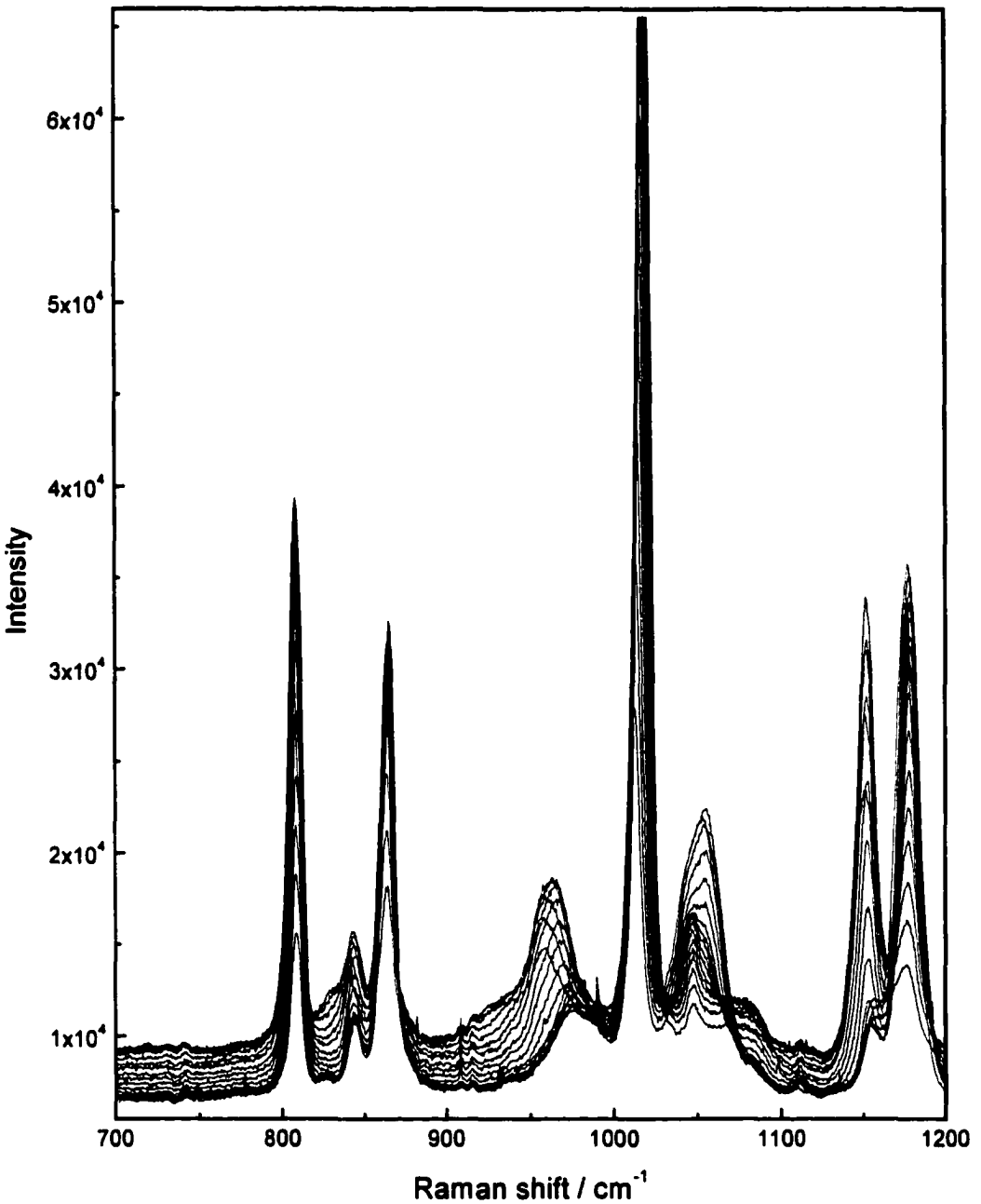

Figure 5.2b SERS of piperidine at different electrode potentials (from bottom to top: 0.0V to –0.90V, 0.05V interval)

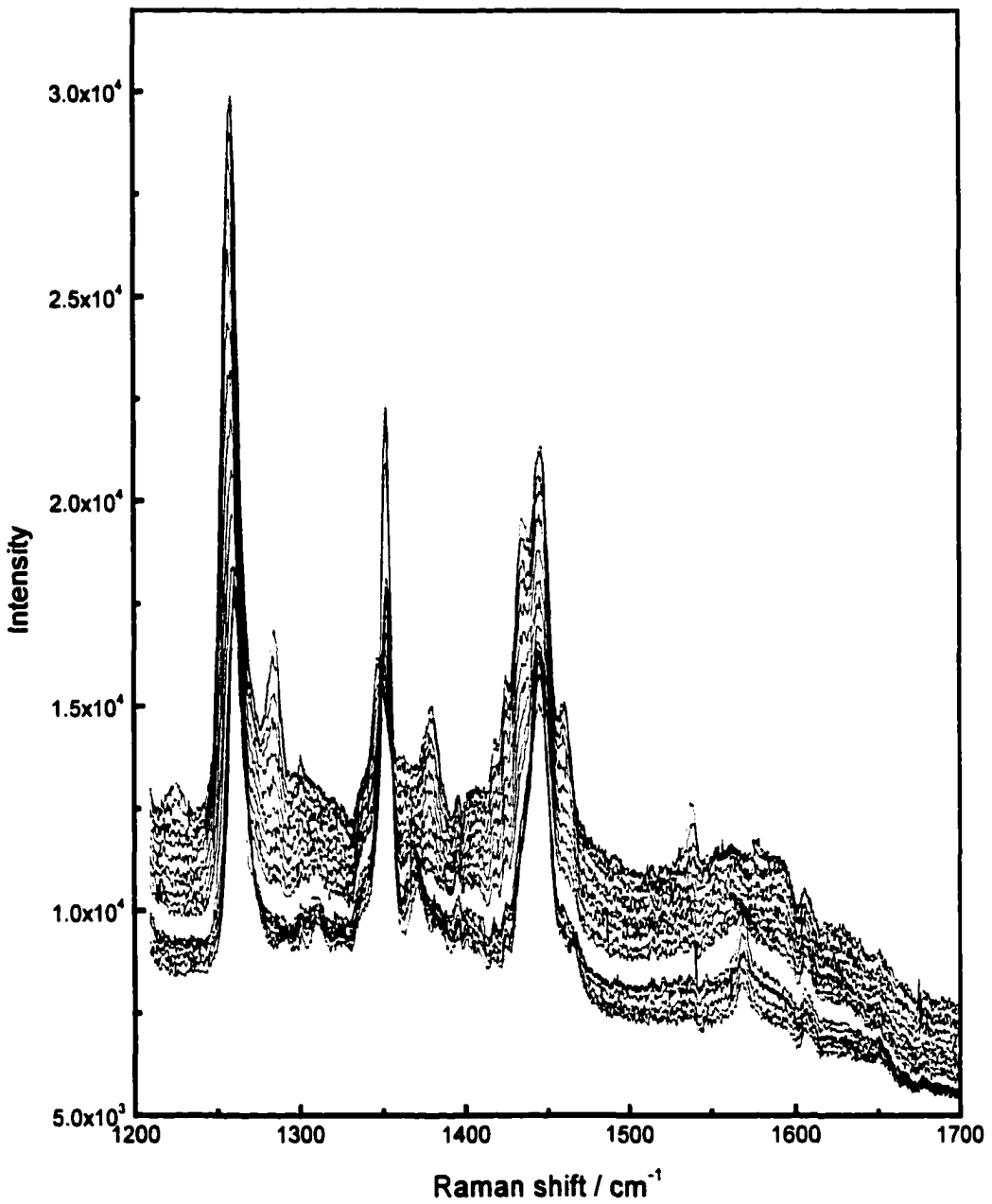

Figure 5.2c SERS of piperidine at different electrode potentials (from bottom to top: 0.0V to –0.90V, 0.05V interval)

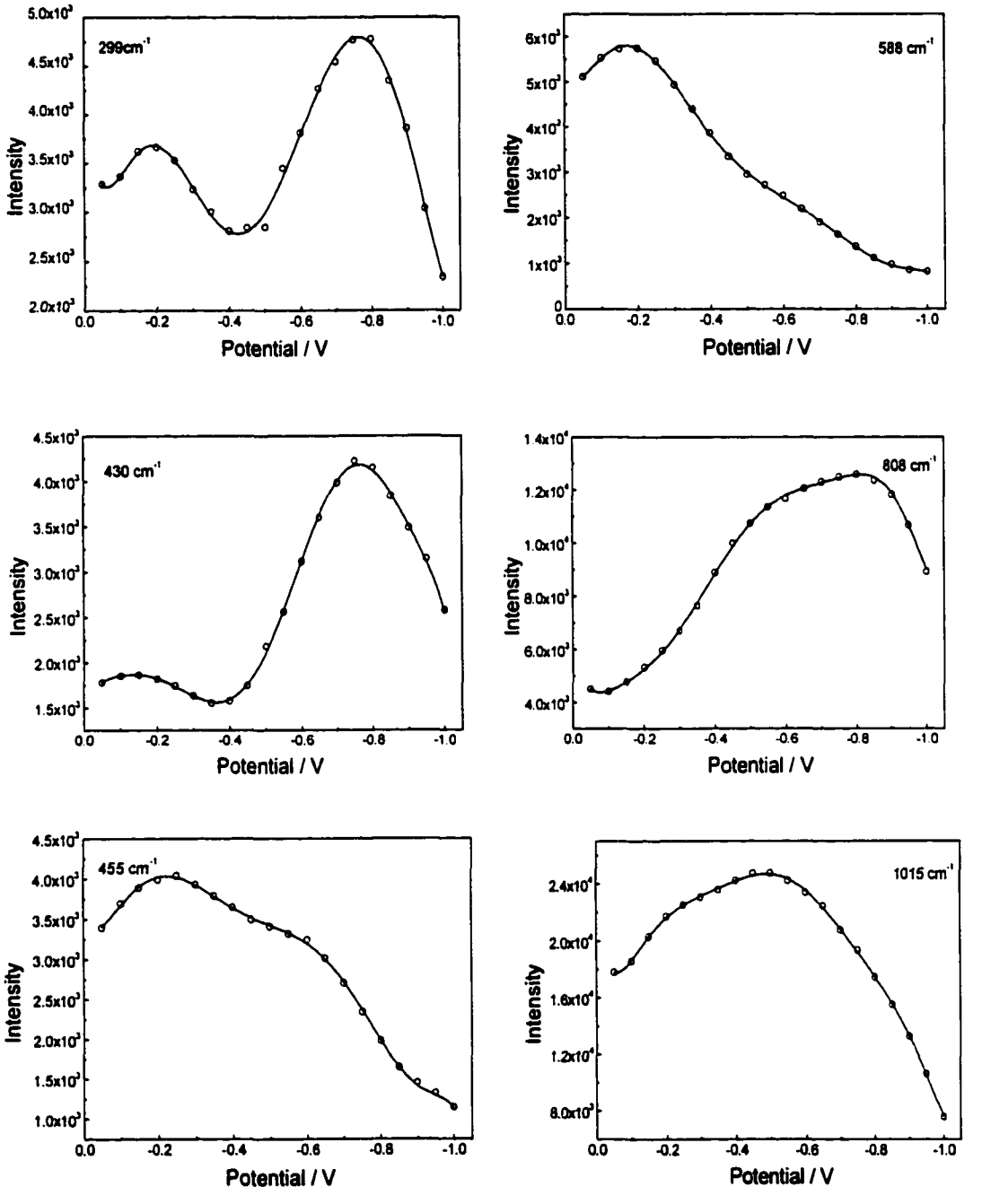

Figure 5.3a Intensity ~ potential profiles for some selected bands in SERS of piperidine

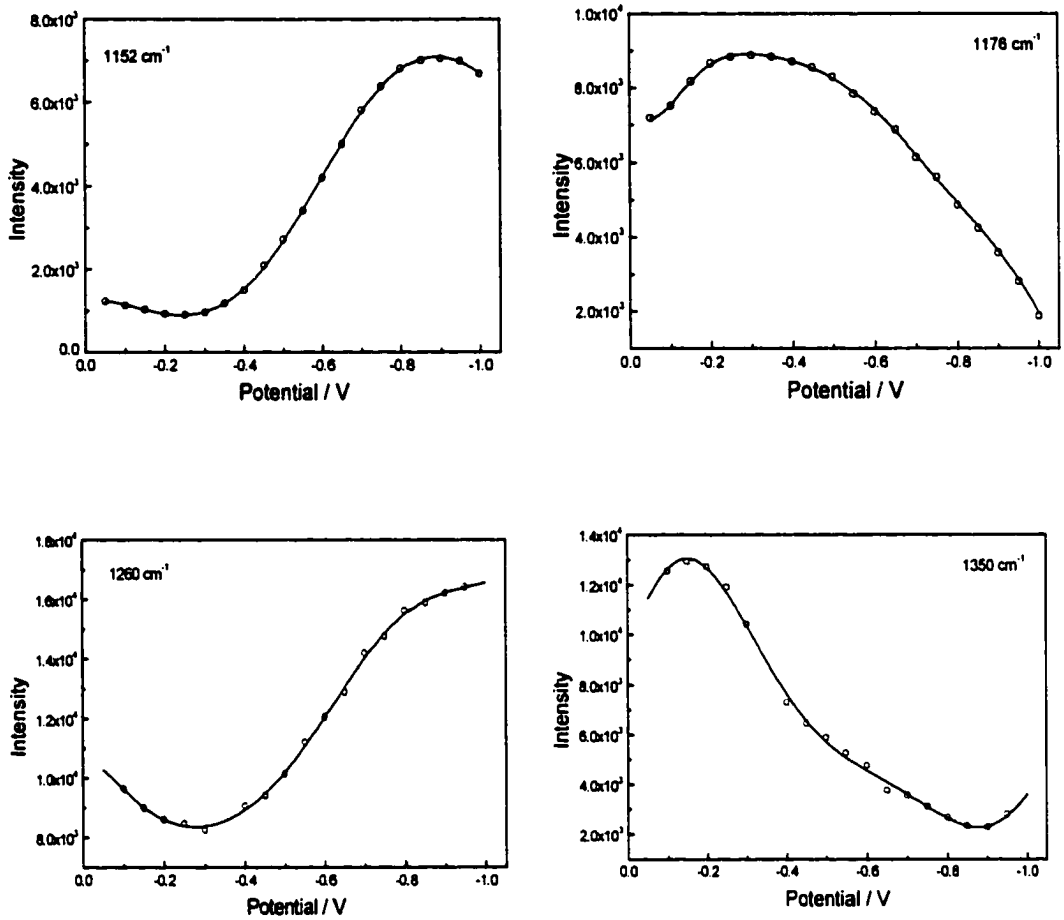

Figure 5.3b Intensity ~ potential profiles for some selected bands in SERS of piperidine

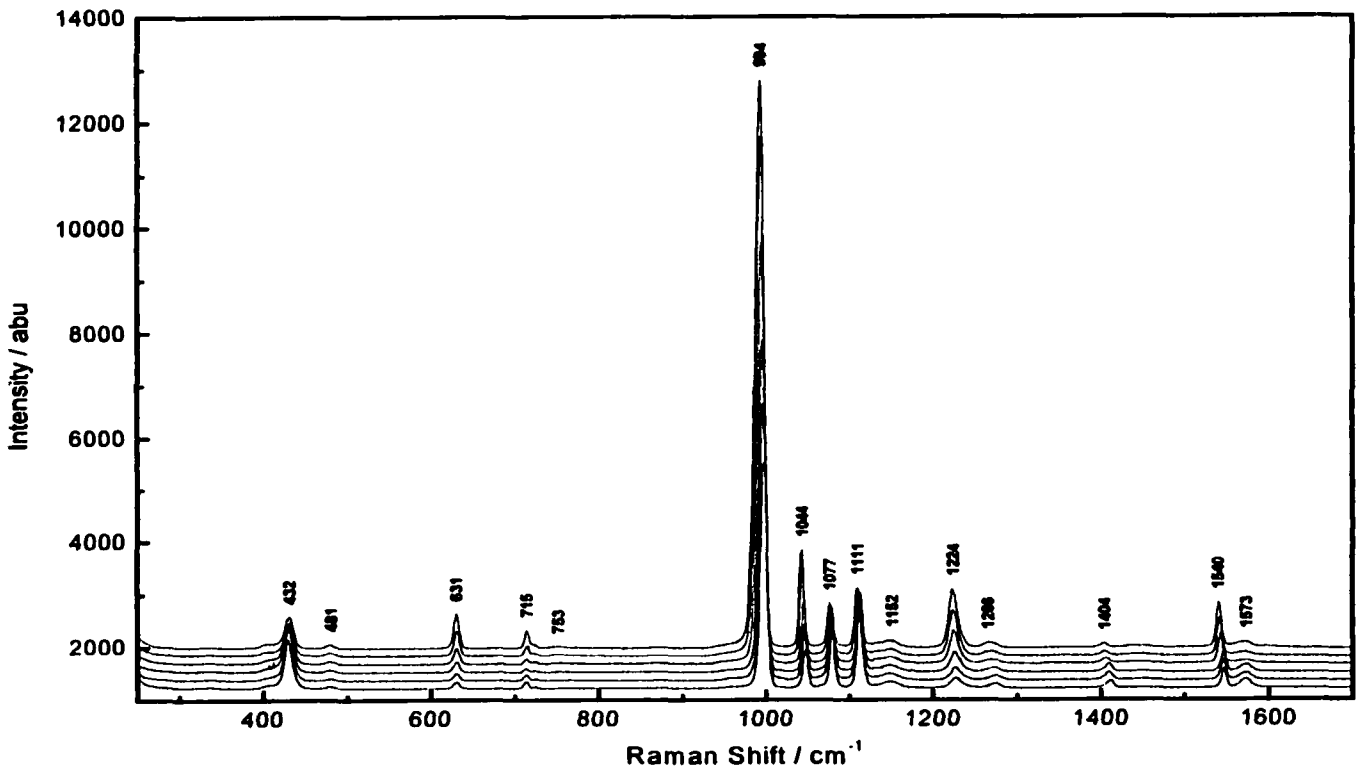

Figure 5. 4 SERS of 2-MP on the Ag electrode at different potentials (from bottom to top: 0.0V, -0.20V, -0.40V, -0.60V, -0.80V, and –1.0V vs. SCE)

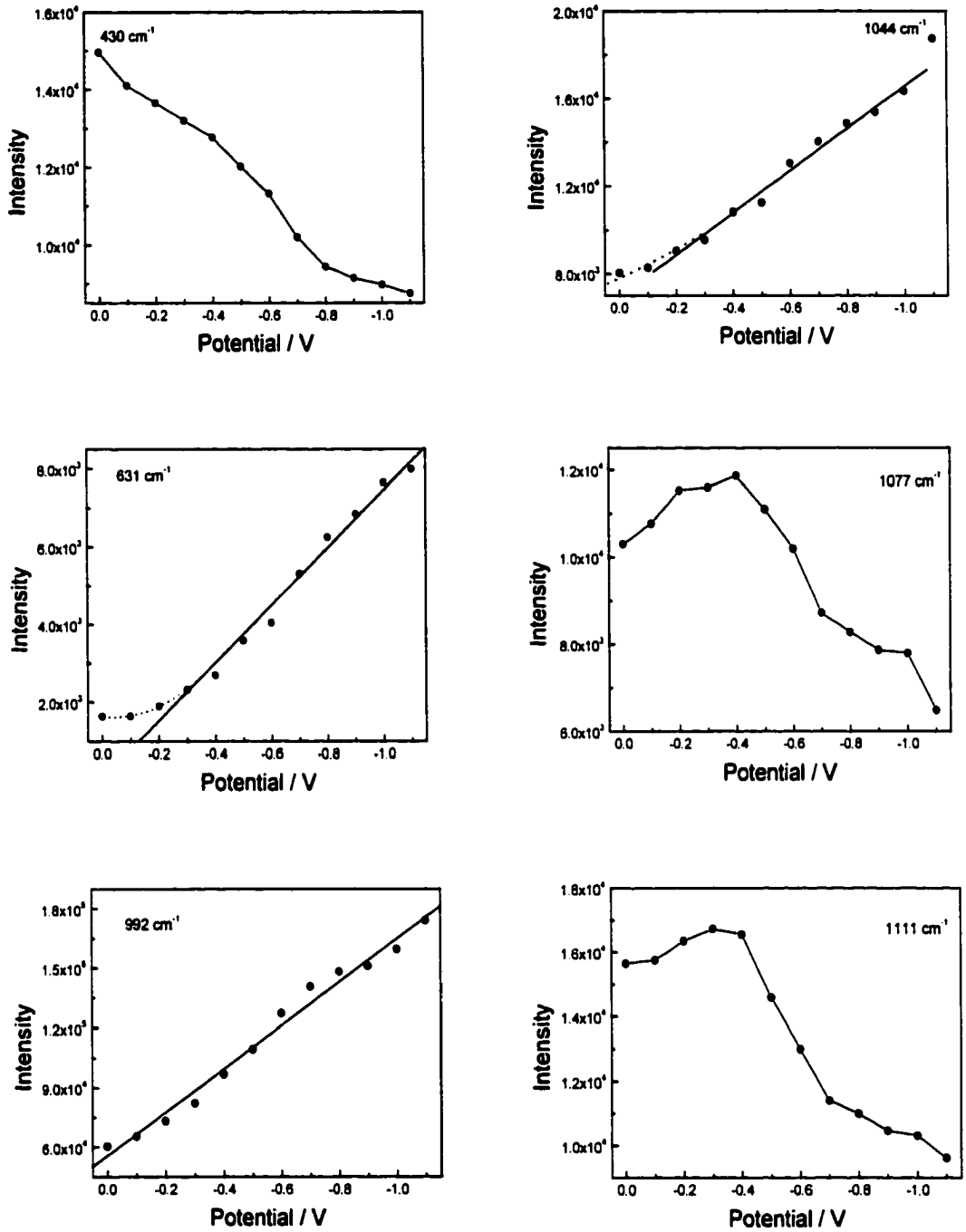

Figure 5.5a Intensity ~ potential profiles for some selected bands in SERS of 2-MP

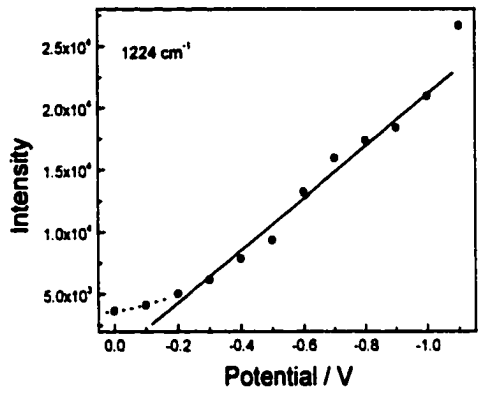

Figure 5.5b Intensity ~ potential profiles for some selected bands in SERS of 2-MP

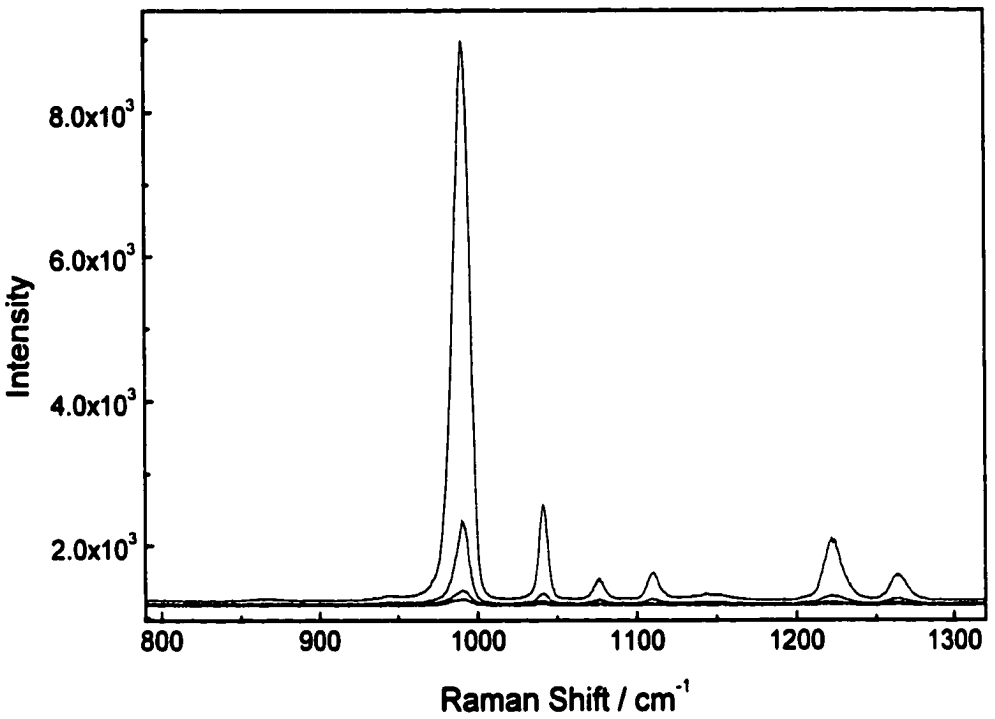

Figure 5.6 SERS of 2-MP decayed with time, time interval 10s, pH=7, at potential –1.1V.

BIBLIOGRAPHY

CHAPTER 1

(1) Advances in Catalysis; D. D. Eley, H. Pines and P. B. Weisz, Eds.; Academic Press, Inc.; Orlando, **1985**

(2) J Kijenski and A. Baiker; Catalysis Today, **1989**, 5, pp1-107

(3) Laser-Controlled Chemical Processing of Surfaces, Materials Research Society Symposia Proceedings, V29; A. W. Johnson, D. J. Ehrlich and H. R. Schlossberg, Eds.; North Holland, New York, **1984**

(4) S. R. Morrison; Electrochemistry at Semiconductor and Oxidized Metal Electrodes; Plenum Press, New York, **1980**

(5) Advances in Corrosion Science and Technology, Vol. 7; M. G. Fontana Chapman and Hall, London, **1985**

(6) G. Wranglen; An Introduction to Corrosion and Protection of Metals; Vol. 28; F. Mansfeld, Ed.; Marcel Dekker, New York, **1987**

(7) X. L. Zhou and J. M. White; Surf. Sci., **1988**, 194, 438

(8) X. Y. Zhu, S. Akhter, M. E. Castro and J. M. White; Surf. Sci., **1988**, 195, L145

(9) Low Energy Electron Diffraction: Experiment, Theory and Surface Structure Determination; Springer Series in Surface Sciences, Vol. 6; M.

A. Van Hove, W. H. Weinberg, C. M. Chan, Eds., Springer-Verlag, **1986**, Berlin, New York, 1986 (LEED).

(10) J. Dericbourg; Surf. Sci., **1992**, 269/270, 1157

(11) Scanning Tunneling Microscopy 1: Springer Series in Surface Sciences, Vol. 20; D. Anselmetti, et. al. Eds., Springer-Verlag, Berlin, 1986, Berlin, New York, **1986**

(12) G. Bracco, M. Canepa, P. Cantini, F. Fossa, L. Mattera, S. Terreni and D. Truffelli; Surf. Sci., **1992**, 269/270, 61

(13) A, Ausmees, M. Elango, A. Kikas, E. Nommiste and A. Saar; Surf. Sci., **1992**, 269/270, 583

(14) H. Ibach, M. Balden, D. Bruchmann and S. Lehwald; Surf. Sci., **1992**, 269/270, 94

(15) Vibrational Spectroscopies for Adsorbed Species, ACS Symposium Series, 137; A. T. Bell and M. L. Hair, Eds.; American Society; Washington. D. C., **1980**

(16) A. Smekal, Naturwiss, **1928**, 11, 873

(17) C. V. Raman and K. S. Krishnan; Nature, 1928, 121, 501

(18) M. Fleischmann and I. R. Hill; in 'Raman Spectroscopy'; Palph. E. White, J. O'M. Bockris (eds); Comprehensive Treatise of Electrochemistry, Vol.8, Plenum Press, **1984**, New York and London, pp373-432

(19) R. L. Birke and J. R. Lombardi; 'Surface-Enhanced Raman Scattering', in J. R. Gale (ed.), Spectroelectrochemistry: Theory and Practice, Plenum Press, Mew York, **1988**, pp263-348

(20) A. C. Albrecht; J. Chem. Phys., **1961**, 34, 1476

(21) M. Fleischman, P. J. Hendra and A. J. McQuillan; J. Chem. Phys. Letter, **1974**, 26, 163

(22) D. L. Jeanmaire and R. P. VanDuyne; J. Electroanal. Chem., **1977**, 84, 1-20

(23) M.G. Albrecht and J. A. Creighton; J. Am. Chem. Soc.; **1977**, 99, 5215

(24) R. P. Van Duyne; in 'Chemical and Biochemical Applications of Lasers'; C. B.Moore Ed.; Academic Press, New York, **1979**, Vol.4, pp101-184

(25) R. L. Paul. A. J. McQuilan, P. J. Hendra, and M. Fleischman; J. Electroanal. Chem., **1975**, 66, 248

(26) M. L. A. Temperini, H. C. Chagas, and O. Sala; Chem. Phys. Letters; **1981**, 79(1), 75

(27) J. R. Lombardi, and R. L. Birke; Surf. Sci.; **1980**, 95, 1259

(28) M. Fleischman, I. R. Hill, and G. Sundholm; J. Electroanal. Chem., **1983**, 157(2), 259

(29) M. Fleischman, I. R. Hill, and G. Sundholm; J. Electroanal. Chem., **1983**, 157(1), 153

(30) L. –W. H. Leung, M. J. Weaver, J. Sm. Chem. Soc.; **1987**, 109, 5113

(31) M. Fleischmann, Z. Q. Tian, L. J. Li; J. Electroanal. Chem.; **1987**, 217, 397

(32) Jia Xu, 'Surface-enhanced Raman Spectroscopy on Electrodes: Enhancement Mechanisms and Application to the studies of Flavin Molecules" PH.D thesis, 1987, The City University of New York

(33) T. M. Davine, in 'Electrochemical and Optical Techniques for the Study and Monitoring of Metallic Corrosion', M. G. S. Ferroira and C. A. Melendres (eds). Kluwer Academic Publishers, **1991**, 389-437

(34) J. A. Creighron, M. G. Albrecht, R. E. Hester, and J. A. D. Matthew; Chem. Phys. Letters, **1978**, 55, 55

(35) D. L. Jeanmaire, and R. P. Van Duyne; J. Electroanal. Chem., **1977**, 84, 1

(36) R. R. Smardzewski, R. J. Coltion, and J. S. Murday; Chem. Phys. Lett., **1979**, 68(1), 53

(37) J. E. Rowe, C. V. Shank, D. A. Zwemer, and C. A. Murray; Phys. Rev. Lett., **1980**, 44(26), 1770

(38) H. Seki, and R. Philpott; J. Chem. Phys., **1980**, 73(10), 5376

(39) J. D. Jackson, Classical Electrodynamics, 2nd Edition, John Wiley and Sons, New York, **1975**, p50

(40) S. Efrima, and H. Metiu; J. Chem. Phys. **1979**, 70, 1602, 2297, 1939

(41) F. W. King, R. P. Van Duyne, and G. C. Schatz; J. Chem. Phys.; **1978**, 69, 4472

(42) A. Otto; Surf. Sci.; **1978**, 75, L392

(43) A. Otto, in: Proc. Conf. On Vibrations in the Adsorbed Layer, Jülich, Germany, **1978**, p162

(44) S. L. McCall, and P. M. Platzman; Bull. Am. Phys. Soc. **1979**, 24, 340

(45) A. Otto, J. Timper, J. Billmann, G. Kovacs and I. Pockrand; Surf. Sci., **1980**, 92, L55

(46) R.K. Chang; 'Raman Spectroscopic Techniques in Interfacial Electrochemistry', in C. Gutierrez and C. Melendres (eds.), Spectroscopic and Diffraction Techniques in Interfacial Electrochemistry, Kluwer Academic Publishers, Netherlands, pp155-180

(47) J. A. Creighton; 'The Selection Rules for Surface-Enhanced Raman Spectroscopy', in R. J. H. Clark and R. E. Hester (eds.), Spectroscopy of Surfaces, Hohn Wiley and Sons Ltd., 1988, pp57-89

(48) P. B. Johnson and R. W. Christy; Phys. Rev., **1972**, B6, 4370

(49) H. J. Hagemann, W. Gudet, and C. Kunz; J. Opt. Soc. Am., **1975**, 65, 742

(50) R. L. Birke, and J. R. Lombardi; 'Surface Enhanced Raman Scattering', in J. R. Gale (ed.), Spectroelectrochemistry: Theory and Practice' Plenum Press, New York, **1988**, 263-348

(51) R. L. Birke, T. Lu, and J. R. Lombardi: 'Surface-enhanced Raman Spectroscopy', in R. Varmi and J. R. Selman (eds.), Techniques for the characterization of Electrodes and Electrochemical Process, John Wiley and Son, Inc., New York, **1992**, 211-277

(52) A. Otto, in 'Light Scattering in Solids III', (M. Cardona and G. Guntherodt. Eds.), Springer-Verlag, Heidelberg.

(53) G. J. Schulz, in 'Principles of Laser Plasmas" (George Bekefi, ed.), Wiley, New York, **1976**, 33

(54) John R. Lombardi, Ronald L. Birke, Tianhong Lu and Jia Xu; J. Chem. Phys., **1986**, 84(8), 4174

(55) E. Koglin and J. M. Sequaris; in 'Analytical Problems', Springer-Verlag, Berlin Heidelberg, New York, Tokyo, **1986**, Vol.134, pp1

(56) T. M. Cotton; in 'Surface and Interfacial Aspects of Biomedial Polymers', J. D. Andrade, (Ed.), Plenum Press, New York, **1985**, vol.2, pp161-187

(57) Y. J. Chen, G. M. Carter and S. K. Tripathy; Solid State Commun., **1985**, 54, 19

(58) R. Aroca and D. Battisti; Langmuir, 1990, 6, 250

(59) R. Aroca and U. Guhathakurta-Ghosh; J. Am. Chem. Soc., **1989**, 111, 7681

(60) J. H. Kim, T. M. Cotton, R. A. Uphaus and D.Mobius; J. Phys. Chem., **1989**, 93, 3713

(61) T. M. Cotton, R. A. Uphaus and D. Mobius; J. Phys. Chem., **1986**, 90, 6071

(62) M. Takahashi, M. Goto and M. Tto; J. Electroanal. Chem., **1989**, 93, 3753

(63) P. J. Tarcha, T. E. Rohr, J. J. Markese and T. Cotton; Surface Enhanced Raman Spectroscopy Immunoassay or Other Specific-Binding Assay, Eur. Pat. Appl. Ep587, 008, Mar., **1994**, US Appl. 944, 138, Sept., **1992**

(64) I. Nabiev, I. Chourpa and M. Manfait; J. Raman Spectrosc., **1994**, 25(1), 13

(65) S. L. Wright, K. J. Latas, A. N. Mortensen, E. A. Orr, J. V. Paukstelis, R. M. Hammaker and W. G. Fateley; Proc. SPIE-Int. Soc. Opt. Eng., **1993**, 1857

(66) T Vo-Dinh; in 'XVth International Conference on Raman Spectroscopy', edited by S. A. Asher and P. B. Stein, **1996**, pp1210

(67) Therese. M. Cotton, Steven G. Schultz, Richard P. Van Duyne; J. Am. Chem. Soc., **1980**, 102, 7960-7962

(68) James F. Rusling and Alaa-Eldin F. Nassar; J. Am. Chem. Soc., **1993**, 115, 11891-11897

(69) Lars H. Eng, Vicki Schlegel, Danli Wang, et al.; Langmuir **1996**, 12, 3055-3059

(70) Katrin Kneipp, Yang Wang, Ramachandra R. Dasari, and Michael S. Feld; Applied Spectroscopy, **1995**, 49(6), 780

(71) Ronald L. Birke, Chongtie Shi, Wei Zhang, and John R. Lombardi; J. Phys. Chem. B, **1998**, 102(41), 7983

(72) Chongtie Shi, Wei Zhang, Ronald L. Birke and John R. Lombardi; J. Electroanal. Chem., **1997**, 423, 67

(73) Chongtie Shi, Wei Zhang, John R. Lombardi and Ronald Birke; J. Phys. Chem., **1992**, 96(25), 10093

(74) Wei Zhang, Alberto Vivoni, John R. Lombardi, and Ronald L. Birke; J. Phys. Chem., **1995**, 99(34), 12846

(75) T.M. Cotton, G. Chumanov, M. Sibbald and J. Zheng; in 'XVth International Conference on Raman Spectroscopy', Edited by S. A. Asher and P. B. Stein, **1996**, pp28

(76) C. K. Chen, T. F. Heinz, D. Rcard and Y. R. Shen; Chem. Phys. Lett., **1981**, 83(3), 455

(77) k. Kneipp; J. Molec. Struct.; **1990**, 218, 357

(78) S. Sun, R. L. Birke and J. R. Lombardi; J. Phys. Chem.; **1988**, 92, 5965

(79) Ronald L. Birke and John R. Lombardi; Molecular Engineering, **1994**, 4, 277

CHAPTER 3

(1) Abelleira, A.; Galang, R. D.; Clarke, M. J., Inorg. Chem. **1990**, 29, 633-639

(2) Ladenstein, R.; Ritsert, K.; Huber, R.; Richter, G.; Bacher, A., Eur. J. Biochem. **1994**, 223, 1007-1017.

(3) O'Kane, D. J.; Lee, J., Biochemistry, **1985**, 24, 1467-1475.

(4) Xu, Jia; Birke, R. L.; Lombardi, J. R., J. Am. Chem. Soc. **1987**, 109, 5645.

(5) Wei, Zhang; Vivoni, A.; Lombardi, R. J.; Birke, R. L., J. Phys. Chem. **1995**, 99, 12846-12857.

(6) Shi, Chongti, Zhang, Wei, Lombardi, J. R.; Birke, R. L., J. Phys. Chem. **1992**, 96, 10093-10096.

(7) Burgmayer, S. J.; Nieter, Inorg. Chem. **1988**, 27, 4059-4065.

(8) Goodgame, M.; Schmidt, Inorg. Chim. Acta **1979**, 36, 151-154.

(9) Lehnen, J.; White, B. M.; Kendric, M. J., Inorg. Chim. Acta **1990**, 167, 257-259.

(10) Heilman, O.; Hornung, F. M.; Kaim, W.; Fiedler, J., J. Chem. Soc., Faraday Trans. **1996**, 92, 4233-4238.

(11) Lee, J.; Wang, Yanyun; Gibson, B., Biochemistry **1991**, 30, 6825-6835.

(12) O'Kane, D. J.; Lee, J., Biochemistry **1984**, 24, 1484-1488.

(13) Visser, A. J. W. G.; Lee, J., Biochemistry **1980**, 19, 4366-4372.

(14) Lee, J.; O'Kane, D. J.; Visser, A. J. W. G., Biochemistry **1985**, 24, 1476-1483.

(15) Glenn Dryhurst, Electrochemistry of Biological Molecules **1977**

(16) Foresman, J. B.; Frisch, A. Exploring Chemistry with Electronic Structure Methods, 2nd ed., Gaussian: Pittsburgh, PA, 1995-96.

(17) Nishina, Y.; Kitagawa, T.; Shiga, K.; Horiike, K.; Matsumura, Y.; Watari, H.; Yamano, T. J. Biochem. (Tokyo) **1978**, 84, 925-932.

(18) Kitagawa, T.; Nishina, Y.; Kyogoku, Y.; Yamano, T.; Ohishi, N.; Takai-suzuki, A.; Yagi, K. Biochemistry **1979**, 18 (9), 1804-1808.

(19) Vervoort, J.; O'Kane, D. J.; Carreira, L. A.; Lee, J. Identification of a Lumazine protein from Photobacterium Leignathi by Coherent Anti-strokes Raman Spectroscopy. Photochem. Photobiol. **1993**, 37 (no. 1), 117-119.

(20) Irwin, Richard M.; Visser, A. J. W. G.; Lee, John; Carreira, Lionel A. Protein-Ligand Interactions in Lumazine Protein and in Desulfovibrio Flavodoxins from Resonance Coherent Anti-Strokes Raman Spectroscopy. Biochemistry **1980**, 19, 4639-4446.

(21) Brutovsky, B.; Ulicny, J.; Miskovsky, P.; Lisy, V.; Chinsky, L. Resonance Raman Spectra of Selected Pterin Molecules. Genetic Algorithms Approach to Force Field Scaling. J. Raman Spectrosc. **1998**, 29, 833-839

(22) Norrestam, R.; Stensland, B.; Soderberg, E. The Crystal and Molecular Structure of Lumazine Hydrate. Acta Crystallog., B **1972**, 28, 659.

(23) Cotton, F. A.; Wilkinson, G. Advanced Inorganic Chemistry, 4th ed.; Wiley & Sons: New York, 1980, p 969.

(24) Benecky, M.; Yu, T.-J.; Watters, K. L.; McFarland: Metal-Flavin Complexation A resonance Raman Investigation. Biochim. Biphys. Acta **1980**, 627, 197.

(25) P. N. Moorthy and E. Hayon; J. Phys. Chem., **1975**, 79 (11).

(26) Inorganica Chimica Acta, **1979**, Vol. 36, 151-154.

CHAPTER 4

(1) Abelleira, A.; Galang, R. D.; Clarke, M. J. Synthesis and Electrochemistry of Pterins Coordinated to Tetraammineruthenium (II) (Inorg. Chem. **1990**, 29, 633-639).

(2) Ladenstein, R.; Ritsert, K.; Huber, R.; Richter, G.; Bacher, A. The Lumazine Synthase/Riboflavin Synthase complex of Bacillus Subtilis X-ray Structure Analysis of Hollow Reconstituted B-Subunit Capsids. Eur. J. Biochem. **1994**, 223, 1007-1017.

(3) O'Kane, D. J.; Lee, J. Chemical Characterization of Lumazine Protein from Photobacterium leignathi: Comparison with Lumazine Protein from Photobacterium. Biochemistry, **1985**, 24, 1467-1475.

(4) Xu, Jia; Birke, R. L.; Lombardi, J. R. Surface-Enhanced Raman Spectroscopy from Flavins Adsorbed on a Silver Electrode: Observation of the Unstable Semiquinone Intermediate. (J. Am. Chem. Soc. **1987**, 109, 5645.

(5) Wei, Zhang; Vivoni, A.; Lombardi, R. J.; Birke, R. L. Time Resolved SERS Study of Direct Photochemical Charge-Transfer Between FMN and a Silver Electrode. J. Phys. Chem. **1995**, 99, 12846-12857.

(6) Shi, Chongti, Zhang, Wei, Lombardi, J. R.; Birke, R. L. Nanosecond Time Scale Kinetics in the Flavin Mononucleotide on an Electrode Surface Using Time-Resolved Surface-Enhanced Raman Spectroscopy. J. Phys. Chem. **1992**, 96, 10093-10096.

(7) Burgmayer, S. J.; Nieter, Transition-Metal Pteridine Complexes. Preparation and Characterization of Cobalt (II) Pteridines. Inorg. Chem. **1988**, 27, 4059-4065

(8) Goodgame, M.; Schmidt, A. Metal Complexes of 2, 4-(1H,3H)-Pteridinedione. Inorg. Chim. Acta **1979**, 36, 151-154

(9) Lehnen, J.; White, B. M.; Kendric, M. J. Electrochemical Studies of Biologically Significant Pterin Compounds. Inorg. Chim. Acta **1990**, 167, 257-259

(10) Heilman, O.; Hornung, F. M.; Kaim, W.; Fiedler, J. Structure, EPR, UV-VIS and IR Spectroelectrochemistry of Reversibly Reducible Compounds $[(C_5Me_5)IrCl(L)](PF_6)$, L = 1,3-dimethyllumazine or 1,3-dimethylalloxazine. J. Chem. Soc., Faraday Trans. **1996**, 92, 4233-4238

(11) Lee, J.; Wang, Yanyun; Gibson, B. Electronic Excitation Transfer in the Complex of Lumazine Protein with Bacterial Bioluminescence Intermediates. Biochemistry **1991**, 30, 6825-6835

(12) O'Kane, D. J.; Lee, J. Physical Characterization of Lumazine Proteins from Photobacterium. Biochemistry **1984**, 24, 1484-1488

(13) Visser, A. J. W. G.; Lee, J. Lumazine Protein from the Bioluminescent Bacterium Photobacterium phosphoreum. A Fluorescence Study of the Protein-Ligand Equilibrium. Biochemistry **1980**, 19, 4366-4372

(14) Lee, J.; O'Kane, D. J.; Visser, A. J. W. G. Spectral Properties and Function of Two Lumazine Proteins from Photobacterium. Biochemistry **1985**, 24, 1476-1483

(15) Birke, R. L.; Lombardi, J. R. In Spectroelectrochemistry: Theory and Practice; Gale, James R., Ed.; Plenum: New York, 1988.

(16) Foresman, J. B.; Frisch, A. Exploring Chemistry with Electronic Structure Methods, 2nd ed., Gaussian: Pittsburgh, PA, 1995-96.

(17) Nishina, Y.; Kitagawa, T.; Shiga, K.; Horiike, K.; Matsumura, Y.; Watari, H.; Yamano, T. J. Biochem. (Tokyo) **1978**, 84, 925-932

(18) Kitagawa, T.; Nishina, Y.; Kyogoku, Y.; Yamano, T.; Ohishi, N.; Takai-suzuki, A.; Yagi, K. Biochemistry **1979**, 18 (9), 1804-1808

(19) Vervoort, J.; O'Kane, D. J.; Carreira, L. A.; Lee, J. Identification of a Lumazine protein from Photobacterium Leignathi by Coherent Anti-strokes Raman Spectroscopy. Photochem. Photobiol. **1993**, 37 (no. 1), 117-119

(20) Irwin, Richard M.; Visser, A. J. W. G.; Lee, John; Carreira, Lionel A. Protein-Ligand Interactions in Lumazine Protein and in Desulfovibrio Flavodoxins from Resonance Coherent Anti-Strokes Raman Spectroscopy. Biochemistry **1980**, 19, 4639-4446

(21) Brutovsky, B.; Ulicny, J.; Miskovsky, P.; Lisy, V.; Chinsky, L. Resonance Raman Spectra of Selected Pterin Molecules. Genetic Algorithms Approach to Force Field Scaling. J. Raman Spectrosc. **1998**, 29, 833-839

(22) Frisch, M. J.; Trucks, G. W.; Schlegel, H. B.; Gill, P. M. W.; Johnson, B. G.; Foresman, J. B.; Robb, M. A.; Cheeseman, J. R.; Keith, T.; Peterssons, G. A.; Montomery, J. A.; Raghavachari, K.; Al-Laham, M. A.; Zakrzewski, V. G.; Oritz, J. V.; Foresman, J. B.; Cioslowski, J.; Stefanov, B. B.; Nanayakkara, A.; Challacombe, M.; Peng, C. Y.; Ayala, P. Y.; Chen, W.; Wong, M. W.; Andres, J. L.; Replogle, E. S.; Gomperts, R.; Martin, R. L.; Fox, D. J.; Binkley, J. S.; Defrees, D. J.; Baker, J.; Stewart, J. J. P.; Head-Gordan, J.; Gonzalez, C.; Pople, J. A. Gaussian-94, Rev. D.1; Gaussian: Pittsburgh, PA 1995.

(23) Spartan 5.0; Wavefunction: Irvine, CA, 1997.

(24) Norrestam, R.; Stensland, B.; Soderberg, E. The Crystal and Molecular Structure of Lumazine Hydrate. Acta Crystallog., B **1972**, 28, 659

(25) Cotton, F. A.; Wilkinson, G. Advanced Inorganic Chemistry, 4th ed.; Wiley & Sons: New York, 1980, p 969.

(26) Benecky, M.; Yu, T.-J.; Watters, K. L.; McFarland: Metal-Flavin Complexation A resonance Raman Investigation. Biochim. Biphys. Acta **1980**, 627, 197

CHAPTER 5

(1) Lombardi, R. L. Birke, Tianhong Lu and Jia Xu, J. Chem. Phys. **1986**, 84(8), 4174-4180

(2) T. E. Furtak and S. H. Macomber, Chem. Phys. Letters, **1983**, 95, 328

(3) T. E. Furtak and D. Roy, Phys. Rev. Lett, **1983**, 50, 1301

(4) S. Venkatersan, Gayle Erdheim, John R. Lombardi and Ronald L. Birke, Surface Science **1980**, 101, 387-398

(5) Otto, J. Electron Spectrosc. Relat. Phenom. **1982**, 44, 105

(6) Luis A. Sanchez, Ronald L. Birke, and John R. Lombardi, J. Phys. Chem. Vol. 88(9), 1984.

(7) Pemble, M.E. Ph.D. Thesis, University of Southampton, Southampton, England, 1980.

(8) Jean A, Baldwin, Blanka Vickova, Mark P. Andrews, and Ian S. Butler, Langmuir, **1997**, 13, 3744-3751

(9) Yoon Soo Pang, Hyun Jin Hwang, Myung Soo Kim, J. Mol. Struct. **1998**, 441, 63-67

(10) Hee Sook Jung, Kwan Kim, Myung Soo Kim, J. Mol. Struct. **1997**, 407, 139-147

(11) T. Sueoka, J. Inukai and M Ito, J. Electron Spectroscopy and Related Phenomena, **1993**,64/65, 263-270

(12) W. H. Li, B. W. Mao and Z. Q. Tian, J. Raman. Spectroscopy, **1995**, 26, 233-237

(13) Suncheng Sun, Ronald L. Birke and John R. Lombardi, J. Phys. Chem. **1990**, 94, 2005-2010

(14) Jun-Ho Choi and Hojing Kim, Bull. Korean Chem. Soc., 14(3), **1993**